RÉPUBLIQUE ALGÉRIENNE DÉMOCRATIQUE ET POPULAIRE
MINISTÈRE DE L'ENSEIGNEMENT SUPÉRIEUR ET DE LA RECHERCHE SCIENTIFIQUE

ÉCOLE NATIONALE POLYTECHNIQUE

المدرسة الوطنية المتعددة التقنيات
Ecole Nationale Polytechnique

CRTSE

Material Engineering Department

End of Studies Project

Submitted for the fulfillment of the State Engineer Degree in Materials Engineering

---

Improvement of the performance of the synthesized NPO-Li layer on the lithium metal anode

---

BOUCHEBBAT Asma & ABED MERAIM Nesrine Ines

Under the supervision of **M.CHERIET Abdelhalk** (CRTSE)
And the co-supervision of **M.LARIBI Merzak** (ENP)

Presented and publicly defended on (29/06/2025)

Jury Members :

President : Dr. DJEMA Oussama ENP
Examiner : Dr. ZOUZOU Chaima ENP

ENP 2025

RÉPUBLIQUE ALGÉRIENNE DÉMOCRATIQUE ET POPULAIRE
MINISTÈRE DE L'ENSEIGNEMENT SUPÉRIEUR ET DE LA RECHERCHE SCIENTIFIQUE

ÉCOLE NATIONALE POLYTECHNIQUE

المدرسة الوطنية المتعددة التقنيات
Ecole Nationale Polytechnique

CRTSE

Material Engineering Department

End of Studies Project

Submitted for the fulfillment of the State Engineer Degree in Materials Engineering

---

Improvement of the performance of the synthesized NPO-Li layer on the lithium metal anode

---

BOUCHEBBAT Asma & ABED MERAIM Nesrine Ines

Under the supervision of **M.CHERIET Abdelhalk** (CRTSE)
And the co-supervision of **M.LARIBI Merzak** (ENP)

Presented and publicly defended on (29/06/2025)

Jury Members :

President : Dr. DJEMA Oussama ENP
Examiner : Dr. ZOUZOU Chaima ENP

ENP 2025

RÉPUBLIQUE ALGÉRIENNE DÉMOCRATIQUE ET POPULAIRE
MINISTÈRE DE L'ENSEIGNEMENT SUPÉRIEUR ET DE LA RECHERCHE SCIENTIFIQUE

ÉCOLE NATIONALE POLYTECHNIQUE

المدرسة الوطنية المتعددة التقنيات
Ecole Nationale Polytechnique

CRTSE

Département du Génie de Matériaux

Mémoire de projet de fin d'études

Pour l'obtention du diplôme d'ingénieur d'état en Génie des matériaux

---

Amélioration des performances de la couche NPO-Li synthétisée sur l'anode en lithium métal

---

BOUCHEBBAT Asma & ABED MERAIM Nesrine Ines

Sous la direction du promoteur **M.CHERIET Abdelhalk** (CRTSE)
Et de l'encadrant **M.LARIBI Merzak** (ENP)

Présenté et soutenu publiquement le (29/06/2025)

Composition du jury :

Président :	Dr. DJEMA Oussama	ENP
Examinatrice :	Dr. ZOUZOU Chaima	ENP

ENP 2025

الملخص

يركّز هذا العمل على تحسين الأداء الكهروكيميائي لِمَصنّعات الليثيوم المعدني في البطاريات الليثيوم-أيون من خلال تطبيق معالجات سطحية باستخدام محاليل وظيفية. فرغم أن الليثيوم المعدني يتميز بسعة نظرية عالية وجهد كهربائي منخفض، إلا أنه يواجه تحديات كبيرة مثل تكوّن التفرعات الشجرية (dendrites)، وعدم استقرار واجهة الإلكتروليت الصلب (SEI)، وانخفاض كفاءة دورات الشحن والتفريغ. وللتغلب على هذه المشكلات، تم تطبيق معالجات سطحية بهدف تكوين طبقات واقية وناقلة من مركبات Li_3N وLi_3PO_4 لتعزيز التوصيلية الأيونية واستقرار الواجهة. تم استخدام هذه المصعدّات المعالَجة مع مهبطات مصنوعة من عجينة السيليكون. وقد تم توصيف العينات المحضّرة باستخدام تقنيات مثل DRX وSEM وEDS، كما تم تقييم أدائها الكهروكيميائي من خلال اختبارات الشحن/التفريغ الجلفاني (GCD)، والتحليل الطيفي للممانعة الكهربائية (EIS)، والفلتمترية الدورية (CV). أ.

الكلمات المفتاحية :

مصعد الليثيوم المعدني؛ التفرعات الشجرية؛ الأداء الكهروكيميائي؛ واجهة الإلكتروليت الصلب (SEI)؛ مهبط عجينة السيليكون؛ البطاريات.

Résumé

Ce travail porte sur l'amélioration des performances électrochimiques des anodes en lithium métal dans les batteries lithium-ion grâce à des traitements de surface utilisant des solutions fonctionnelles. Le lithium métal, malgré sa capacité théorique élevée et son faible potentiel électrochimique, présente des défis majeurs tels que la formation de dendrites, une interphase électrolytique solide (SEI) instable et une faible efficacité de cyclage. Pour remédier à ces problèmes, des traitements de surface ont été appliqués afin de former des couches protectrices et conductrices de Li_3N et Li_3PO_4, dans le but d'améliorer la conductivité ionique et de stabiliser la SEI. Les anodes traitées ont été associées à des cathodes à base de pâte de silicium. Les échantillons synthétisés ont été caractérisés par DRX, MEB et EDS, et évalués électrochimiquement à l'aide de tests de charge/décharge galvanostatique (GCD), de spectroscopie d'impédance électrochimique (EIS) et de voltampérométrie cyclique (CV).

Mots-clés : Anode en lithium métal – dendrites – performance électrochimique – interphase électrolytique solide (SEI) – cathode en pâte de silicium – batteries.

Abstract

This work focuses on improving the electrochemical performance of lithium metal anodes in lithium-ion batteries by applying surface treatments using functional solutions. Lithium metal, despite its high theoretical capacity and low electrochemical potential, faces significant challenges such as dendrite formation, unstable solid electrolyte interphase (SEI), and poor cycling efficiency. To address these issues, surface treatments were applied to form protective and conductive layers of Li_3N and Li_3PO_4, aiming to enhance ionic conductivity and stabilize the SEI. The treated anodes were paired with silicon slurry-based cathodes. The synthesized samples were characterized by XRD, SEM, and EDS, and evaluated electrochemically through galvanostatic charge–discharge (GCD), electrochemical impedance spectroscopy (EIS), and cyclic voltammetry (CV).

Keywords : Lithium metal anode – dendrites – Electrochemical performance – Solid electrolyte interphase (SEI) – Silicon slurry cathode – Batteries.

Acknowledgements

At the threshold of this academic journey, we would like to express our deepest gratitude to all those who guided, supported, and inspired us throughout the realization of this work.

First and foremost, we extend our heartfelt thanks to Mr. Cheriet Abdelhak, our thesis supervisor, whose unwavering guidance, insightful feedback, and generous support have been instrumental from the early stages of our project to its final completion. His expertise and kindness made a significant impact on our experience, and we are truly grateful for his mentorship.

We also wish to express our sincere appreciation to Mr. Laribi Merzak, our co-supervisor, who has been a pillar of support not only during this thesis but also throughout our three years of specialization in Materials Engineering. His dedication to our academic and professional growth has left a lasting impression on us.
Our thanks extend to the École Nationale Polytechnique, where we received a solid and enriching education. We are particularly grateful to the professors and staff of the Materials Engineering Department, whose continuous support and rigorous training helped shape us into the engineers we are today. Their guidance was not only academic but also human, and their support during challenging moments of our journey was both uplifting and essential to our progress.

We are also deeply thankful to the Centre de Recherche en Technologie des Semiconducteurs pour l'Énergétique (CRTSE) for hosting our research and providing us with an exceptional working environment. We express our appreciation to the researchers, technicians, and staff—especially those in the Thin Films and Interfaces Division—for their valuable technical assistance, their warm hospitality, and for making our research journey both productive and enjoyable.

To everyone who, in one way or another, contributed to the success of this thesis, we extend our heartfelt thanks.

BOUCHEBBAT Asma and ABED MERAIM Nesrine Ines.

Dedication

To my dearest parents
This work is first and foremost dedicated to you.

To my beloved mother *Thank you for everything you have done for me. For always standing by my side, for supporting every decision I made, for lighting my way when things felt uncertain, for your help, your patience, and your unconditional love. I am so incredibly lucky to have you as my mom.*
To my father *Thank you for your strength, your constant support, and your presence. Thank you for driving me to school every single morning and picking me up every day — not just during these past five years, but throughout my entire school life. For bearing with me through early mornings, for always showing up, thank you. To both of you — thank you for your eternal love and support. You are my hope, my strength, and the reason I kept going, even when it was hard and felt impossible. This achievement is yours as much as it is mine.*

To my sister *The one because of whom I am who I am today. My sister, my best friend, my partner in crime, the keeper of all my secrets, my constant support, and my guiding light. Thank you for being there in ways words can hardly express — for lifting me up, for believing in me, and for always knowing how to bring strength to my heart. I love you more than you could ever imagine.*

To my brother Mohamed *Thank you for being there for us when no one else was. Thank you for helping me find my way when I felt lost, and for making things feel easy and simple when they seemed impossible. You are more than just my big, protective brother — you are a source of strength, comfort, and quiet courage. I love you so much, and I'm deeply grateful for everything you are.*

To Ines *You are more than a best friend — you are a second sister to me, my soulmate, my comfy person.Thank you for being there, always — through every moment, every silence, every storm. I'll never forget how much you did for me when I couldn't do it on my own.I'll say it again : if it weren't for you, I wouldn't be graduating this year. If you know, you know.....I'll carry your presence with me, always — and I can't wait to see what's waiting for us after graduation.*

To Tati Madina, Malak, and Meriem
Thank you for your love, your kindness, and your constant support. Tati, your presence has always brought warmth and reassurance — like a second mother to me. Madina, Malak and Meriem, you've been more than cousins — you've been friends, sisters, and a source of joy in my life. I'm truly grateful to have you all by my side.

To Tata Hayet and Tonton Tarik *Thank you for your constant encouragement, your kindness, and your unwavering support.Your presence has always brought comfort, strength, and inspiration throughout this journey.With all my gratitude and affection.*

To Houda, Bouchra, and Ines *My university friends — and my life friends. We've been through a lot together, faced some really hard moments side by side. Thank you for making even the most impossible times feel lighter — for finding laughter in the chaos and turning stress into stories we'll never forget. This journey was tough, but you made it amazing, unforgettable, and filled with moments I'll always treasure. I'll never regret any part of it — because it led me to you.and also To* ***Kassia*** *Thank you for the laughs and the support .I'm grateful we shared this journey together.*

BOUCHEBBAT Asma

Dedication

To my Beloved mother *The one who was with me through every high and low, who always supported me. Your love is my strength, your prayers my protection, and your sacrifices the silent pillars behind every step I take. This work is a reflection of the values you instilled in me : patience, perseverance and the will to rise.*

To my Beloved father *Your quiet strength, constant guidance, and unwavering belief in me have shaped the person I am today. Thank you for your endless support, and for always encouraging me to aim higher.*

To my brother Raouf *Thank you for being my unpaid psychologist, the one who always had my back and my constant source of support and laughter. Through every high and low, you've been there without asking for anything in return. This journey wouldn't have been the same without you.*

To Asma *You are more than a university friend, more than a teammate — you are my sister, my soulmate, my voice of guidance whenever I felt lost. You brought light into the hardest moments and calm into the chaos. You made me believe in the invisible string theory, and I'll always be grateful our paths were tied. Thank you for being my anchor, my mirror, and my safe place.*

To my university friends, Houda, Bouchra, Amel, Hiba, Kassia *You have become more than friends ; you are a second family to me. Your presence throughout this journey has made the weight of every challenge lighter, and every stressful moment bearable. In your laughter, I found joy ; in your words, I found comfort ; and in your unwavering support, I found strength. Thank you for the late-night talks, the shared stress, the encouragement, and the unforgettable memories.*

To my childhood friends, Aya, Maya, Dorra *You were there before the dreams had names, before the goals had shape. Your support began when everything was still just a possibility, and it has stayed with me ever since. Thank you for growing beside me, for believing in me long before I believed in myself.*

To Tonton Moussa and Tata Fatiha *Your presence, kindness, and quiet support throughout the years never went unnoticed. From those early school mornings to every small gesture — I am forever grateful . Tata Fatiha Your warmth and care always made me feel safe, supported, and seen. Thank you both for being part of the comfort and stability that helped me move forward with confidence.*

To my beloved grandmother *Your strength, wisdom, and unconditional love have been a guiding light in my life. This work is dedicated to you, with deep gratitude and endless affection.*

To my cousin Amira *More than family — you are a friend, a confidante, a constant presence. Thank you for your love, your encouragement, and for always reminding me of who I am when I forget.*

To Tonton Tahar and Nawel *Your kindness, care, and sincere support have been a true blessing throughout this journey. Thank you for always being there with words of encouragement, comforting presence, and unwavering belief in me. I am truly grateful for everything you've done.*

ABED MERAIM Nesrine Ines

Table of Contents

List of Tables

List of Figures

List of Acronyms

- **LIB** : Lithium-Ion Batteries
- **SSLB** : All-Solid-State Lithium Batteries
- **LE** : Liquid Electrolyte
- **SE** : Solid Electrolyte
- **SEI** : Solid Electrolyte Interphase
- **EIS** : Electrochemical Impedance Spectroscopy
- **DRX** : X-ray Diffraction
- **EDS** : Energy Dispersive Spectroscopy
- **SEM** : Scanning Electron Microscope
- **CC** : Current Collector
- **GCD** : Galvanostatic Charge–Discharge
- **CV** : Cyclic Voltammetry
- **CE** : Coulombic Efficiency
- **THF** : Tetrahydrofuran
- **GEB** : Gel Electrolyte Batteries
- **LEB** : Liquid Electrolyte Battery
- **HEB** : Hybrid Electrolyte Batteries
- **SEB** : Solid Electrolyte Batteries
- **PPEB** : Plasticized Polymer Electrolyte Battery
- **DPEB** : Polymer Electrolyte Battery
- **EC :DMC** : Ethylene carbonate and dimethyl carbonate
- **VRE** :variable renewable energy

List of Symbols

- **T** : Temperature (°C)
- **V** : Voltage (mV)
- **i** : Electric current (mA)
- **e** : Elementary charge (Coulomb)
- **C** : Molar concentration (mol/L)
- **n** : Amount of substance (mol)
- **Q** : Electric charge (Coulombs)
- **j** : Electric current density (mA/cm^2)
- $\mathbf{C_{cap}}$: Capacity (mAh/g)
- **Em** : Migration energy (eV)
- **EA** : Apparent activation energy (eV)
- **Et** : Trap energy (eV)
- **Ef** : Defect formation energy (eV)
- **Ea** : Activation energy (kJ/mol or eV)

Introduction

"**To unlock the full potential of renewable energy, we must learn to store the sun and the wind — and that's what batteries make possible.**"

Inspired by energy researchers

The increasing global demand for reliable and high-capacity energy storage systems has made batteries a cornerstone of modern technology. From consumer electronics to electric vehicles and grid-scale storage, lithium-ion batteries (LIBs) have become the standard due to their favorable energy density, cycle life, and efficiency. However, with growing pressure to enhance battery performance and safety, conventional LIBs are now approaching their practical limitations.

One of the most promising strategies for pushing beyond these limits involves the use of lithium-metal anodes. Lithium metal possesses an ultra-high theoretical specific capacity of 3860 $mAh\,g^{-1}$ and the lowest electrochemical potential (0 V vs. Li^+/Li) among all known anode materials, making it an ideal candidate for next-generation high-energy batteries. If successfully integrated, lithium-metal-based systems could dramatically increase energy density, potentially reaching 400 $Wh\,kg^{-1}$, and thus unlock the full potential of advanced applications such as long-range electric vehicles and high-capacity portable devices.

However, the use of lithium metal anodes presents significant technical challenges. Uncontrolled dendrite formation, unstable SEI layers, and parasitic reactions with liquid electrolytes often lead to rapid capacity fading, short circuits, and safety hazards. To address these critical issues, research has increasingly focused on improving the lithium-electrolyte interface by stabilizing the SEI and minimizing dendritic growth.

In this work, we explore an approach to enhance the performance and stability of lithium metal anodes by applying a surface treatment using functional solutions, designed to create a robust artificial SEI. This interphase mimics the behavior of a solid electrolyte, improving interfacial stability and ionic conductivity while suppressing dendrite growth. While lithium metal anodes are often associated with all-solid-state configurations, our system uses a liquid electrolyte, making it a hybrid configuration that combines the high-energy potential of lithium metal with the practical benefits of liquid electrolytes.

This study aims to contribute to the development of safer, higher-capacity, and longer-lasting lithium-based batteries by engineering the lithium/electrolyte interface.

Organization of the Thesis :

Chapter 1 : Introduces batteries as vital components in modern energy systems, covering their energy storage role, working principles, and key components (electrodes, electrolytes, separators). It classifies batteries as primary (non-rechargeable) or secondary (rechargeable), categorized by electrolyte type (aqueous, organic liquid, solid-state) and performance metrics (energy density, cycle life, safety).

Chapter 2 : explores lithium-based batteries, focusing on their high energy density and key challenges, particularly with lithium-metal anodes. These anodes face critical issues like dendrite growth (causing short circuits), unstable SEI layers (leading to capacity fade), and mechanical degradation from cycling. To overcome these, research strategies are examined, including arti-

ficial SEI layers, 3D host structures, and hybrid/solid-state electrolytes. The chapter highlights progress toward practical lithium-metal batteries while noting remaining challenges.

Chapter 3 : presents the chemical synthesis of inorganic thin-film NPOLi solid electrolytes deposited on lithium metal anodes, along with the fabrication and assembly of battery cells employing silicon slurry cathodes. The chapter details the working principles of these systems and comprehensively describes the characterization techniques used in this study.

Chapter 4 : presents the electrochemical performance, compositional analysis, and structural characterization results of the fabricated lithium metal anode cells with silicon slurry cathodes, including their cycling stability evaluation.

The thesis concludes with key findings and proposes future research directions for advanced solid-state battery development.

Chapter 1

Energy and Batteries

> ""The holy grail of energy is storage. Once we figure out how to store energy effectively, we will be in a completely different place." "
> — *Dr. Steven Chu*

1.1 Energy storage

1.1.1 What's "energy storage"

Energy storage is one key to unlocking a future of the power sector that can be designed to be more flexible and predictable in terms of operating costs and the revenue streams that recoup capital costs. In recent years, many storage technologies have emerged that allow for short-duration, rapid-response energy storage and longer-duration applications that can economically shift energy to periods of high seasonal demand, such as scorching summer months, or low supply, such as during droughts. All signs indicate that new storage technologies will continue to emerge.

With the proliferation of renewable energy technologies, energy storage can also serve a role in decarbonising grids as it enables (VRE) generation technologies to attain a level of total power system share that in years past was not technically feasible. Energy storage solutions can provide flexible daily renewable ramp rates, balance out power capacity changes during weather abnormalities, optimise renewable outputs to achieve maximum payback during peak periods, and enhance operations when these solutions integrate with existing assets to benefit the overall operations of a power network.[32].

This balance between energy and power performance is clearly illustrated in the Ragone plot below. It compares key storage technologies — such as fuel cells, batteries, and supercapacitors — highlighting their respective strengths. While fuel cells excel in energy density and supercapacitors in power delivery, batteries offer a versatile compromise between the two. This visual representation underscores the importance of selecting appropriate storage solutions based on specific application needs within an evolving energy landscape.

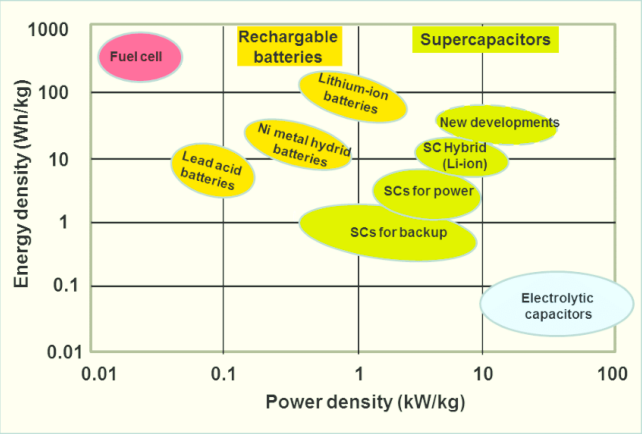

Figure 1.1 – Ragone plot comparing energy density and power density of various energy storage technologies, illustrating the trade-offs between fuel cells, batteries, and supercapacitors.[2]

1.1.2 The different forms of energy storage

1.1.2.1 Hydrogen storage

Hydrogen as an energy carrier can be produced by electrolysis of water*, stored and then used in a fuel cell to produce electricity . There are several means of storage : pressurized, liquid (20 K) and solid in metal hydrides and absorbent materials . In the latter case, reversible storage of interesting density (1.5 times that of liquid hydrogen) takes place under near-ambient temperature and pressure conditions. Research into these materials remains very active, with a view to improving their performance in terms of kinetics, aging under cyclic conditions, increasing their mass capacity, etc.

1.1.2.2 Supercapacitors

Supercapacitorsare devices capable of delivering high currents for times of the order of seconds A supercapacitor consists of two porous electrodes, usually activated carbon*, impregnated with electrolyte, separated by an electrically insulating membrane with a porous texture ensuring ionic conduction. Storage is electrostatic, with no electrochemical reaction. The number of charge/discharge cycles is therefore very high. Electrolytes with good ionic conductivity are either aqueous or organic.
Current research is focused on increasing energy density. The exploration of new systems involving metal oxides or nitrides materials and new environmentally-friendly aqueous electrolytes is also under development.

1.1.2.3 Mechanical storage

A flywheel stores electrical energy in the form of rotational kinetic energy An electric motor sets the disk into rotation and holds it there, while energy is recovered via an electric generator. These systems store small quantities of energy (10 Wh/Kg) which are instantly available and can be restored in a very short time (1 to 10 W/Kg). An important aspect of current research to improve performance is the replacement of metallic materials by lighter composite materials. Compressed-air energy storage (CAES) is a mass storage system ranging from MW to GW . It consists of massively compressing air in a geological cavity with the excess electricity produced, then recovering the energy by turbining. It is a means of smoothing out daily electricity production. The main focus of research is on adiabatic* CAES, in which the heat of compression is recovered and stored independently of the compressed air, to be re-injected during turbining.

1.1.2.4 Magnetic storage

These systems consist of a superconducting coil including a cryostat* and an interface power converter* for charging or discharging. They are suitable for fast operation of the order of a few milliseconds to a few seconds. It is a pulsed source of current, with moderate energy density (a few Wh/Kg). Research focuses not only on superconducting materials, but also on the implementation of the constituent elements, the cryogenic system, connections, mechanical structures, etc.

1.1.2.5 Thermal storage

Among the performance criteria for the storage process, energy density (quantity of heat stored per unit of mass or volume) is the one that most clearly distinguishes the three methods (sensible heat, latent heat, heat of reaction). The other criteria are efficiency, storage and restitution capacity, cost and ease of management [33, 34].

1.1.2.6 Electrochemical storage

The enormous growth in world population, particularly in the developing world, coupled with technological developments are considered as the key factors behind the immense increase in electrical energy consumption over the past half century. Further increases in the world energy consumption are expected with its energy demand projected to be doubled by the middle and tripled by the end of the century [35] as a result of further population growth (with world population expected to reach 9 billion by 2048) and increased electrical energy demands in industrial and commercial sectors [36].

Currently, fossil fuels such as oil, gas and coal are the primary sources of energy, with more than 85% of the world's total energy generation achieved through these conventional sources [37]. Over-reliance on fossil fuels for production of energy has led to numerous environmental challenges including poor air quality, unexpected climatic variations, water/soil contamination and a colossal increase in greenhouse gas emissions [38, 39].

To contain or reverse these trends, deployment of more sustainable and low carbon or even carbon free renewable sources of energy such as wind, solar or tidal are essential. However, these renewable sources of energy are location-specific and, in some cases, unpredictable in nature and therefore operational flexibility is key for their integration into the power systems. This flexibility is attainable when using appropriate energy storage technologies that can help in managing fluctuations and mismatches in energy supply and demands, ultimately improving the efficiencies in energy and power supply systems by reducing the gap between production and consumption. Furthermore, growth in energy proportion added to national grid through the integration of renewable sources such as wind and solar results in curtailments which can be addressed by using appropriate storage technologies [40].

There are a broad range of energy storage and conversion technologies available including chemical, thermochemical, mechanical, electrical and electrochemical storage systems. Among these, electrochemical energy storage and conversion systems such as electrochemical capacitors/batteries and fuel cells respectively, have received the most intensive attention and have been adopted in everyday applications due to their high columbic efficiencies. Basically energy storage devices perform two important tasks : (a) time shifting bulk energy from renewables production to time of energy demand (supplied by batteries + fuel cells), (b) production of clean, stable power and frequency, avoiding voltage spikes (important for digital economy) by supercapacitors and high power batteries.

However, challenges related to their durability, high cost, environmental concerns, and operability problems must be addressed in order to improve their effectiveness and further increase uptake. For instance, even though lithium-ion batteries have transformed the technology of electric vehicles (EV) and portable electronics such as mobile phones and laptops, this technology still suffers from issues such

as high lithium cost and safety concerns [41]. In 2011, almost 78% of lithium was extracted from brines (in Chile, Argentina and USA), and the rest came from hard rock mines (in China and Australia) [42]. Environmental impact of lithium mining including human health, effect on biodiversity and availability of clean/fresh water for consumption and agriculture use are other key concerns. Since major lithium reserves are located in salt lakes and pans where lithium is extracted through evaporation and flooding of reserves with fresh water [43].

Similarly, electrochemical capacitors (ECs) have inferior energy densities whereas fuel cells have operability and system issues [44, 45].

The aim of this review is to make comprehensive classification of electrochemical energy storage, conversion systems as shown in Figure 1, explain their basic working principles, and technical characteristics, highlight the distinctive properties of each system, and discuss their fields of application.

A diverse range of energy storage and conversion devices is shown in figure 1.2,based on their energy delivery time varying with the type of mechanism involved in energy storage or conversion systems. For example, electrochemical capacitors are considered as high power density devices and their delivery time is in the range of few seconds to minutes since these devices utilise only the material on the electrode surface unlike batteries or fuel cells where bulk of the material is involved in energy storage and conversion respectively. Other characteristics of these devices vary as well due to the fundamental difference in the mode of energy storage or conversion (physical/electrochemical). In case of electrochemical capacitors, most of the commercially used devices use electric double layer charge storage phenomenon, which results in inferior energy densities as compared to other electrochemical energy storage or conversion devices shown in Figure 1.3 beginfigure

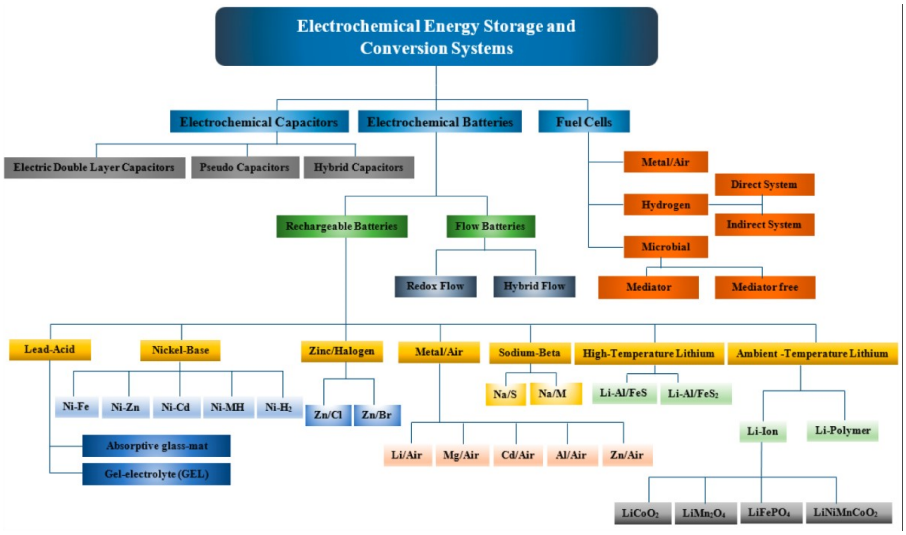

Figure 1.2 – Classification of electrical energy storage and conversion devices[3].

Electrochemical capacitors/batteries and fuel cells are key electrochemical energy storage and conversion technologies respectively, used in commercial applications with their particular selection dependent on performance limitations such as energy densities, power densities, and cycle life. Electrochemical batteries and fuel cells are considered as high energy density devices with typical gravimetric energy densities in the range of 100–200 Wh kg^{-1} and 600–1200 Wh kg^{-1} respectively, whereas current ECs have significantly lower energy densities with typical values between 0.05–30 Wh kg^{-1} [46]. However, ECs are considered as high-power density devices with very short charge/discharge times (of the order of seconds) which is difficult to achieve by other electrochemical energy storage and conversion devices. Figure 1.2 shows a comparison of specific energy, specific power and their delivery timescale for different energy storage and conversion devices. At present, none of these devices has the capability to meet the wide spectrum of requirements demanded by the diverse range of renewable energy sources such as wind, tidal and solar. However, they can respond to a broad range of requirements such as fast charge/discharge, peak power demands and high energy storage needs over a longer

period of time when used in a combination of two or more.

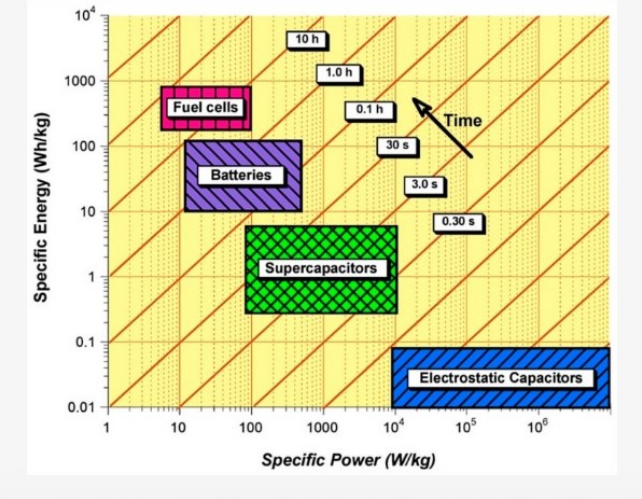

Figure 1.3 – Energy density, power density, and delivery timescale for different energy storage and conversion devices [4].

1.1.3 Energy storage and batteries

1.1.3.1 Electrochemical Energy Storage in Batteries

Electrochemical storage relies on the conversion of electrical energy into chemical energy and vice versa within an electrochemical cell. This primarily includes batteries, such as lithium-ion batteries, in which redox (oxidation-reduction) reactions enable the transfer of electrons and the storage of energy. These systems offer the advantages of good energy density, high efficiency, and quick response time, making them particularly well-suited for storing electricity for both mobile and stationary applications.[47]

An understanding of the state-of-the-art of Li ion batteries, their future trend, and the prospects and limits of electrochemical energy storage in general are extremely important to technologists involved in the design and development of new consumer products and scientists and engineers engaged in the invention and development of advanced materials for future high energy density batteries. This account is not a comprehensive review of rechargeable batteries ; rather, it is a narrative of the author's perspective on the prospects for electrochemical energy storage, its limitations, and the challenges for developing advanced batteries.[48]

1.2 Batteries

> "Batteries are not just a power source ; they are a critical technology to achieving a sustainable future"
> *Akira Yoshino (Co-inventor of the lithium-ion battery)*

1.2.1 Why Batteries ?

The use of fossil fuels has undeniably played a pivotal role in the advancement of human civilization, powering industrial development, transportation, and modern lifestyles. However, the extensive and prolonged reliance on these non-renewable energy sources has led to a series of critical challenges, including the depletion of natural resources, escalating greenhouse gas emissions, and severe environmental degradation. These issues have prompted the urgent need to transition towards more sustainable and environmentally friendly energy systems.

In response to this global energy and environmental crisis, renewable energy sources such as wind, hydroelectric, solar, and hydrogen fuel cells have emerged as promising alternatives. These systems offer the potential for clean, abundant, and sustainable energy production, significantly reducing the carbon footprint and mitigating the harmful effects of climate change. Nevertheless, the intermittent and variable nature of renewable energy sources necessitates the development of efficient and reliable energy storage technologies to ensure stability and continuity in energy supply.

Among the various energy storage methods, electrochemical energy storage—commonly known as battery storage—has gained significant attention. Batteries have the unique capability to directly convert chemical energy into electrical energy and vice versa, making them essential for both stationary applications (such as grid energy storage) and mobile uses (such as electric vehicles and portable electronics). Their scalability, responsiveness, and ability to store energy over short to moderate durations make them a cornerstone of the modern energy landscape.

As a result, electrochemical energy storage systems are increasingly recognized not only as technological tools but as key enablers in the global transition to a low-carbon economy. Their continued development and integration into energy infrastructures are indispensable to achieving energy security, improving the efficiency of renewable energy systems, and ultimately supporting a sustainable future for society.[49]

1.2.2 Generals about batteries

1.2.2.1 Introduction

A battery is an electrochemical device that directly transforms the chemical energy stored in its active materials into electrical energy through oxidation-reduction (redox) reactions. Unlike conventional thermal systems, where energy is converted via combustion and subject to the limitations imposed by the Carnot cycle, batteries operate through electron transfer mechanisms without intermediate heat production, which enables them to achieve higher conversion efficiencies. In rechargeable systems, this process is reversible—electrical energy is applied to drive the redox reaction in the opposite direction, thus restoring the battery's initial state. The fundamental principle involves electrons flowing from the anode to the cathode through an external circuit, while ions travel through the electrolyte to maintain charge balance. In contrast to non-electrochemical redox reactions like rusting or combustion, where electron transfer occurs directly and results in heat, the electrochemical approach allows for controlled and efficient energy harnessing. This makes batteries a cornerstone technology in modern energy systems, particularly in applications requiring portable or decentralized power.

1.2.3 Cell vs a battery

1.2.3.1 From Cells to Batteries : Electrochemical Energy Conversion

A cell is the basic electrochemical unit providing a source of electrical energy by direct conversion of chemical energy. The cell consists of an assembly of electrodes, separators, electrolyte, container and terminals. A battery consists of one or more electrochemical cells, electrically connected in an appropriate series/parallel arrangement to provide the required operating voltage and current levels, including, if any, monitors, controls and other ancillary components (e.g. fuses, diodes), case, terminals and markings. (Although much less popular, in some publications, the term "battery" is considered to contain two or more cells.) Popular usage considers the "battery" and not the "cell" to be the product that is sold or provided to the "user." Most often, the electrical data is presented on the basis of a single-cell battery. The performance of a multicell battery will usually be different than the performance of the individual cells or a single-cell battery.
While the term "battery" is often used, the basic electrochemical unit being referred to is the "cell." A battery consists of one or more of these cells, connected in series or parallel, or both, depending on the desired output voltage and capacity. [50]

1.2.3.2 Key Components of an Electrochemical Cell

1. **The anode or negative electrode**—the reducing or fuel electrode—which gives up electrons to the external circuit and is oxidized during the electrochemical reaction.
2. **The cathode or positive electrode**—the oxidizing electrode—which accepts electrons from the external circuit and is reduced during the electrochemical reaction.
3. **The electrolyte**—the ionic conductor—which provides the medium for transfer of charge, as ions, inside the cell between the anode and cathode. The electrolyte is typically a liquid, such as water or other solvents, with dissolved salts, acids, or alkalis to impart ionic conductivity. Some batteries use solid electrolytes, which are ionic conductors at the operating temperature of the cell [50].

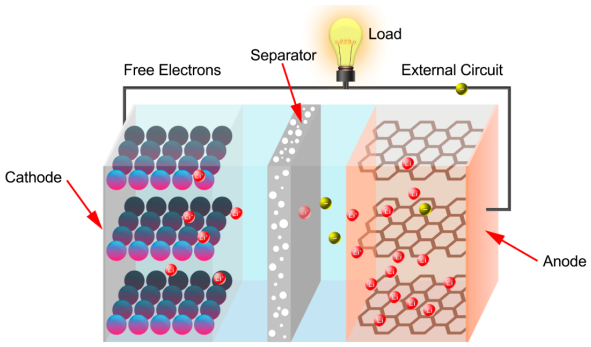

Figure 1.4 – Components of a lithium-ion battery cell[5]

1.2.4 Operations of batteries

1.2.4.1 Intercalation and Deintercalation vs Charging and Discharging Phenomena

1.2.4.1.1 generals

In rechargeable batteries, especially lithium-ion batteries, two closely related processes occur during operation : intercalation/deintercalation and charging/discharging. Although they are connected, they describe different aspects of battery behavior.

The term 'intercalation' refers to a process where by a guest molecule or ion is inserted into a host lattice. The structure of the guest–host or intercalation compound is only slightly perturbed from the host structure and the reaction used to form the compound is reversible [51].

Intercalation is the process by which ions, such as lithium ions (Li^+), are inserted into the layered structure of an electrode material without significantly changing its crystal framework. Conversely, deintercalation is the removal of these ions from the electrode's structure. These processes take place at the microscopic level inside the electrode materials.

On the other hand, charging and discharging describe the macroscopic electrical operation of the battery. During charging, electrical energy is supplied to the battery, causing lithium ions to move from the cathode through the electrolyte to the anode, where they intercalate. Meanwhile, during discharging, the battery delivers electrical energy to an external circuit as lithium ions move in the opposite direction.
move back from the anode to the cathode, involving deintercalation from the anode and intercalation into the cathode.[52]

1.2.4.1.2 Charging and discharging Methodology

The batteries are charged by supplying constant voltage at the terminal of the battery by a power supply. Charging rate is set to **C/5** for Lithium-ion batteries. After setting this voltage and current values, the battery is left for charging. After every half an hour, the value of battery voltage and current are noted down by using a multimeter and clamp meter. Charging characteristics are plotted as current and voltage versus time.

The battery is charged up to end of charge voltage (voltage at which the battery should disconnect from the supply to prevent it from overcharge). To determine the discharging voltage and current, the battery is discharged through a LED load. Voltage and current readings are noted down after each half an hour to plot the voltage and current versus time graph. The battery is discharged up to the end of discharge voltage ; it is the voltage at which the battery should be disconnected from the load to prevent it from over discharging. [53]

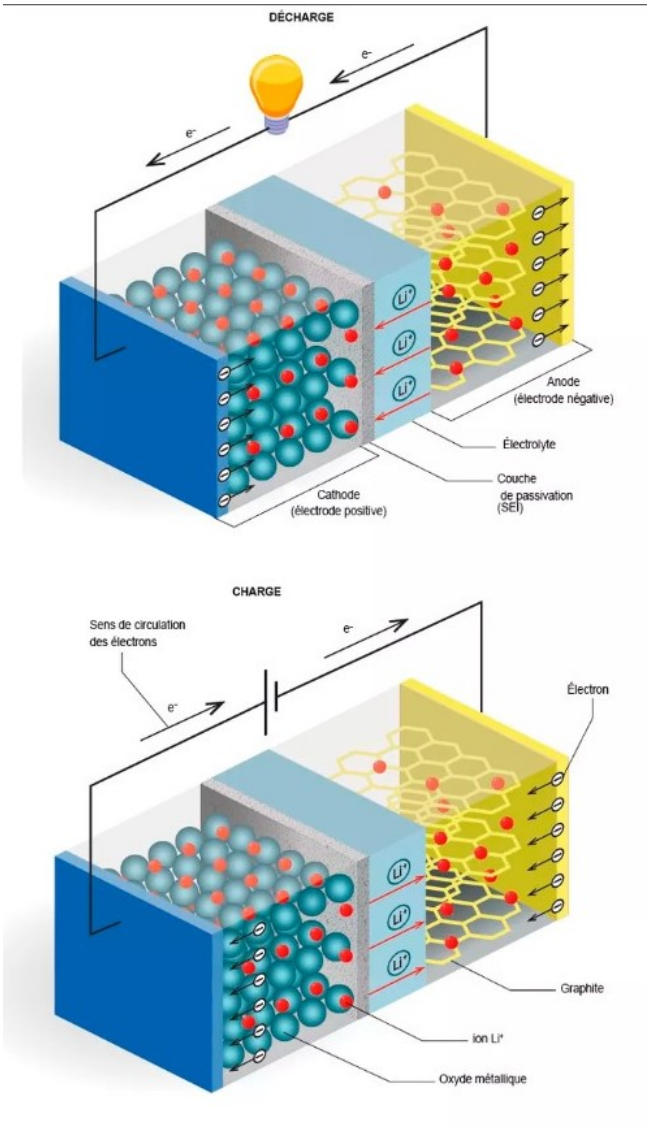

Figure 1.5 – Schematic illustration of the charge and discharge processes in a lithium-ion battery[6]

1.2.5 Classification of Cells and Batteries

1.2.5.1 Generalities

Batteries are broadly classified into two main categories : primary and secondary batteries. Primary batteries are non-rechargeable systems designed for single-use applications ; once their stored energy is depleted, they must be discarded. In contrast, secondary batteries are rechargeable and capable of undergoing multiple charge–discharge cycles, making them suitable for long-term use in various applications.
Beyond this fundamental distinction, both primary and secondary batteries can be further categorized according to several criteria, including their physical configuration, intended application, operating temperature range, and most notably, the nature of the electrolyte employed. Among these classification parameters, the electrolyte type holds particular importance, as it significantly influences the battery's performance, safety, and energy density.
Electrolytes may exist in various forms, such as aqueous solutions, organic solvents, gel polymers, solid-state materials (including ceramics and solid polymers), or molten salts, each offering distinct advantages depending on the specific use case.[54]

1.2.5.2 Primary Batteries

Primary Cells are designed for single use. Once discharged, they are disposed of. Their chemical reactions are non-reversible. [55]

Table 1.1 – Comparison of Primary Batteries

Aspect	**Aqueous Electrolyte Batteries**	**Nonaqueous Electrolyte Batteries**
Definition	Non-rechargeable, water-based electrolytes and Irreversible reactions.[55]	Non-rechargeable, non-aqueous solvents (often organic) and Supports lithium chemistries.[56]
Popular Types	1. Zn/MnO_2 (KOH), 1.5 V 2. Zn/Air (KOH), 1.6 V 3. Zn/HgO (KOH), 1.35 V	1. Li/MnO_2, 3.0 V, 280 Wh/kg 2. $Li/(CF)_n$, 290 Wh/kg 3. $Li/SOCl_2$, 3.6 V, up to 700 Wh/kg
Advantages	High energy per volume (225 Wh/L), inexpensive	High energy (150–300 Wh/kg), high voltage (3.6–4.0 V), lightweight, long life (>1000 cycles)
Applications	Flashlights, toys, remote controls, hearing aids, medical devices	Consumer electronics, military and medical devices

1.2.5.3 Secondary Batteries

Secondary Cells are capable of multiple charge-discharge cycles Forcing current through the cells in the reverse direction can reverse the electrochemical reactions that occur during discharge[54]

Table 1.2 – Comparison of Secondary Batteries Based on Electrolyte Type

Type	**Secondary cells with aqueous electrolytes**	**Secondary batteries with nonaqueous electrolytes**
Definition	Rechargeable electrochemical energy storage devices using water-based electrolytes. Can be recharged and reused multiple times. [57]	Rechargeable batteries using non-water-based electrolytes (organic solvents or solid-state materials). [57]
Popular Types	Lithium-ion batteries are the most advanced and widely used type of rechargeable battery today. Key components : -Anode : Carbon (usually graphite), which hosts Li ions. -Cathode : Metal oxides -Electrolyte	-Lithium Metal Solid-State Batteries -All-Solid-State Lithium-Sulfur (Li–S) -Solid-State Lithium-Air (Li–O) -Thin-Film Solid-State Batteries
Key Components	Electrolyte : water-based Anode and cathode vary depending on chemistry	Anode : carbon (usually graphite) Cathode : metal oxides Electrolyte : organic solvent or solid-state
Advantages	Low cost Easy recycling Good performance for specific applications Long cycle life	High energy density High voltage Longer cycle life Lightweight Enhanced safety Wider temperature range Compatible with advanced chemistries
Applications	Consumer electronics Backup power Electric bikes Medical equipment	Renewable energy storage Medical devices Aerospace Electronics Electric vehicles (EVs)

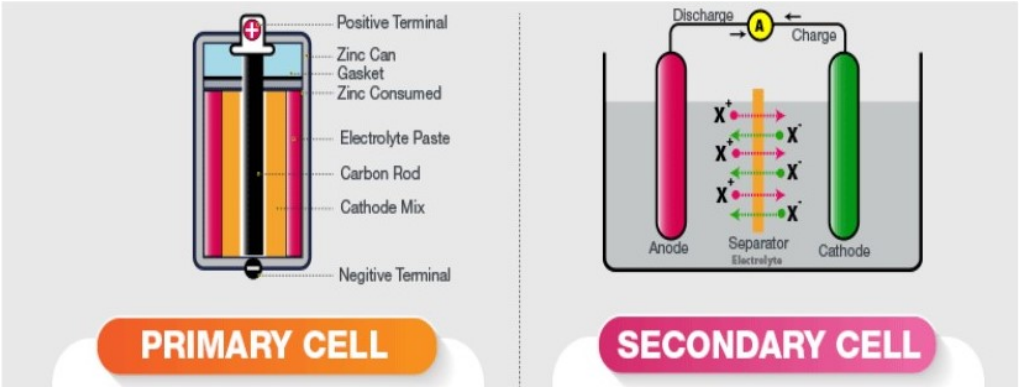

Figure 1.6 – Comparison between primary and secondary batteries[7]

1.2.5.4 Classification Based on the Electrolyte

1.2.5.4.1 A Universal Battery Classification Based on the Ion Conduction Mechanism

The chemistry and physical properties of the electrolyte significantly influence battery manufacture and performance. An ideal electrolyte should exhibit a unity transference number and high ionic conductivity at least comparable to that of liquid electrolytes. Both parameters are important for faster ion transport and the reduction of internal cell resistance.

In addition, interface-related challenges, such as dendrite formation, instability of electrolytes with electrodes, and sluggish electrode kinetics play an important role. In particular, the following parameters are crucial in governing the advantages and disadvantages of each electrolyte type :

- Ion conduction mechanism
- Ionic conductivity
- Transference number
- Mechanical properties
- Thermal properties
- Surface properties
- Electrochemical windows

These parameters strongly influence battery performance and manufacture [8, 58].

Presently, electrolytes are classified simply according to their composition and physical state of matter. For example, the terms solid, inorganic solid, ceramic, solid polymer, soggy sand, semi-solid, quasi-solid, almost solid, gel polymer, composite, hybrid, and liquid are used to describe and categorize electrolytes. However, these descriptors leave room for interpretation as to the predominant ion conduction mechanism that occurs in the electrolyte.

In our view, the most relevant parameter to classify electrolytes is their ion conduction mechanism. Following this perception, we suggest the following classification of electrolytes into four types of predominant ion conduction mechanisms :

1. Mobile ion-solvent complexes define a liquid electrolyte (LE) or gel electrolyte (GE).
2. Ion transport through polymer chain segmental motion defines a dry polymer electrolyte (DPE) or plasticized polymer electrolyte (PPE).
3. Ion transport by vacancies and interstitial sites defines a solid electrolyte (SE).
4. A hybrid electrolyte (HE) is defined as any combination of the above in which at least two types of conduction mechanism are present in the electrolyte or cell.

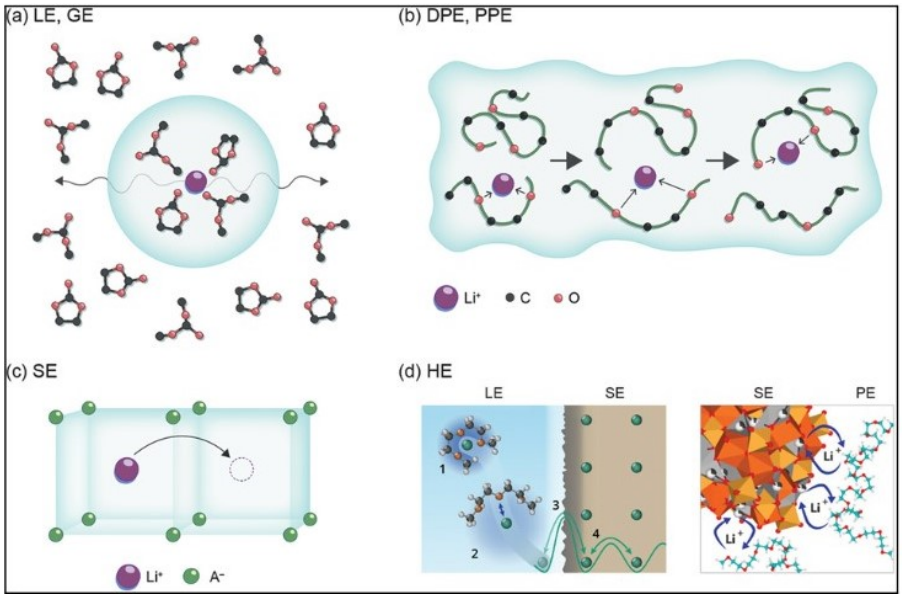

Figure 1.7 – Schematic representation of different types of electrolytes and their ion conduction mechanisms : (a) mobile ion–solvent complexes in LEs and GEs [8, 9], (b) polymer chain segmental motion in DPEs and PPEs [9], (c) ion transport via vacancies and interstitial sites in SEs [9, 10], and (d) interface behavior in HEs, including LE–SE and PE–SE interfaces [11, 12].

It is evident that the large spread of achieved conductivities, spanning two orders of magnitude, results in vastly different battery performance. Since the conduction mechanism and the type of electrolyte are fundamental to battery operation, we extend the same principles to the classification of battery cells. In our proposed terminology, the types of batteries corresponding to each class of electrolyte are denoted as follows :

1. Liquid Electrolyte Battery (LEB) or Gel Electrolyte Battery (GEB),
2. Dry Polymer Electrolyte Battery (DPEB) or Plasticized Polymer Electrolyte Battery (PPEB),
3. Solid Electrolyte Battery (SEB),
4. Hybrid Electrolyte Battery (HEB).

For example, an LEB refers to a cell using a liquid electrolyte, a prominent example of which is commonly known as the lithium-ion battery.

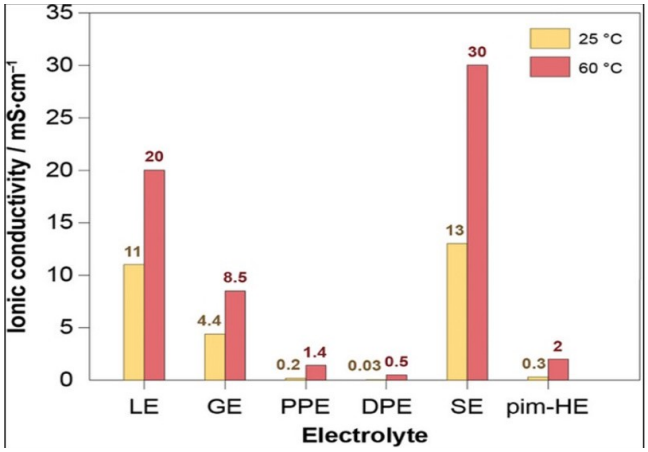

Figure 1.8 – Ionic conductivity values of representative examples for each class of electrolyte : liquid electrolyte (LE) : 1 M $LiPF_6$ in ethylene carbonate-dimethyl carbonate [13] ; gel electrolyte (GE) : mixture of 10 wt.% cross-linked poly(methyl methacrylate) and 90 wt.% LE [14] ; plasticized polymer electrolyte (PPE) : PEO :LiTFSI :Pyr_{14}TFSI in a 20 :2 :2 ratio [15] ; dry polymer electrolyte (DPE) : PEO–$LiClO_4$ [16] ; solid electrolyte (SE) : $Li_{10}GeP_2S_{12}$ [17] ; hybrid electrolyte (HE) : composite of $Li_{1.3}Al_{0.3}Ti_{1.7}(PO_4)_3$ fibers, poly[bis(2-(2-methoxyethoxy)ethoxy)phosphazene], and lithium(4-styrenesulfonyl) [18].

Note : these examples demonstrate high conductivities achieved within each electrolyte type ; conductivity of other examples may deviate significantly from the values shown here.

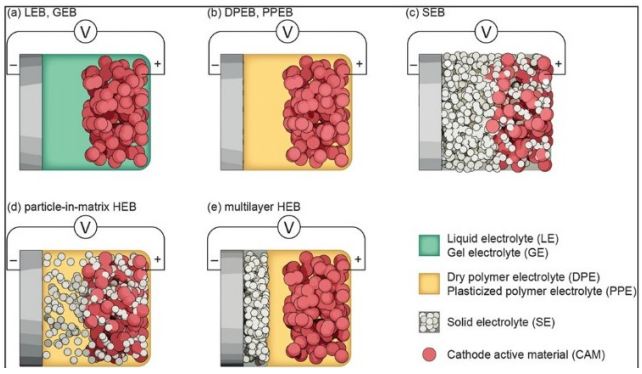

Figure 1.9 – Schematics of batteries made of a metal negative electrode (for example lithium), a positive electrode containing cathode active material (CAM) particles, and an electrolyte, forming either a a) liquid electrolyte battery (LEB) or gel electrolyte battery (GEB), b) dry polymer electrolyte battery (DPEB) or plasticized polymer electrolyte battery (PPEB), c) solid electrolyte battery (SEB), d) particle-in-matrix hybrid electrolyte battery (HEB), or e) multilayer HEB.

Note : Even though the solid electrolyte–polymer electrolyte (SE–PE) combination depicted in the HEB schematics is a commonly investigated configuration, it is used here as an illustrative example. In principle, any combination of electrolytes may be prepared in the form of a particle-in-matrix or multilayer HEB.

1.2.5.4.2 Liquid Electrolyte Battery and Gel Electrolyte Battery

1.2.5.4.2.1 Gel Electrolyte Batteries (GEB)

The combination of liquid and polymer provides several intermediate cases dependent on composition and miscibility. With increasing polymer content, the properties of the mixture change continuously from liquid polymer solution, via gel polymer (polymer in solvent), and plasticized polymer (solvent in polymer), to dry polymer [59].

As the transition between all of these cases is continuous, careful classification must be made on a case-by-case basis for polymer-containing electrolytes.

In general, gels are formed by entrapping liquid in a miscible polymer matrix, often a cross-linked polymer network [60]. Thus, a gel electrolyte (GE) combines the cohesive structure of polymers and the conduction properties of liquids [61, 62].

The ion transport occurs predominantly through the entrapped liquid electrolyte (LE), provided that the gel contains a high content of liquid solvent [63].

In general, gel electrolytes have comparable ionic conductivity and conduction properties to those of the corresponding liquid electrolytes. However, due to their distinctive mechanical properties, they are clearly distinguishable from LEs. This distinction justifies identifying gel electrolyte batteries (GEBs) as a separate class.

Common polymers used to form gels include polyacrylonitrile (PAN), polyvinylidene fluoride (PVDF), and poly(methyl methacrylate) (PMMA). These are typically swollen with molecular solvents or plasticizers such as propylene carbonate, ethylene carbonate, dimethyl formamide, or tetraglyme [62].

1.2.5.4.2.2 Liquid Electrolyte Battery (LEB)

LEs are made by dissolving salt in liquid solvents with low molecular weight and viscosity. For example, lithium-ion batteries typically use 1 m solutions of lithium salts ($LiPF_6$, LiTFSI, etc.) dissolved in non-aqueous organic solvents, such as ethylene carbonate, dimethyl carbonate. In exceptional cases, aqueous electrolytes are also used [64].

In LEs, both solvated cations and solvated anions are mobile species. Typically, the ionic conductivity of LEs reaches 10^{-2} S cm^{-1} [65].

Ion transport requires the migration of solvated ions, created by the dissociation and solvation of a conducting salt in a solvent [66]. During solvation, solvent molecules coordinate to the ions and the ion migrates along with a solvation sheath [67]. The fast exchange of solvated ions and solvating compounds creates a uniform ionic environment [67].

Therefore, ion transport is diffusion-limited and coupled with the viscosity of the liquids [68, 69]. Ion conduction is facilitated by :

- Reduced viscosity of the solvent (increased ion mobility)
- Dissociation of ion pairs (increased concentration of mobile ions)

Even though LEBs present the most advanced technology to date, lithium LEBs with organic electrolytes may suffer from several issues :

- Thermal runaway
- Leakage or drying up of the electrolyte
- Side reactions between lithium metal and electrolyte
- Unstable interface and dead lithium formation → irreversible capacity loss [70]

Cell aging tests (e.g., Tesla 18650 lithium-ion cells) show that capacity fade and impedance rise are strongly linked to the composition of the solid electrolyte interface (SEI) formed with a graphite anode [19].

Current LEB research focuses on optimizing electrolytes to :

- Produce a uniform SEI
- Ensure uniform ion flux
- Achieve favorable SEI composition

Advanced electrolyte engineering includes :

- Additive optimization
- Solvent ratio modification
- Use of fluorinated solvents and salts
- High salt concentration electrolytes [71]

The oxidation of electrolyte with high-voltage cathodes is another crucial factor contributing to capacity fading [72].

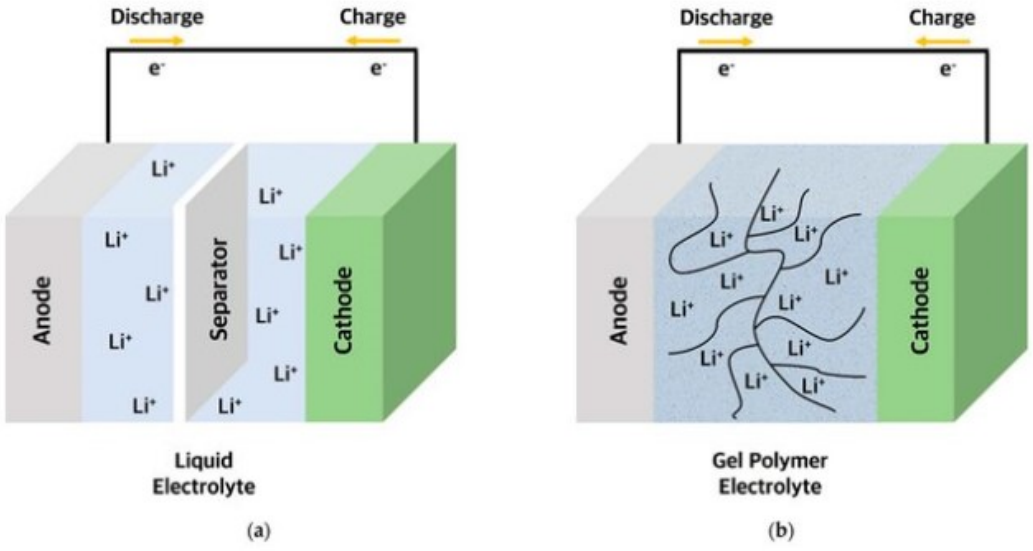

Figure 1.10 – Comparison between liquid and gel electrolytes [19]

1.2.5.4.3 Hybrid Electrolyte Batteries (HEB)

Hybridization of electrolytes opens the pathway to a manifold of subtypes of cells [**?**]. In order to avoid complications from a plethora of combinations with individual names, we propose to simply classify all cells as HEBs that contain at least two electrolytes with different ion conduction mechanisms.

Therefore, there are four possible combinations :

- LE–PE
- LE–SE
- PE–SE
- LE–PE–SE

Among these, the PE–SE combination is the most prominent case. These combinations are usually present in HEBs either in the form of :

- A particle-in-matrix assembly, or
- Separate electrolyte layers in a multilayer assembly

Effective ion conduction through an HEB requires efficient transfer of lithium ions from one electrolyte type to another, implying a transition from one ion conduction mechanism to another [**?**]. However, across the interface, ion transport depends on the interface structure and composition.

Neither the SE–LE nor the SE–PE interfaces are without challenges : both have been found to produce degradation products that hinder ion transfer [**? ?**].

Figure 1.11 – Schematic illustration of single vs. hybrid electrolytes [20]

1.2.5.4.4 Dry Polymer Electrolyte Battery and Plasticized Polymer Electrolyte Battery

1.2.5.4.4.1 Dry Polymer Electrolyte Battery (DPEB)

In contrast to LEs and GEs, PEs use complexes of polymers and conducting salt for ion conduction.

Although they are sometimes called "solid polymer electrolyte", here, we denote this class simply as PE, as the physical state depends on the temperature and may be very soft or even liquid during cell operation.

The concept of PEs was first proposed in 1973 by Fenton et al., who observed ionic conductivity improvement in polyethylene oxide (PEO) when dissolving metal salt complexes.

A common example of dry polymer electrolytes (DPEs) is
polyethylene oxide lithium bis(trifluoromethanesulfonyl)imide (PEO-LiTFSI).

Alternatively, other polymers with polar functional groups, polymer blends [73], copolymers, block copolymers, or polyelectrolytes [74] are used as polymer host for lithium salts.

The achievable ionic conductivity in polymer salt complexes is typically in the range of $\sim 10^{-6}$ to 10^{-4} S cm^{-1} at room temperature.

1.2.5.4.4.2 Plasticized Polymer Electrolyte Battery (PPEB)

Plasticizers are additives that increase polymer mobility, leading to decreased glass transition temperature and increased polymer chain dynamics [75, 76].

Such plasticized polymers are similar to gels, but the plasticizer content is typically lower.

Recently, Bai et al. [77] reported a high salt content plasticizer composed of *acetonitrile* and *LiTFSI* for poly(dimethyl(methacryloyloxy)methyl phosphonate) (PMAPC1) polymers, achieving an ionic conductivity of 1.6 mS cm^{-1} at 100 °C.

The plasticizer enhances segmental motion of polymer chains ; for example, acetonitrile doping decreases the glass transition temperature of PMAPC1 and enhances salt dissociation and ion mobility, thereby accelerating ion transport through the polymer matrix.

As long as the polymer matrix is the predominant mode of conduction and the added plasticizer merely acts to mobilize polymer chains, this type of cell is classified as a plasticized polymer electrolyte battery (PPEB).

For instance, Bai et al. assembled a PPEB with configuration :
Li | 1 PMAPC1 + 2 LiTFSI + 1 AN | $LiFePO_4$, which delivered a specific capacity of approximately 147 mAh g^{-1} in the first discharge cycle and showed a capacity retention of 91.4% after 500 cycles, along with stable SEI characteristics [77].

1.2.5.4.5 Solid Electrolyte Battery (SEB)

Solid electrolytes (SEs) conduct ions through an ordered anion structure without requiring salt additives. Several inorganic SEs are reported for oxides, thiophosphates, and other ionic compounds, some reaching conductivities beyond 10^{-2} S cm^{-1} at room temperature with near-unity transference number.

Common examples include LISICON [78], garnet-type [79], NASICON [80], lithium nitride [81], lithium borohydrides [82], perovskites [83], mixed halides [84], argyrodite-type electrolytes [85, 86, 87], and sulfide-based solid solutions [88].

Increasing ionic conductivity (up to 24 mS cm^{-1}) can be achieved through structural and compositional tuning within a given family of structures [85].

Ion transport in SEs is generally governed by the sequential and discrete movement of ions through crystallographic vacancies and interstitial sites [89]. For instance, argyrodite-type Li_6PS_5X (X = Cl, Br, I) exhibits anion site disorder, which promotes conductivity. In the cubic polymorph, the anions form an fcc framework, with S^{2-} and PS_4^{3-} units occupying voids.

Enhanced site disorder—as seen in Li_6PS_5Cl—leads to increased conductivity. Correlated ion transport with halogen disorder was confirmed via solid-state NMR and impedance [90]. Additionally, PS_4^{3-} rotation facilitates ion diffusion.

Advantages of SEBs include :

- Unity transference number (no concentration polarization),
- Absence of solvated species,
- Enhanced safety and higher energy density vs LEBs.

Challenges include :

- Crack formation and contact loss at interfaces,
- Dendritic growth causing short-circuits.

Tan et al. employed a μSi anode in a μSi | Li_6PS_5Cl | NCM811 cell to address interfacial instability [91]. Other strategies include :

- Thicker cathode composites [92],
- High areal cathode loading (25.2 mg cm^{-2}) [93],
- Thinner electrolytes and higher densities for energy density gain.

Lee et al. demonstrated pressure-free sheet-type multi-stacked cells with Ag/C composite, achieving 942 Wh L^{-1} with 10 parallel bi-cells [94].

Future directions :

- **Nanostructured Si anodes** (e.g., 3D columnar) [95],
- Silver-carbon anodes,
- Conversion-type and high-voltage cathodes,
- Low-binder content fabrication [96],
- New binder chemistries and catholyte microstructures [97],
- Dry processing and cycling pressure maintenance.

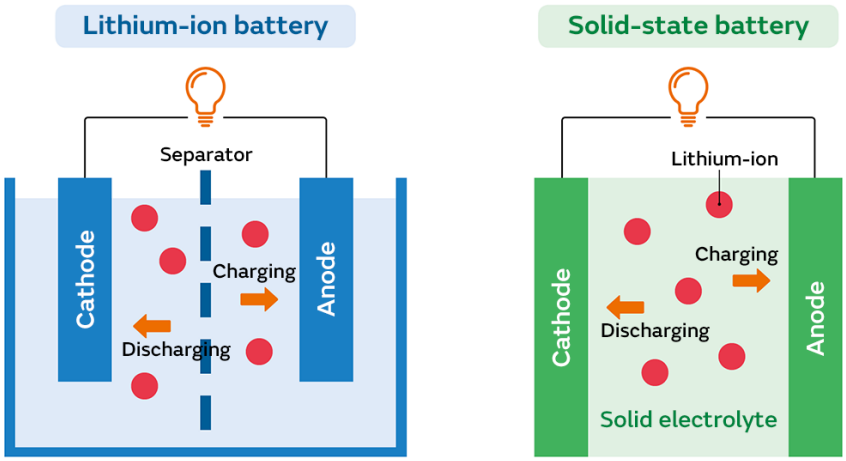

Figure 1.12 – Comparaison entre une batterie lithium-ion conventionnelle et une batterie tout solide [21]

Chapter 2

Lithium Batteries

> ""I think lithium-ion batteries will continue to evolve and contribute to the realization of a sustainable society" "
> — *Akira Yoshino*

2.1 Historical Overview

Research in lithium batteries began in 1912, when Gilbert N. Lewis took his position as professor of physical chemistry and dean of the College of Chemistry at the University of California, Berkeley. The first primary lithium batteries entered the market in the 1970s. Two more decades passed before Sony Energytec commercialized the first rechargeable Li-ion battery in 1990 [98]. This battery used a $LiCoO_2$ cathode and a graphitic carbon anode. Soon after, one of these lithium-ion batteries (LIBs) exploded in a handheld video camera. Since then, the issue of thermal runaway and battery fires has been recognized as a major concern.

These safety problems are also costly : for example, in 2006, Dell had to recall 4.1 million notebook computers due to Sony-manufactured batteries catching fire, leading to an estimated loss of $300 million. Another key challenge has been the need to increase both energy and power densities—first for portable electronics, then for hybrid electric vehicles (HEVs) and electric vehicles (EVs). The importance of developing green energy has long been understood by scientists. What is more recent is the awareness by governments worldwide that the transition to green energy and the reduction of greenhouse gas emissions is not only essential, but also urgent.

The increase in population combined with higher energy consumption per person (due to rising GDP per capita globally) leads to a dramatic increase in energy demand. In this context, electrochemical energy storage has become a major issue. LIBs, in particular, can help solve the intermittency problems of renewable sources like wind and solar by stabilizing electricity production. Moreover, electric vehicles emit no gas and are therefore considered "clean".

These factors—combined with the explosive growth of smartphones and personal computing—explain why the lithium-ion battery market, valued at $11.7 billion in 2012, was projected to grow to $33.1 billion in 2019. This rapid market growth and profitability have driven intense industrial competition to produce batteries with the highest energy density and/or power density. Scientists too feel this pressure. Sometimes, in pursuit of recognition or funding, some publish papers—especially in high-impact journals—that are more akin to media hype than rigorous science. Unfortunately, this can mislead decision-makers who may interpret marketing claims as scientific facts. That is why it is crucial to periodically write critical reviews on the current state of lithium battery research and discuss realistic prospects for the near future [99].

2.2 Why Lithium ?

Lithium is a highly versatile element, but one of its most valuable applications is as a key component in high energy-density rechargeable lithium-ion batteries. Its exceptional electrochemical properties—particularly its **high charge-to-weight ratio**—make it ideal for use in energy storage systems, especially in the context of **portable electronics** and **electric mobility**. With growing concerns over carbon dioxide emissions and the rising cost of hydrocarbon fuels due to limited supply, lithium is expected to play an even more critical role in large-scale batteries used to power all-electric and hybrid vehicles. For instance, it is estimated that a single 40-mile trip in an electric vehicle could require 1.4 to 3.0 kilograms of lithium equivalent (7.5 to 16.0 kilograms of lithium carbonate), which could significantly increase global lithium demand.

Projections of future lithium demand vary widely depending on several factors, including advancements in battery recycling, the public's acceptance of electric vehicles, and government incentives promoting the transition to lithium-powered transportation. Greater reliance on electricity could lead to rising energy prices, while reduced demand for hydrocarbon fuels might lower their cost, potentially shifting market dynamics.

As of 2009, approximately 13 percent of the world's lithium reserves—expressed in terms of contained lithium—were found in hard rock mineral deposits, while 87 percent were located in brine sources. The majority of lithium recovered from brine originated in Chile, followed by smaller contributions from China, Argentina, and the United States. In addition, both Chile and Australia possess significant lithium mineral reserves. Recycled batteries are also an increasingly important source of lithium. As lithium-ion batteries become more common in electric vehicles, recycling systems are expected to scale up, allowing the reuse of lithium to manufacture new battery cells [100].

2.3 Lithium Battery Types

Lithium batteries contain metallic lithium and are not rechargeable. The button-sized cells that power watches, hand-held calculators, and small medical devices are usually lithium batteries. These are also called primary lithium batteries, and they provide more usable power per unit weight than lithium-ion batteries (called secondary batteries). Lithium-ion batteries use lithium compounds, which are much more chemically stable (less likely to oxidize spontaneously) than the elemental lithium used in lithium batteries [101].

There are many lithium-ion battery types and configurations. These batteries are not generally available in standard household sizes but are specifically manufactured for a particular electronic device. It is possible to classify lithium-ion battery types according to their battery chemistry and packaging. The major difference between batteries for electronics and batteries for electric vehicles is the size. Increased size can be achieved either by assembling many small cells or by developing single large cells. A detailed cost and technical analysis of lithium-ion battery development for automobiles is beyond the scope of this summary, but can be found in several detailed studies [102, 103, 104, 105, 106].

Rechargeable lithium-ion batteries can be categorized by packaging into the following types :

- **Cylindrical cells** – the most widely used packaging for wireless communication, mobile computing, biomedical instruments, and power tools [22]
- **Prismatic cells** – developed in the early 1990s, made in various sizes and capacities, custom-made for electronic devices such as cell phones [22]
- **Pouch cells** – introduced in 1995, allow tailoring to the exact dimensions of the electronic device, and are easily assembled into battery packs [22]

- **button cells**- Also known as coin cells, these are small, non-rechargeable batteries commonly used in compact, low-power devices such as watches, calculators, hearing aids, and small medical instruments. They provide high energy density for their size and are designed for long shelf life and steady, low-current discharge. [22]

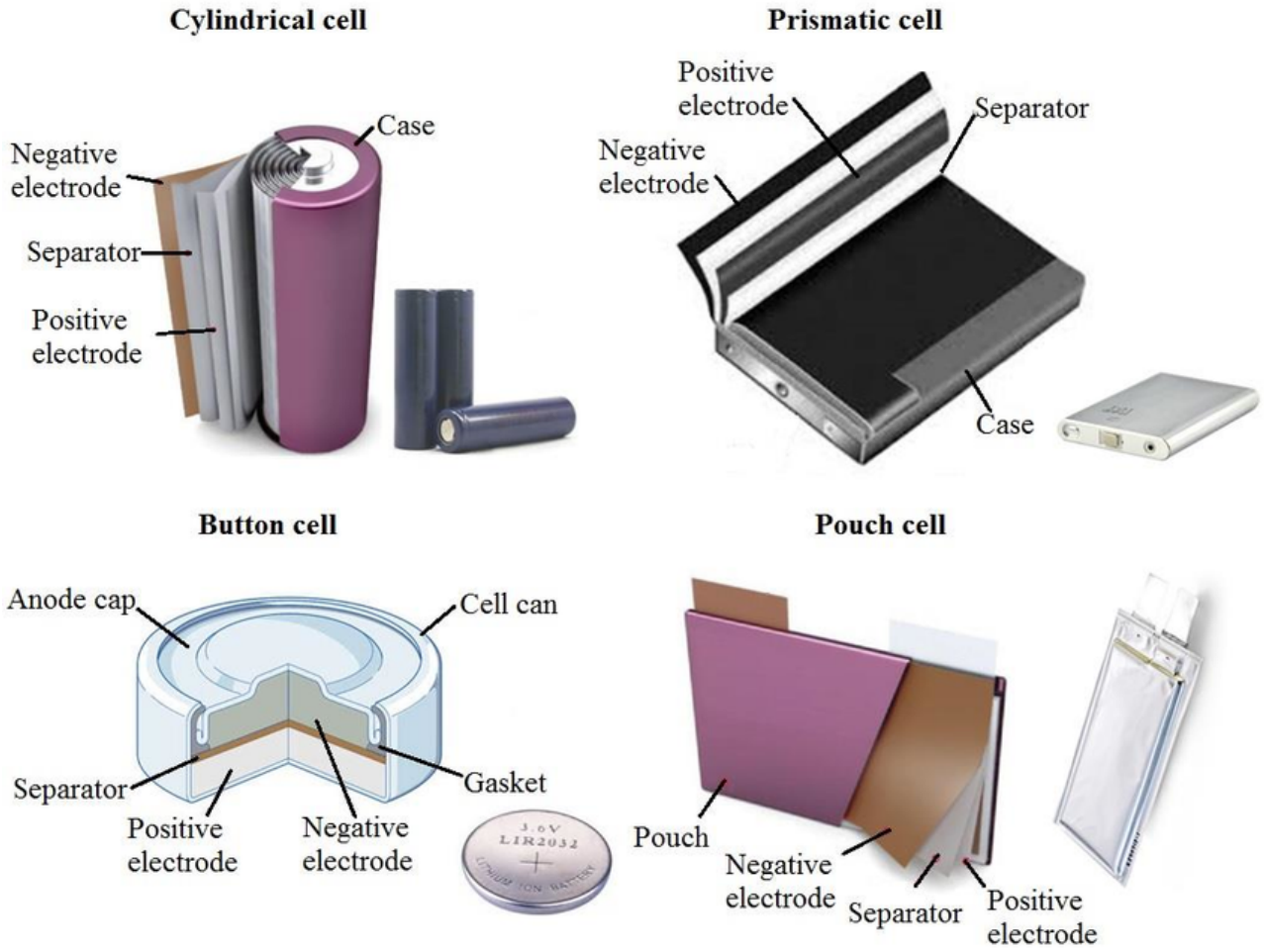

Figure 2.1 – The most common lithium-ion cell types. . [22]

2.4 Classification of Lithium Batteries Based on Electrode/Electrolyte Material

Table 2.1 – Electrode and electrolyte materials [1]

Cathode Materials	**Anode Materials**	**Electrolyte Materials**
Lithium iron (II) phosphate, LFP ($LiFePO_4$)	Lithium titanate, spinel, LTO nano-powder ($Li_4Ti_5O_{12}$)	Lithium aluminum titanium phosphate, LATP ($Li_{1.3}Al_{0.3}Ti_{1.7}(PO_4)_3$)
Lithium cobalt phosphate, LCP ($LiCoPO_4$)	Lithium titanate, LTO (Li_2TiO_3)	Lithium difluoro (oxalato) borate, LiFOB; LiODFB; LiBOB ($LiB(C_2O_4)_2F_2$)
Lithium nickel manganese cobalt oxide, NMC ($LiNi_{0.33}Mn_{0.33}Co_{0.33}O_2$)	Lithium-aluminum alloy (AlLi)	Lithium bis (oxalato) borate, LiBOB ($LiB(C_2O_4)_2$)
Lithium nickel cobalt aluminum oxide, NCA	Tin (IV) oxide (SnO_2)	Lithium hexafluorophosphate ($LiPF_6$)
Lithium manganese nickel oxide, (LMNO $Li_2Mn_2NiO_8$)	Lithium (Li)	Lithium trifluoromethanesulfonate, (LiTF CF_3SO_3Li)
Lithium nickel cobalt oxide, LNCO ($LiNi_{0.8}Co_{0.2}O_2$)	Graphite (C)	Lithium tetrachlorogallate ($LiGaCl_4$)
Lithium manganese oxide, LMO ($LiMn_2O_4$)	Carbon, mesoporous (C)	Lithium tetrachloroaluminate ($LiAlCl_4$)
Lithium manganese (III, IV) oxide, LMO $LiMn_2O_4$ Lithium manganese dioxide ($LiMnO_2$) Lithium nickel dioxide, LNO ($LiNiO_2$) Lithium trivanadate, LTV (LiV_3O_8) Lithium iron (III) oxide ($LiFeO_2$) Lithium cobalt (III) oxide ($LiCoO_2$) Lithium molybdate (Li_2MoO_4) Germanium (IV) sulfide (GeS_2) Manganese nickel Carbonate ($Mn_{0.75}Ni_{0.25}CO_3$)	Carbon (C)	Lithium tetrafluoroborate ($LiBF_4$) Lithium perchlorate ($LiClO_4$) Lithium hexafluoroarsenate (V) ($LiAsF_6$) Lithium phosphate Monobasic (LiH_2PO_4)

2.5 Lithium Metal Anodes

Li metal has been considered as the ultimate anode material due to its high theoretical capacity (3860 mA h g^{-1}) and low redox potential (3.04 V vs SHE) [107, 108]. The energy densities of batteries using Li metal anodes surpass those with graphite or silicon anodes. However, two critical challenges—dendritic Li growth and an unstable electrode–electrolyte interface—hinder practical applications [109]. Due to high diffusion barriers and weak interaction energy, Li tends to grow into 1D filament-like dendrites [110], which possess high surface area, inducing parasitic reactions with the electrolyte. This leads to low Coulombic efficiency, short circuits, and thermal runaway risks. Detached Li also becomes "dead Li," further reducing efficiency and increasing porosity [111, 112].

Another issue is the unstable solid electrolyte interphase (SEI). Li metal reacts with the electrolyte to form a fragile SEI that continuously consumes both Li and electrolyte during cycling. Cracking of the SEI promotes dendrite growth, dead Li formation, capacity fading, and volume expansion [113]. An ideal Li anode should thus be dendrite-free, highly efficient, and stable over long cycles. Rational electrolyte design has shown promise : for example, Cui's group added $LiNO_3$ and lithium polysulfides, forming a uniform SEI that boosted Coulombic efficiency to 99% over 300 cycles [114]. Other additives such as FEC, $CsPF_6$, $LiPF_6$, $AlCl_3$, LiTFSI, and LiFSI have also been investigated [115].

However, under high current density, even optimized electrolytes may fail. Recent work shows that 3D current collectors with high nucleation site density can promote uniform Li deposition. Structures such as porous Cu, graphene frameworks, and carbon nanofibers reduce local current density, limit dendrite growth, and accommodate Li volume change [116, 117, 118, 119]. Guo's group reported that Li deposited on a submicron-fiber 3D Cu host achieved higher efficiency and longer lifespan compared to traditional 2D Cu foil [120]. Nonetheless, poor wettability and high nucleation overpotentials remain challenges. Solutions include surface treatments, noble metal coatings, composite alloys, and lithiophilic functionalization [121, 122]. To simplify manufacturing, Ye et al. developed a surface nanocrystallization method to improve molten Li wettability [123].

However, 3D current collectors usually show an undesirable affinity with lithium metal, which may lead to large nucleation overpotential and poor electrode contact. To overcome this limitation, various strategies have been developed to improve the lithiophilicity, such as the incorporation of noble metals, Li-rich composite alloys, functional organic coatings, elemental additives, and functional group modifications [124].

In a notable study, Ye et al. proposed a facile surface nanocrystallization strategy to enhance the rapid wettability of molten lithium. This was achieved by dispersing metal nanoparticles on a 3D current collector, which reduced the surface energy and induced a Laplace pressure, enabling uniform Li deposition and low nucleation overpotential [125].

More recently, composite anodes integrating the benefits of SEI protective layers and 3D conductive frameworks have become a research hotspot. Zheng and co-workers developed a hybrid host structure in which lithium is encapsulated inside a 3D scaffold coated with metal-organic frameworks (MOFs). This structure not only minimized volume changes during cycling but also promoted uniform distribution of Li ions, achieving even Li deposition with a dimensional variation of less than 5% [126].

Various 3D collectors have been proposed, including both metal-based and carbon-based hosts [125, 124]. However, due to the internal and external consistency of the 3D structure, lithium may still deposit on the surface, forming dendrites and potentially causing local short circuits. Future strategies aim to induce lithium nucleation deep within the 3D host or apply lithiophilicity gradients to redirect lithium growth away from unsafe zones near the separator.

Finally, the large effective surface area of 3D current collectors inevitably promotes excessive SEI formation, leading to severe consumption of both lithium and electrolyte during repeated cycling.

Thus, one of the pressing challenges is to develop advanced architectures that can limit SEI growth while maintaining high electrochemical performance.

2.5.1 Rise of the Lithium Metal Anode

Rechargeable batteries have markedly reshaped our lives – from electric vehicles to portable electronic and optoelectronic devices. For a battery anode, lithium (Li) metal is considered the "Holy Grail" because of its extremely low density (0.534 g cm^{-3}), ultra-high theoretical capacity (3860 mAh g^{-1}), and exceptionally negative electrochemical potential (-3.04 V vs. standard hydrogen electrode) [127].

The Li metal anode was first adopted in the TiS_2–Li prototype in 1976 [128, 129], but was soon replaced by intercalation compounds like graphite due to severe capacity fading and potential explosion hazards resulting from dendritic Li growth [130].

Since C/$LiCoO_2$-based Li-ion batteries delivered an energy density of 120–150 Wh/kg—twice that of Ni-Cd batteries at the time [128]—they rapidly supplanted Ni-Cd, becoming the dominant technology. Since then, Li-ion chemistry research has intensified to increase energy and power density. Meanwhile, the use of lithium metal anodes has resurged after 20 years of dormancy. Around 2010, with the booming electric-vehicle and electronics markets, a strong demand emerged for high-energy-density storage (targeting 500 Wh/kg or more), fueling renewed interest in high-Ni NMC–Li or S–Li batteries [131].

Current research is primarily focused on strategies to suppress Li dendrite formation, improve Coulombic efficiency (CE), and gain deeper insights into Li plating/stripping via advanced characterization and modeling. These aspects have been thoroughly reviewed recently [132, 133]. Dense Li deposition with CE ∼99% is now achievable using high salt concentration or localized high concentration electrolytes [134, 135, 136, 137].

A major milestone is the application of cryo-electron microscopy (Cryo-EM) to observe the nanostructure of electrochemically deposited lithium (EDLi) and the complex solid electrolyte interphase (SEI) [138, 139], enabling the correlation of structure with performance. Based on these findings, it is a timely opportunity to revisit the challenges and prospects of Li metal anodes. In this Opinion, we explore key controversies, assess proposed strategies, and propose future directions for realizing a practical lithium metal anode.

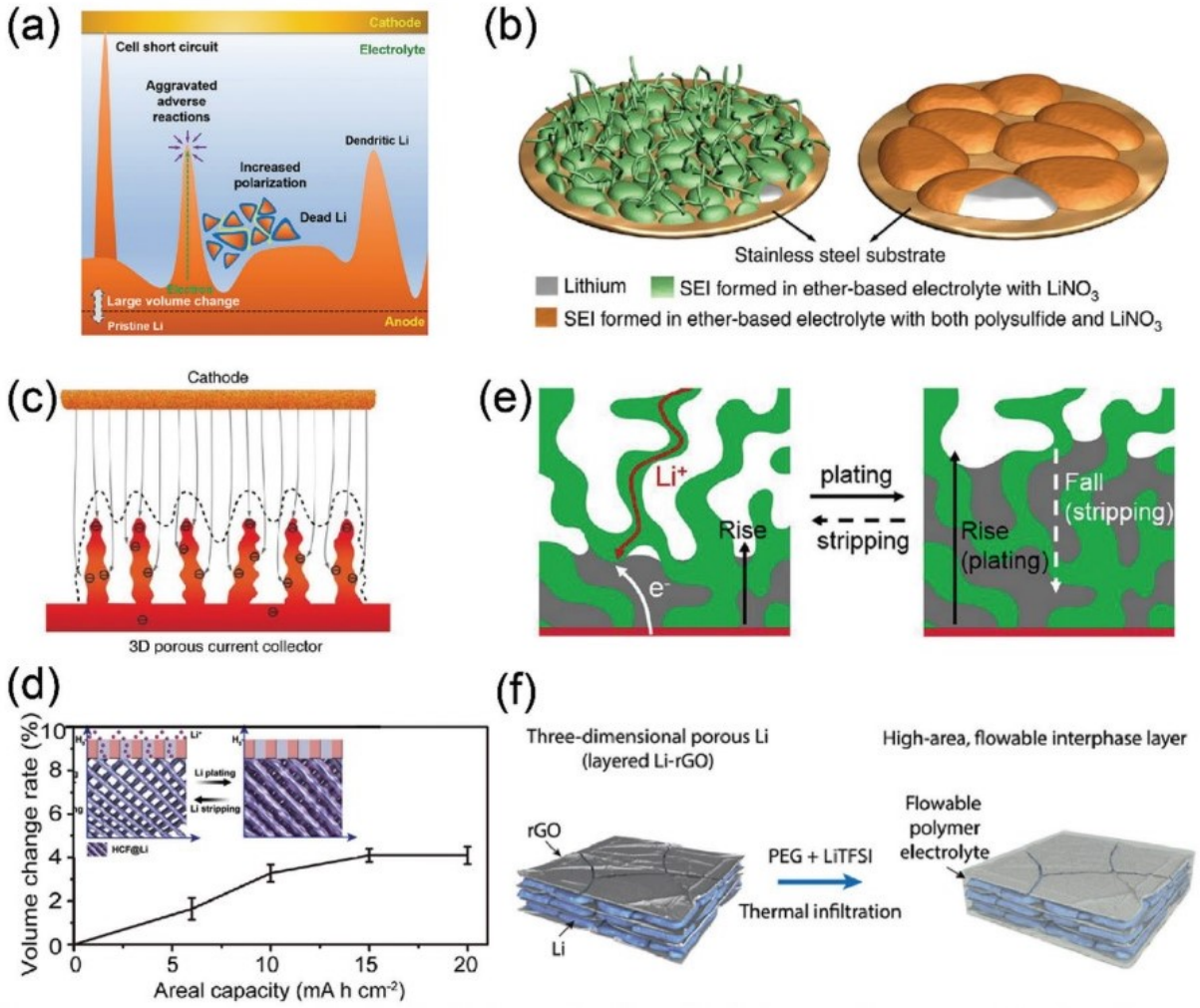

Figure 2.2 – a) Dilemmas of Li-metal Anodes. Reproduced with permission [23]. Copyright 2017, American Chemical Society. b) Schematic illustration showing the morphology difference of lithium deposited on stainless steel, with or without the polysulfide and $LiNO_3$. Reproduced with permission [24]. Copyright 2015, Nature Publishing Group. c) Illustration of the proposed electrochemical deposition processes of Li metal on a 3D current collector. Reproduced with permission [25]. Copyright 2015, Nature Publishing Group. d) Electrode volume change rate of MOF-HCF@Li anode after plating ; inset shows a schematic illustration of the Li plating/stripping process. Reproduced with permission [26]. Copyright 2019, Elsevier. e) Schematic for the process of Li deposited in the 3D ion-conductive host from the bottom current collector. Reproduced with permission [27]. Copyright 2018, National Academy of Sciences. f) Schematics illustrating the fabrication process of the 3D Li anode with flowable interphase for solid-state Li battery. Reproduced with permission [28]. Copyright 2017, American Association for the Advancement of Science.

2.5.2 Main Challenges with Li Metal : Dendrite Formation or Low Coulombic Efficiency ?

It is widely accepted that Li dendrite formation and low Coulombic efficiency (CE) are two primary obstacles hindering the performance of lithium metal batteries [140]. In addition to these issues, other significant challenges include volume expansion, poor cycle life, capacity fading, increased overpotential, and potential safety hazards.

One of the most widely discussed safety concerns is the idea that Li dendrites can mechanically pierce the separator, resulting in an internal short circuit that may cause thermal runaway or explosion [140]. This concept is often illustrated using a Li dendrite growth model figure, originally observed in a beaker cell via optical microscopy [141]. However, such dendritic morphology is rarely seen in real coin cells or pouch cells.

Instead, in commercial carbonate-based electrolytes and even in solid-state systems, whisker-like Li deposits are typically observed. These whiskers tend to grow *parallel* to the separator, rather than perpendicularly. Only when a whisker grows perpendicularly can it penetrate the separator and cause a short circuit [142]. Moreover, in several recently developed advanced electrolytes, researchers have observed chunky Li deposits with large granular dimensions, as shown in Figure. These findings indicate that the focus on dendrite-induced internal shorts may be somewhat exaggerated.

In fact, Lu et al. [143] refuted the dendrite penetration mechanism as the main failure mode by conducting SEM analysis on a cycled Li anode. They concluded that active Li consumption and electrolyte depletion are more likely to be responsible for cell failure than direct short circuits.

Even when advanced electrolytes allow highly efficient Li plating/stripping with a CE of around 99%, the remaining 1% inefficiency presents a critical limitation. To achieve long cycle life, large excesses of fresh Li and electrolyte are often required. This requirement complicates the design of practical batteries and limits energy density at the cell level [29].

Therefore, improving the Coulombic efficiency of Li metal is an inescapable requirement for extending the cycle life and safety of Li metal batteries.

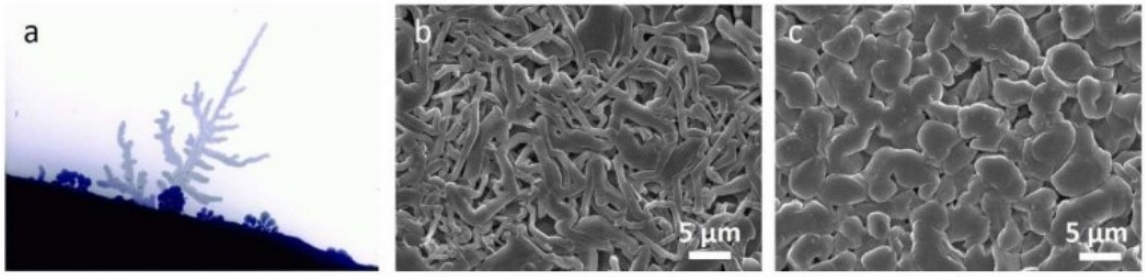

Figure 2.3 – The morphologies of electrochemically deposited Li under different conditions. (a) the famous optical microscope image representing Li dendrites ; (b) whisker-like Li deposited in commercial carbonate electrolyte (1M LiPF6 in EC/EMC, 3 :7 with 2 [29]).

2.5.2.1 The Failure of the Lithium Anode

Before the lithium metal battery can evolve into a viable technology, major challenges related to **stability** and **safety** must be addressed [30]. These issues are intrinsically tied to the behavior of the lithium metal anode, which faces several key limitations that hinder its practical application.

2.5.2.2 Dendrite Formation

Lithium tends to deposit in the form of dendrites on the anode current collector. Once these dendrites become large enough to pierce the separator, they can cause short circuits. The resulting high current through dendritic bridges rapidly generates heat, posing serious safety risks such as fire or explosion. This significantly restricts the commercialization of lithium metal batteries since user-side safety must be ensured.

Lithium deposition is often uneven, and this inhomogeneity becomes more severe with cycling. Mechanical stress accumulates under the solid electrolyte interphase (SEI), leading to cracks. Lithium then grows from these cracks and forms initial dendrites, which progressively extend until internal short circuits occur. Both thermodynamic and kinetic factors contribute to this behavior.

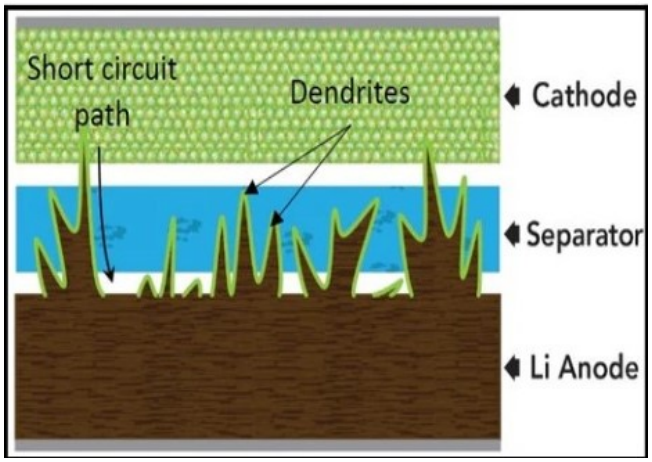

Figure 2.4 – Schematic illustration of lithium dendrite growth through the separator [30]

2.5.2.3 Dead Lithium

Dead lithium refers to lithium that has lost electrical contact with the anode and can no longer participate in electrochemical reactions, resulting in irreversible capacity loss. Even in optimal conditions, the Coulombic efficiency (CE) of lithium plating/stripping in non-aqueous electrolytes rarely exceeds 99.2%, primarily due to dendrite formation and dead lithium [30].

Dead lithium typically originates from fractured dendrites. The breaking points usually occur at thin necks, where curvature-induced electron density is high, leading to faster electro-dissolution. Once broken, the exposed fresh lithium reacts with the electrolyte, forming a poorly conductive SEI, isolating it from the circuit.

Dead lithium formation is more pronounced in systems with abundant slim dendrites. Additional factors such as cycling protocol and mechanical stress also influence its formation. In porous current collectors with large pores, uneven current distribution causes lithium in the center to lose contact with

the host, leading to isolated, inactive lithium. Therefore, controlling pore size is critical to minimizing dead lithium.

2.5.2.4 Corrosion and Volume Expansion

Lithium metal, due to its highly negative redox potential, spontaneously reacts with electrolytes to form a solid electrolyte interphase (SEI). However, this layer is often unstable and breaks during repeated cycling, exposing fresh lithium to further reactions. This results in continuous electrolyte consumption, lithium corrosion, and a drop in Coulombic efficiency [144].

Three main factors affect this corrosion process :

- **Electronic structure of the electrolyte** : Electrolytes with a higher LUMO (Lowest Unoccupied Molecular Orbital) energy are less likely to be reduced by lithium. For example, ethers exhibit better stability than esters.
- **Viscosity of the electrolyte** : Low-viscosity solvents like DME and THF are generally less stable against lithium compared to more viscous ones like EC or PC.
- **Stability of the SEI** : A robust SEI layer prevents the exposure of fresh lithium. Its stability depends on the electrolyte composition. For instance, EC-based electrolytes form unstable SEI, whereas fluorinated carbonates promote LiF-rich, stable SEI layers that improve lithium protection.

By optimizing electrolyte formulations and enhancing SEI robustness, lithium corrosion and its negative impacts on battery performance can be significantly reduced.

2.6 Inactive Li Formation Causes Low CE : SEI Li+ or Unreacted metallic Li ?

Low Li-metal CE stems from the loss of active Li as it forms the SEI and unreacted metallic Li, which together comprise inactive Li (also known as “dead” Li). SEI formation is a result of the (electro)chemical reaction between highly reactive Li metal and the electrolyte, whereas unreacted metallic Li is isolated from the electronically conductive network during stripping by the insulating SEI, thus becoming inactive [145, 146].

The importance of the SEI has been reviewed exhaustively [147, 148] ; however, quantitative characterization of SEI properties remains elusive, including : chemical composition, nanostructure, and mechanical properties. This is partly due to the brittle and heterogeneous nature of the SEI. It is generally believed that dramatic volume changes yield fractures in the SEI during Li stripping/plating. This fracturing results in continuous SEI formation that consumes both the active Li and electrolyte. This process is further accelerated by growth of porous Li whiskers. With this in mind, many researchers attribute the continuous formation of SEI as the primary reason for capacity loss and low CE, without further quantitative verification.

However, it was recently reported that this picture is not correct following quantification of both the SEI Li^+ and unreacted metallic Li after stripping via the recently developed titration gas chromatography (TGC). Importantly, TGC results reveal that the capacity loss of Li metal anodes is primarily dominated by unreacted metallic Li that is trapped by the insulating SEI. The overall SEI Li^+ amount in the inactive Li remains almost identical and at a relatively low amount under different testing conditions. This suggests that the main loss of CE in Li metal batteries does not come from SEI formation but rather from the unreacted metallic Li. The capacity loss from forming SEI has been over-blamed for decades.[149]

Although the amount is low, we still want to emphasize that the SEI cannot be overlooked since its chemical and mechanical properties directly dictate the surface properties of the EDLi, directly affecting the dynamic Li plating and stripping process. Much work is still needed to correlate the SEI properties to the electrochemical behavior and performance of Li metal anodes.

2.7 Silicon as a Future Material for Batteries

Silicon has attracted tremendous research interest in recent years due to its potential to revolutionize the performance of lithium-based batteries. While it is commonly explored as an anode material in lithium-ion batteries, its intrinsic properties and electrochemical behavior make it an important candidate in the broader context of electrode materials. In conventional LIBs, graphite has served as the dominant anode material due to its acceptable specific capacity (372mAhg^{-1}), low cost, and cycling stability. However, the need for higher energy density, longer cycle life, and faster charge/discharge rates has driven the exploration of materials with much higher lithium storage capacities [150, 151, 152].

Silicon stands out in this regard. Its theoretical capacity can reach 3590mAhg^{-1} at room temperature (corresponding to the formation of $Li_{15}Si_4$), nearly 10 times that of graphite, and even 4200mAhg^{-1} at elevated temperatures through the formation of $Li_{22}Si_5$ [153]. Furthermore, it is the second most abundant element in the Earth's crust, allowing for cost-effective and scalable manufacturing. These properties place silicon at the forefront of next-generation electrode materials [154].

Nevertheless, silicon's application faces significant practical barriers. The most critical among them are drastic volume expansion, structural instability, and poor electrical conductivity. In light of these challenges, a substantial body of work has been dedicated to modifying silicon's structure, composition, and morphology to enhance its electrochemical performance and durability.

In our study, although silicon was not used as an anode, its properties and associated research are of critical bibliographic relevance. The information compiled here from the literature serves to contextualize the broader role of silicon as an electrode material, including the rational design principles that underlie its successful integration into lithium battery systems.

2.7.1 Advantages of Silicon

Silicon's foremost advantage lies in its extraordinarily high lithium storage capacity. As previously mentioned, it can theoretically host up to 15 lithium atoms per silicon atom in the $Li_{15}Si_4$ phase, giving it a specific capacity of 3590mAhg^{-1} at room temperature. This is nearly an order of magnitude higher than graphite and offers a path toward substantially improving energy density at the cell level.[155]

In addition to its capacity advantage, silicon has a low average lithiation potential ($\sim$0.4 V vs. Li^+/Li), which is sufficiently low to ensure high cell voltage and thus high energy output. At the same time, this slightly elevated potential compared to graphite reduces the risk of dendritic lithium plating, thereby improving safety margins[156], especially under high-rate charging conditions.

Moreover, silicon is naturally abundant and environmentally benign, which makes it a sustainable and economically viable option for large-scale applications. Its widespread availability allows for low raw material costs, and its compatibility with existing silicon-processing industries presents further economic and technological incentives.[157, 158] Another key advantage of silicon is its tunability via nanostructuring and composite design. By modifying the size, shape, porosity, and surface chemistry of silicon particles, researchers have demonstrated impressive improvements in performance. For example, engineered structures such as yolk-shell nanoparticles, porous silicon frameworks, and nanowires have enabled much more stable cycling performance by mitigating volume-induced degradation and enhancing electrical contact.[159]

As shown in a study cited by Ashuri et al, a pomegranate-inspired nanoscale architecture achieved 1160mAhg^{-1} and 1270mAhcm^{-3} after 1000 cycles at C/2, showcasing silicon's potential when rationally designed at the nanoscale [160]. In another case, a micro-sized porous Si/C material yielded 1600mAhg^{-1} and 1088mAhcm^{-3} after 150 cycles at 400mAg^{-1} [161].

Several other studies have reported innovative silicon-based materials with promising performance [162]

2.7.2 Limitations and Technological Challenges (Volume Expansion, SEI Instability)

Despite its extraordinary promise, the practical application of silicon is significantly hindered by several interrelated challenges. Chief among them is the extensive volume expansion during lithiation, which can reach as high as ∼300% in crystalline silicon upon the formation of lithium-rich phases like $Li_{15}Si_4$ [163].

This expansion leads to pulverization of silicon particles, mechanical fracture of the active material, and delamination from the current collector. As a result, the electronic and ionic pathways are disrupted, leading to capacity fading and poor cycling stability [164].

Moreover, the solid electrolyte interphase (SEI) layer, which forms spontaneously at the electrode–electrolyte interface, is highly unstable in silicon-based systems. Due to the repeated expansion and contraction, the SEI undergoes continuous rupture and reformation, consuming electrolyte and producing thick, resistive interphases. This not only depletes active lithium but also increases cell impedance, further deteriorating battery performance [165].

Crucially, the volume expansion in crystalline silicon is anisotropic, occurring more readily along certain crystallographic orientations (e.g., the (110) plane) compared to others. This anisotropy contributes to uneven stress distribution, localized failure, and nonuniform SEI growth [166].

In contrast, amorphous silicon exhibits isotropic expansion, which is somewhat less damaging. As shown in in-situ TEM studies, lithiation of crystalline silicon particles leads to a sharp interface between a lithiated amorphous shell and pristine crystalline core, which moves inward during cycling. After the first cycle, silicon typically remains amorphous, and the anisotropic behavior disappears in subsequent cycles [167].

Another factor contributing to capacity fade is electrical disconnection. Even when particle cracking is avoided, the large expansion and contraction can weaken mechanical contact between particles and conductive additives or the current collector. Over multiple cycles, this results in gradual loss of connectivity and active material isolation, leading to performance degradation [164].

Attempts to mitigate these challenges have focused on reducing particle size, introducing void spaces, and coating silicon with flexible, conductive shells. Nanoparticles below 150nm are less prone to cracking. For example, particles smaller than 20nm have been shown to resist fracture entirely. However, this alone is insufficient, as structural rearrangements and electronic disconnection still occur without further design strategies [168].

Furthermore, silicon's intrinsic electrical conductivity is low ($< 10^{-5}$Scm^{-1} for undoped Si). This necessitates the incorporation of conductive additives or coatings, such as carbon shells, graphene, or conductive polymers. These not only enhance electronic transport but also act as mechanical buffers to accommodate silicon expansion and stabilize the SEI layer [166].

Finally, the chemical reactivity of freshly exposed silicon surfaces during cycling promotes parasitic side reactions with electrolyte components. This consumes active lithium and degrades both silicon and electrolyte, posing additional challenges for achieving long cycle life [163, 167].

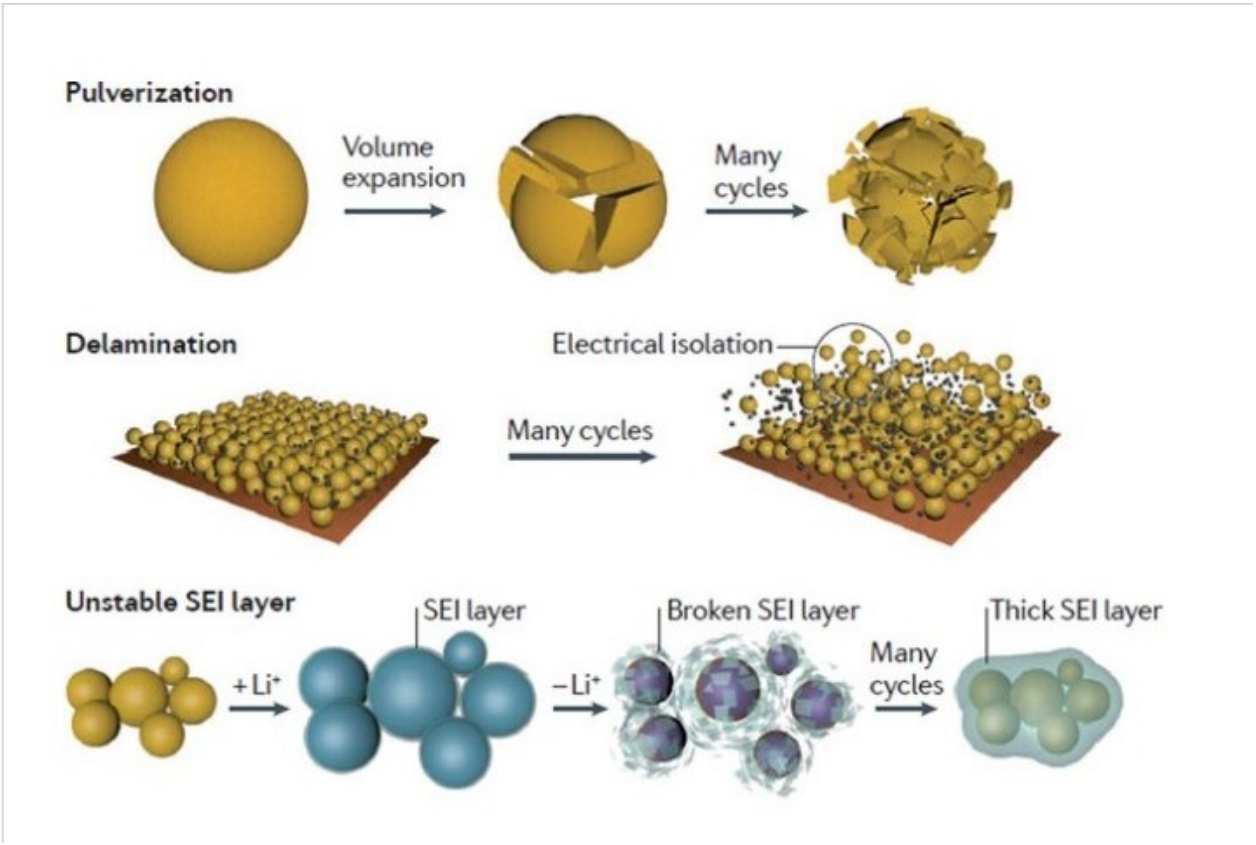

Figure 2.5 – Challenges of Si-based anodes in LIBs.2 Reused with permission [31].

2.8 Design Strategies to Overcome Challenges

Researchers have developed a variety of nanostructuring and composite approaches to overcome silicon's limitations. These include :

a. Nanoparticles and Size Engineering

Reducing silicon particles below 150 nm, and ideally below 20 nm, helps alleviate mechanical stress and prevent cracking during cycling. However, such small particles still suffer from electrical isolation over long-term cycling unless integrated into conductive networks [169].

b. Core-Shell and Yolk-Shell Architectures

Encapsulating Si nanoparticles within conductive carbon shells or flexible oxide matrices (like SiO_2 or TiO_2) can suppress volume-induced stress and stabilize the SEI layer. Yolk-shell designs are particularly effective as the internal void accommodates Si expansion without damaging the shell.

Notably, the yolk-shell structure has shown excellent cycling stability ($\sim$1400 mAh g^{-1} over 1000 cycles at 1C), with minimal capacity fading and high coulombic efficiency [170, 171].

c. Porous Silicon

Porous architectures—both nano- and micro-scaled—provide internal voids for expansion, high surface area for lithium transport, and stable mechanical frameworks. For example, porous Si derived from rice husks retained 1700 mAh g^{-1} over 300 cycles at C/2 without carbon coating [172].

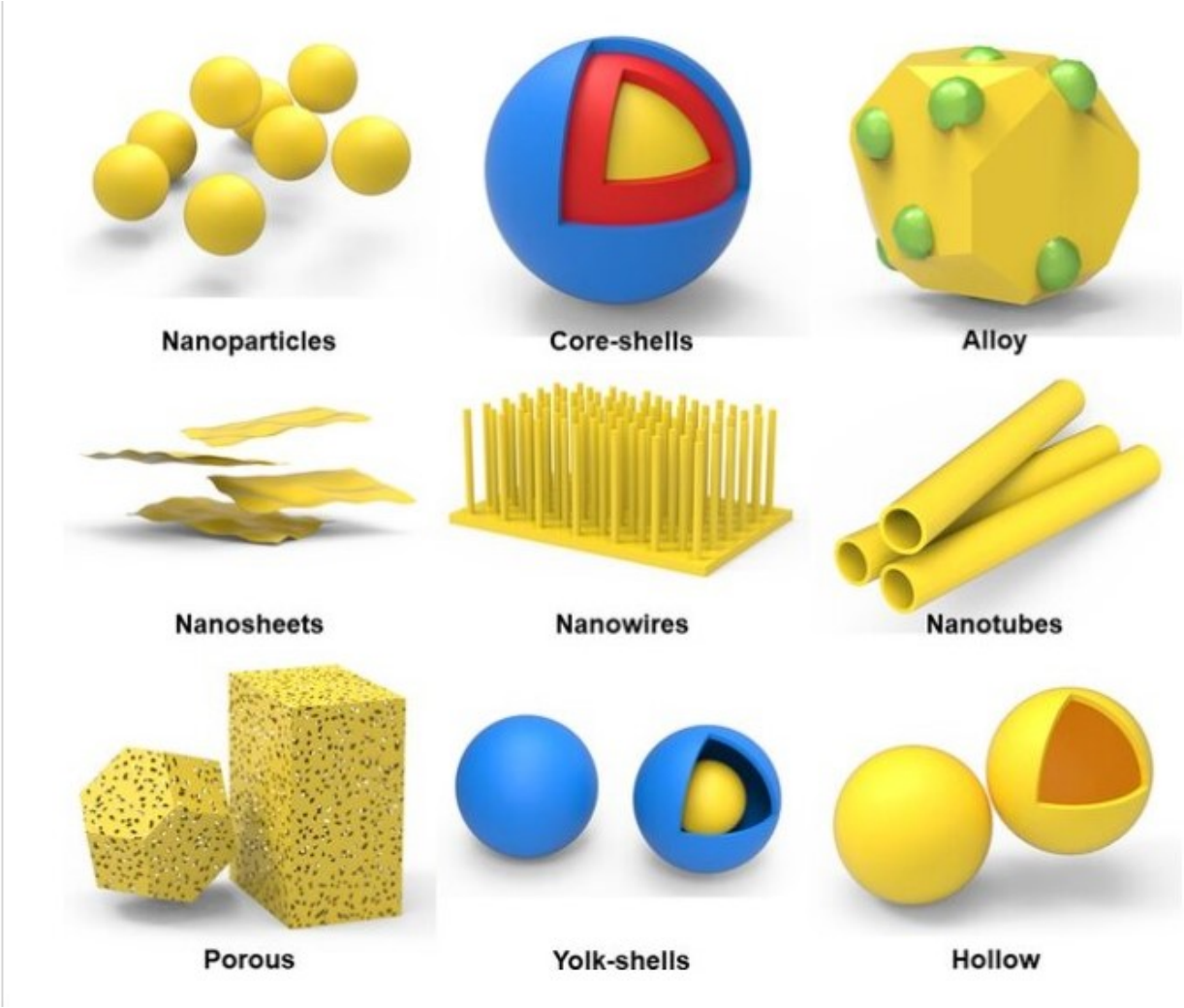

Figure 2.6 – Different representative strategies to solve the major issues of Si-based anodes [31] .

2.9 Relevance Beyond the Anode : General Electrode Design

Although most studies contextualize silicon strictly as an anode material, its fundamental interaction with lithium, structural versatility, and ability to host lithium at high capacity make it relevant for broader electrode engineering purposes, especially in novel architectures where lithium metal is the anode and silicon participates in composite or intermediate electrodes.

In such hybrid systems, understanding the properties, failure mechanisms, and protective strategies developed for Si anodes remains essential, even if the role of silicon shifts from classical anode to a different function. For this reason, silicon-related literature offers valuable insight into interface stabilization, capacity retention, and mechanical resilience that can be transferred to other electrode configurations [173, 174].

Chapter 3

Experimental part

3.1 Introduction

In this chapter, we present the experimental procedures undertaken to address the key limitations of conventional lithium-ion batteries (LIBs). While LIBs have revolutionized portable energy storage, their widespread adoption is constrained by issues such as :

- limited energy density,
- capacity fading over cycles,
- and safety concerns related to dendrite formation and thermal runaway.

To overcome these drawbacks, particular attention has been directed toward replacing the traditional graphite anode with lithium metal, a material known for its ultra-high theoretical capacity (3860 mAh/g) and the lowest electrochemical potential (0 V vs. Li^+/Li).

Despite these promising attributes, lithium metal anodes pose significant challenges, including :

- dendritic lithium growth,
- unstable solid electrolyte interphase (SEI),
- and low Coulombic efficiency.

To mitigate these issues and improve the electrochemical performance of the lithium metal anode, a protective solid electrolyte layer was synthesized and applied directly onto its surface. This layer simultaneously acts as a stable SEI and a solid-state electrolyte, offering :

- enhanced ionic conductivity,
- improved interfacial stability,
- and better protection against dendrite propagation.

Additionally, a conventional separator and a liquid electrolyte were used, resulting in a hybrid configuration combining both solid and liquid electrolytes.

On the cathode side, silicon—typically employed as an anode material due to its high specific capacity—was explored in an unconventional role as a cathode. This choice was driven by the interest in studying its behavior as an insertion host and evaluating its electrochemical performance in this atypical configuration.

The following sections detail the materials, synthesis methods, cell assembly procedures, and characterization techniques implemented throughout the study.

3.2 Materials and methods

3.2.1 Electrolyte synthesis

3.2.1.0.1 Preparation of solutions

To prepare the electrolyte solutions, a 0.25 mol/L solution of phosphoric acid (H3PO4, 85%) was first prepared by accurately measuring 2.45 g of liquid H3PO4 using a micropipette and dissolving it in 100 mL of tetrahydrofuran (THF) inside a 100 mL beaker. The mixture was stirred with a magnetic stirrer until fully homogenized.

Separately, three lithium nitrate (LiNO3, 99.99%) solutions were prepared at concentrations of 0.25 mol/L, 0.5 mol/L, and 0.75 mol/L by dissolving, respectively, 1.72 g, 3.45 g, and 5.17 g of LiNO3 (weighed with a microbalance) in 100 mL of THF using 100 mL volumetric flasks.

THF was added gradually with volumetric pipettes, and each solution was stirred magnetically until the salt was completely dissolved. All solutions were stored in sealed glass containers to avoid evaporation and contamination prior to further use.

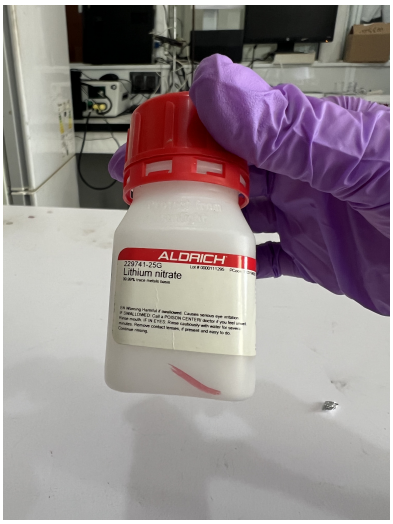

Figure 3.1 – Lithium nitrate

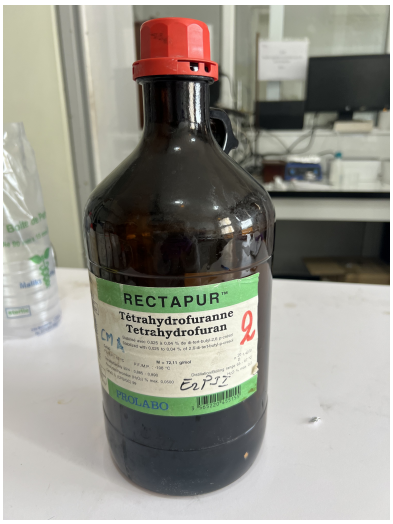

Figure 3.2 – Tetrahydrofuran

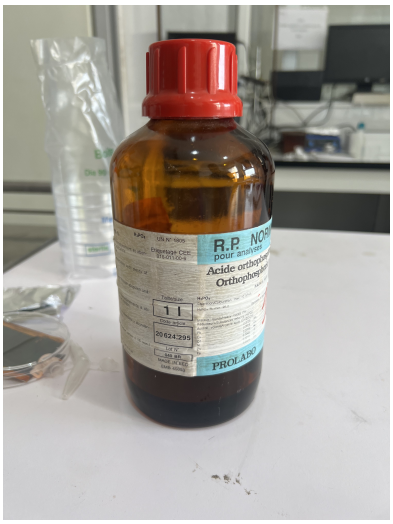

Figure 3.3 – Phosphoric acid

Figure 3.4 – Precision Balance

Table 3.1 – Chemical properties of the reagents used in the preparation of electrolyte solutions.

Chemical	Chemical Formula	Molar Mass (g/mol)	Purity (%)
Phosphoric acid	H3PO4	98.00	85.00
Lithium nitrate	LiNO3	68.95	99.99
Tetrahydrofuran (THF)	THF	72.11	99.99

To calculate the **molar concentration** of the commercially available phosphoric acid (H_3PO_4, 85%), the following formula was used :

$$C = \frac{10 \cdot P \cdot \rho}{M} = \frac{10 \times 85 \times 1.685}{98} = 14.6 \text{ mol/L}$$

Where :

- C is the molar concentration (mol/L)
- ρ is the density of H_3PO_4 (typically 1.685 g/mL)
- P is the mass percentage (85%)
- M is the molar mass of H_3PO_4 (98 g/mol)

To prepare 100 mL of a **0.25 mol/L** phosphoric acid solution, the required amount of commercial H_3PO_4 (85%, $\rho \approx 1.685$ g/mL) was calculated as follows. First, the number of moles needed was determined :

$$n = C \times V = 0.25 \text{ mol/L} \times 0.1 \text{ L} = 0.025 \text{ mol}$$

Given that the molar mass of H_3PO_4 is 98 g/mol, the corresponding **mass of pure acid** is :

$$m_{\text{pure}} = 0.025 \text{ mol} \times 98 \text{ g/mol} = 2.45 \text{ g}$$

To obtain this using the 85% solution, the **actual mass** of commercial acid needed is :

$$m_{\text{solution}} = \frac{2.45 \text{ g}}{0.85} = 2.88 \text{ g}$$

Using the known density, the corresponding **volume to measure** is :

$$V = \frac{2.88 \text{ g}}{1.685 \text{ g/mL}} = 1.71 \text{ mL}$$

Therefore, **1.71 mL** of H_3PO_4 (85%) was measured with a micropipette and diluted with **tetrahydrofuran (THF)** to a final volume of 100 mL to prepare the desired 0.25 mol/L solution.

The choice of **THF** as a solvent contributed to the uniformity and clarity of the solution, enabling better control over ion distribution and avoiding phase separation. Its compatibility with lithium-based systems made it particularly suitable for dissolving both H_3PO_4 and $LiNO_3$ without introducing unwanted side reactions.

During the preparation, care was taken to ensure measurement accuracy using micropipettes and a microbalance, and to maintain clean, sealed conditions for chemical stability. These steps were essential to ensure the reproducibility and quality of the final electrolyte formulation.

3.2.1.0.2 Lithium preparation

Before being used as an electrode in a lithium/silicon cell, the surface of metallic lithium must be properly prepared. Lithium is a highly reactive material that quickly forms an unwanted surface layer when exposed to air or moisture. This layer—composed mainly of lithium oxide, lithium hydroxide, or lithium carbonate—can interfere with the electrochemical interface by limiting lithium-ion conduction, reducing contact with the solid electrolyte, and causing uneven lithium deposition during cycling. These issues can significantly lower battery performance and promote the formation of lithium dendrites, needle-like structures that may lead to short circuits.

To ensure a clean surface, the lithium was gently scraped to remove surface contaminants, then passed through a rolling mill to obtain the desired thickness (approximately 1 mm). All these steps were performed inside a glove box under an inert argon atmosphere, where the oxygen and water content was maintained below 1 ppm. This controlled environment was essential to preserve the integrity of the lithium surface and ensure a stable and efficient interface with the electrolyte.

Since droplets of solution will be added on top of the lithium surface, it was crucial to prevent the liquid from leaking to the sides and damaging the bottom surface. For this reason, as shown in the image, we intentionally shaped the lithium pieces with raised edges by folding or shaping the extremities upward. This design helps contain the solution on the top surface and protects the lithium interface underneath, ensuring better control over the wetting and reaction area.

Figure 3.5 – Surface cleaning of lithium by gentle scraping to remove oxide layers.

Figure 3.6 – Pure Lithium electrode prepared with raised edges before electrolyte application.

3.2.1.0.3 Phosphating process

To form the desired **NPO–Li solid electrolyte layer**, we employ a **synergistic phosphatation process** involving **phosphoric acid** (H_3PO_4) and **lithium nitrate** ($LiNO_3$). The term *synergistic* refers to an interaction between two or more substances or processes that produces a greater effect than the sum of their individual effects. In other words, when these components act together synergistically, the combined outcome is stronger or more effective than what would be expected from each acting alone.

A simple direct mixing of H_3PO_4 and $LiNO_3$ in a THF solution is not effective due to the formation of LiH_2PO_4, which is insoluble in THF. This leads to poor interaction with the lithium surface and limits protective layer formation.

Therefore, the synergistic phosphatation process ensures that the combination of H_3PO_4 and $LiNO_3$ leads to the formation of a more stable and uniform protective layer on the lithium surface than either compound alone. This enhanced effect results from the specific way these two reactants interact during the process, ultimately improving the stability and performance of the lithium anode and the properties of the designed solid electrolyte.

First Reaction :

In the first step, **phosphoric acid (H_3PO_4)** reacts with **lithium metal** to form **lithium dihydrogen phosphate (LiH_2PO_4)**. This reaction is carried out under a heat source (around 40°C) for three hours, promoting both the reaction and the evaporation of the THF solvent. During this step, **hydrogen gas (H_2)** is released as a byproduct :

$$2\,Li + 2\,H_3PO_4 \rightarrow 2\,LiH_2PO_4 + H_2 \tag{3.1}$$

Figure 3.7 – Droplets of functional solution being applied onto the lithium surface.

Figure 3.8 – Treated lithium surface after complete solution deposition.

The formation of hydrogen on the lithium surface leads to porous and loosely packed interfacial layer. This non-dense solid electrolyte interphase (SEI) results in uneven lithium-ion transport and localized current density fluctuations. Such heterogeneities promote the anisotropic growth of lithium dendrites, compromising battery performance and posing safety risks due to short circuits.

Second Reaction :

Next, a drop of lithium nitrate ($LiNO_3$) solution is placed onto the surface already coated with LiH_2PO_4. This step fills the previously formed voids with nitrogen-containing compounds. The reaction proceeds slowly over another three hours at 40°C to enhance reaction kinetics and solvent evaporation, forming a denser, more compact, and homogeneous interphase.

The proton (H^+), released from the decomposition of the metastable intermediate LiH_2PO_4, facilitates

the reduction of $LiNO_3$ into lithium nitride (Li_3N). The acidic environment promotes this reduction through a series of intermediates, yielding various products including :

$$Li + LiNO_3 + LiH_2PO_4 \rightarrow LiNO_2 + Li_xN_yO_z + Li_3N + Li_3PO_4 + Li_2O + H_2 \tag{3.2}$$

The final SEI layer, composed of **Li_3PO_4–Li_3N (NPO–Li)**, appears **black in color** and forms a robust interface with the lithium metal.

3.2.2 Preparation of the slurry

The slurry was prepared by mixing nanometric silicon (60–80%), carbon black (10–25%), and a binder such as PVDF, CMC, or PAA (10–15%) in a suitable solvent to form a homogeneous paste. This mixture was thoroughly stirred to ensure even dispersion of the active materials and optimal coating properties. The resulting slurry was then ready for application using the doctor blade coating technique to produce a uniform electrode layer.

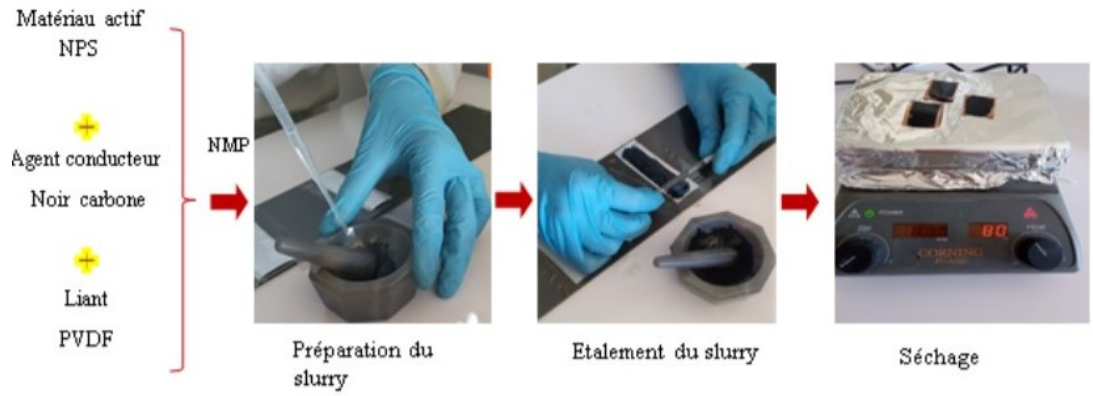

Figure 3.9 – Conventional preparation method of the silicon slurry

3.2.2.1 Doctor blade technology for the preparation of the cathode

Doctor blade coating is a technique used to apply a thin, uniform layer of liquid or slurry onto a flat surface by using a blade (the “doctor blade”) to spread the material at a controlled thickness. It is commonly used in battery electrode fabrication, thin film production, and printing.

Figure 3.10 – Doctor blade coating system used for electrode fabrication.

3.2.2.1.1 Doctor Blade Coating Process

Once the slurry is prepared with the appropriate viscosity and consistency to ensure smooth application, the substrate and blade are set up. Doctor-blade coating is compatible with many different substrates, including individual sheets, continuous rolls, or larger surfaces.

Once the blade and substrate are properly aligned, the coating material is dispensed onto the substrate in front of the blade.

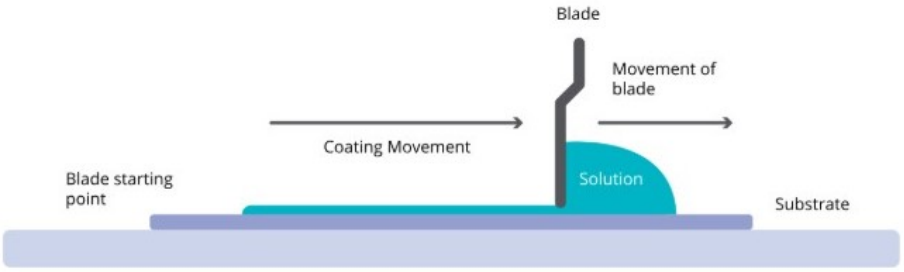

Figure 3.11 – Schematic Illustration of the Deposition Process.

In doctor blade coating, a blade is used to spread a solution over a substrate at a controlled height, allowing for precise film thickness. As the blade moves, it spreads and smooths the coating material across the surface. The thickness of the resulting film is primarily determined by the gap between the blade and the substrate, but factors such as the blade angle, coating speed, and the properties of the solution also play significant roles. Once the wet film is applied, the coated substrate undergoes a drying or curing process, air-blading, to solidify the layer. Both the drying method and the drying rate are crucial in ensuring the uniformity and performance of the final coating

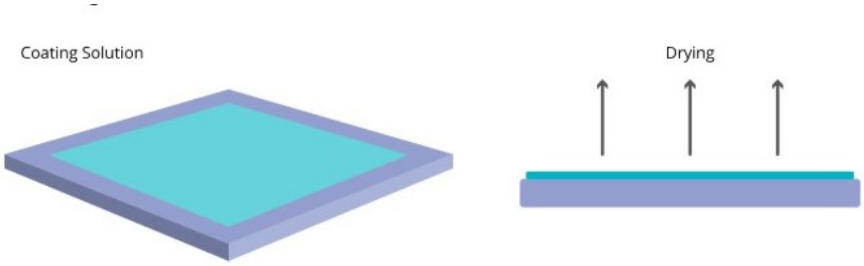

Figure 3.12 – Doctor blade coating post-coating annealing.

3.2.2.1.2 Doctor blade coating system's several components

The blade is one of the most important parts of a doctor blade coating system. It is usually made from stainless steel, ceramic or plastic material. The choice of material depends on the required durability, resistance to corrosion and interaction with the coating material.

The blade edge can be sharp, rounded, or bevelled, depending on the desired coating thickness and the properties of the material being applied. The blade height (the gap between the blade and substrate) is adjustable, along with the blade angle, and applied pressure. There are various types of doctor blades.

The fixed blade is the most common type of doctor blade used. This is where the blade remains stationary at a fixed thickness from the substrate. This blade is ideal for precise and even coatings, such as thin film photovoltaics or electronics where film uniformity is important, where a set film thickness is needed.

Some printing systems use adjustable doctor blades. The flexibility is advantageous for applications which require different film thicknesses. With adjustable systems, you can vary this height without needing to change the blade. The ability to fine tune the gap provides versatility to industries who may specialise in flexible electronics or if coating different viscosities solutions.

There are also rotary blades, like those featured a rolling mechanism, which allow the blade to rotate as it moves across the substrate. This type of blade is advantageous where large scale coating applications are required.

3.2.3 Preparation of Liquid Electrolyte (LE)

To prepare the liquid electrolyte used in this study, a 1 mol/L solution of lithium hexafluorophosphate ($LiPF_6$) was dissolved in a solvent mixture of ethylene carbonate (EC) and dimethyl carbonate (DMC) in a 1 :1 volume ratio.

The $LiPF_6$ was gradually added to the EC :DMC mixture under constant stirring to ensure complete and uniform dissolution.

These solvents were selected for their :

- excellent lithium-ion solvation properties,
- and their ability to form a stable passivation layer on the electrodes.

The resulting liquid electrolyte was then absorbed into a porous fiberglass sheet to facilitate ion transport.

3.2.4 Cell Assembly

As previously mentioned, the fabrication of the battery cell was carried out in an argon-filled glove box, with H_2O and O_2 levels maintained below 0.5 ppm.

The assembly was done using a Swagelok-type cell, which is a compact, reusable electrochemical test cell commonly used in battery research to evaluate electrode and electrolyte performance under controlled conditions.

It features a stainless steel cylindrical body with threaded end caps that securely seal the cell, making it suitable for air-sensitive materials. Springs, spacers, and sealing O-rings are also included to apply uniform pressure, ensure tight contact, and maintain an airtight, stable internal environment for reliable electrochemical testing.

The configuration used was **Cu/Li/SE/LE/Si/Cu**, as shown in the following figures :

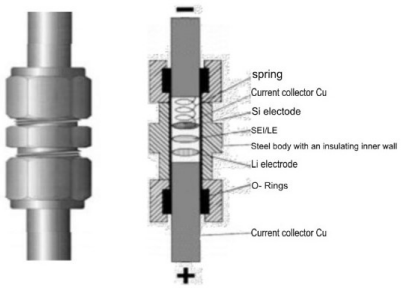

Figure 3.13 – Structure and assembly of a Swagelok cell

Figure 3.14 – Swagelok cell used in the laboratory

Figure 3.15 – Cell during addition of the silicon cathode

Figure 3.16 – Cell during addition of the separator

Figure 3.17 – Cell during addition of the lithium metal anode

Figure 3.18 – Measuring the resistance and potential difference of the assembled cell

3.2.4.1 Use of a Hybrid Electrolyte in the Battery Cell

In this study, a hybrid electrolyte was used to combine the advantages of both liquid and solid electrolytes within the same cell, configured as Li /SE + LE/ Si.

The solid electrolyte formed on lithium (as a result of the phosphatation process) provides structural stability and acts as a protective layer that enhances the safety and mechanical integrity of the cell.

On the other hand, the liquid electrolyte improves ionic conductivity and facilitates better interfacial contact between the electrodes and the electrolyte, thereby reducing internal resistance. It also electrically separates the solid electrolyte from the silicon anode.

The hybrid configuration helps overcome limitations associated with purely solid electrolytes, such as poor wetting and high interfacial resistance, while also minimizing the risks associated with liquid electrolytes, such as leakage or flammability.

This dual approach offers a balanced environment for lithium-ion transport, contributing to the overall performance and stability of the silicon–lithium battery system.

In this study, three solid electrolyte samples were prepared using different lithium nitrate ($LiNO_3$) concentrations in order to obtain electrolytes with varying thicknesses.

The table below summarizes the preparation of the three solid electrolyte solutions, each with a different $LiNO_3$ concentration, while maintaining a constant concentration of H_3PO_4.

Table 3.2 – Composition of the prepared NPO-Li solutions for each sample

Sample	H_3PO_4 Concentration (mol/L)	Volume of THF (mL)	$LiNO_3$ Concentration (mol/L)	$LiNO_3$ Mass (g)
First sample C1	0.25	100	0.25	1.72
Second sample C2	0.25	100	0.50	3.45
Third sample C3	0.25	100	0.75	5.17

3.2.5 Glove box

The **glove box** is a sealed enclosure designed to handle highly reactive, air-sensitive, or moisture-sensitive materials under a rigorously controlled atmosphere. It is an essential piece of equipment in many fields, including battery research, synthetic chemistry, and materials science. The front panel of the glove box is fitted with airtight gloves that allow the operator to safely manipulate materials inside the chamber without breaching its inert atmosphere.

The internal environment of the glove box is continuously purged and maintained using a high-purity inert gas, typically argon or nitrogen. Advanced purification systems are used to remove residual oxygen and water vapor, often reducing their concentrations to below 1 part per million (ppm). This low level of contamination is crucial when working with highly reactive substances such as metallic lithium, alkali metals, or organometallic compounds, which can degrade or react violently upon exposure to air or moisture.

In addition to preserving material stability, the glove box helps ensure reproducibility in experimental conditions by providing a clean and controlled environment. It is commonly equipped with features such as antechambers for safe sample transfer, oxygen and moisture sensors, recirculating gas purification units, and pressure regulation systems. These features collectively maintain a stable internal atmosphere and allow sensitive experimental procedures to be carried out reliably and safely.

Figure 3.19 – Glove Box

3.2.6 Key components of the glove box

- **Oxygen and moisture sensors :** to continuously monitor the internal atmosphere, usually keeping O_2 and H_2O levels below 1 ppm.
- **Gas purification system :** to remove traces of oxygen and moisture and regenerate the inert atmosphere.
- **Vacuum airlock chamber (antechamber) :** to safely transfer materials in and out without contaminating the main chamber.
- **Pressure control system :** to maintain a stable and slightly overpressurized internal environment.
- **Integrated gloves and transparent window :** allowing safe and precise manipulation of materials while observing operations.
- **Sealed chamber (usually stainless steel or polymer) :** ensuring airtight conditions.

3.2.6.1 Transferring materials in and out of the glove box

To introduce or remove materials without compromising the internal atmosphere, a two-door vacuum airlock is used. Materials are first placed in the antechamber and the outer door is sealed. The chamber is then evacuated to remove air and moisture, followed by several argon purges. Once the internal environment is safe, the inner door is opened to access the main chamber, and the process is reversed for removing items.

3.3 Characterization Techniques

3.3.1 Scanning Electron Microscopy (SEM)

Scanning Electron Microscopy (SEM) is a powerful imaging technique developed in the 20th century to overcome the limitations of optical microscopes. Instead of light, SEM uses a focused beam of high-energy electrons to scan the surface of a sample. These electrons interact with the atoms at the surface, producing signals such as :

- **Secondary electrons (SE) :** These are low-energy electrons that are ejected from the very surface of the sample when it's hit by the electron beam. Because they come from just a few nanometers deep, they give very detailed images of the surface texture and fine features. SE imaging is useful for seeing things like cracks, pores, and surface roughness.
- **Backscattered electrons (BSE) :** These are high-energy electrons from the original beam that bounce back after hitting atoms in the sample. They provide contrast based on the atomic number, heavier elements appear brighter, and lighter ones appear darker. BSE images help identify composition differences and larger structural features.

In addition to imaging, SEM is often equipped with **Energy Dispersive X-ray Spectroscopy (EDS)**, which enables elemental analysis of the sample. When the electron beam interacts with the sample's atoms, it can cause them to emit X-rays with energies that are characteristic of each specific element. EDS detects these X-rays to identify the elements present and can also provide approximate quantification. Combined with SEM imaging, EDS allows for both detailed surface observation and chemical composition analysis within the same system.

Figure 3.20 – Picture while putting the solutions inside the glove box

Figure 3.21 – The scanning electron microscope used for characterization

3.3.1.1 Main Components of SEM

- **Electron gun :** Generates the high-energy electron beam.
- **Electromagnetic lenses :** Focus the electron beam onto the sample.
- **Scan coils :** Move the electron beam in a raster pattern across the surface.
- **Sample chamber :** Holds the specimen in a vacuum environment.
- **Detectors :** Capture secondary and backscattered electrons to form images.
- **EDS detector :** Analyzes X-rays emitted from the sample to determine its elemental composition.
- **Computer system :** Controls the microscope and displays the images/data.

In our project, SEM JEOL JCM-7000 model was used to study the surface morphology and elemental distribution of the synthesized solid electrolytes. This helped us evaluate their homogeneity, compactness, and the presence of specific elements (such as lithium, nitrogen, and phosphorus), which are critical for understanding the electrolyte's quality and its role in battery performance. Additionally, post-cycling SEM analysis allowed us to observe changes in the surface, particularly the distribution and evolution of pores that formed after battery cycling.

3.3.2 X-ray Diffraction (XRD)

X-ray diffraction (XRD) is a powerful and non-destructive analytical technique used to investigate the crystallographic structure, phase composition, and other structural parameters of materials. It operates on the principle that X-rays, when directed at a crystalline substance, are diffracted by the orderly arrangement of atoms within the crystal lattice. This diffraction occurs due to the interaction of incident X-rays with the electron clouds surrounding the atoms.

A monochromatic X-ray beam is typically generated using a cathode ray tube with a metal target (commonly Cu or Mo), filtered to select a single wavelength, and collimated before striking the sample. When the X-rays hit the periodic atomic planes in the crystal, constructive interference of the scattered rays occurs only at specific angles that satisfy Bragg's law :

$$n\lambda = 2d\sin(\theta)$$

where n is the order of reflection (an integer), λ is the wavelength of the incident X-rays, d is the spacing between atomic planes, and θ is the angle of incidence.

The diffracted beams are collected by a detector as a function of the 2θ angle, producing a diffraction pattern that is characteristic of the material's crystal structure. This pattern—consisting of peak positions, intensities, and shapes—can be analyzed to determine a variety of material properties, including :

- **Phase identification :** Each crystalline phase has a unique diffraction fingerprint.
- **Crystallite size and strain :** Broadened peaks can indicate small crystallite sizes or lattice strain (analyzed via the Scherrer equation).
- **Lattice parameters :** Precise determination of unit cell dimensions.
- **Preferred orientation (texture) :** Anisotropic distributions of crystallites can be detected.
- **Quantitative phase analysis :** Using Rietveld refinement, the relative amounts of multiple crystalline phases can be quantified.

Because XRD does not destroy or alter the sample, it is especially useful for characterizing materials such as metals, ceramics, minerals, and electrode powders in their as-prepared or cycled states. In

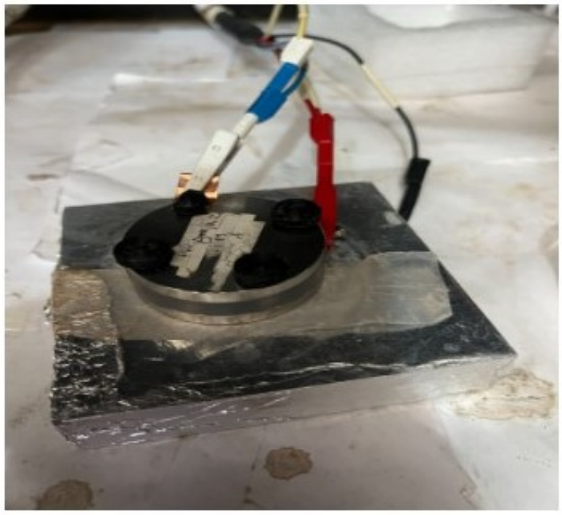

Figure 3.23 – Real image of the cell during electrochemical testing, connected to the potentiostat/-galvanostat setup.

battery research, for example, XRD is commonly used to monitor structural changes during electrochemical cycling, detect phase transitions, and verify the purity of synthesized compounds.

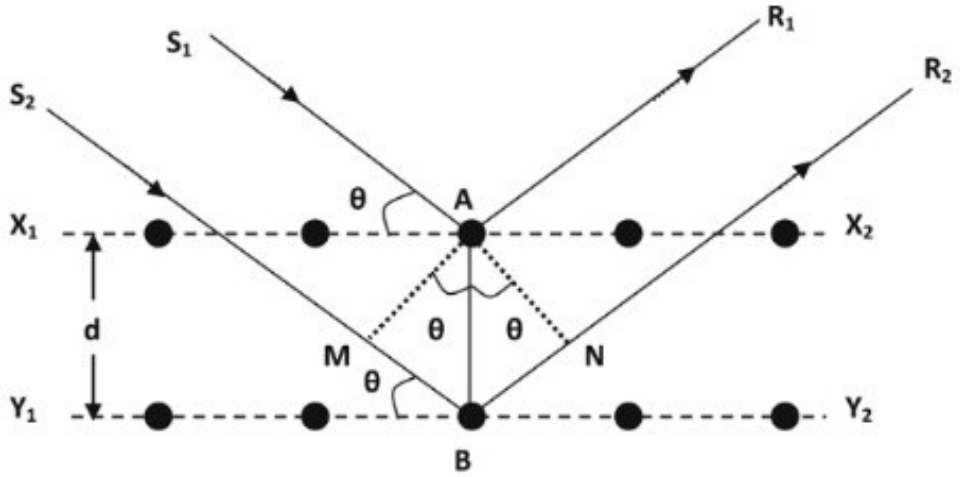

Figure 3.22 – Illustration of X-ray diffraction from solids

3.3.3 Electrochemical Characterization

3.3.3.1 Experimental Setup

All electrochemical measurements, including voltammetry, galvanostatic cycling, electrochemical impedance spectroscopy (EIS), and the electrochemical responses of the cells, were carried out using a Bio-Logic multichannel Potentiostat/Galvanostat.

The cells were directly connected to the Potentiostat/Galvanostat system, which was controlled by a microcomputer equipped with EC-Lab software. This software provides a range of functions for data acquisition, experimental signal control, and data storage, allowing for post-processing and detailed analysis of the electrochemical results.

3.3.3.2 Electrochemical Impedance Spectroscopy (EIS)

Electrochemical Impedance Spectroscopy (EIS) is a powerful diagnostic tool used to investigate the behavior of electrochemical systems by applying a small-amplitude alternating voltage and measuring the resulting current response over a broad range of frequencies. This technique is centered on analyzing the dynamics at the electrode/electrolyte interface by perturbing the system around a steady-state operating point, typically on the current–voltage curve. The frequency sweep usually ranges from a few microhertz (µHz) to several megahertz (MHz), allowing for the resolution of both slow and fast processes occurring in the system.

Because the excitation signal is small, the system response remains nearly linear, enabling the separation and identification of different electrochemical phenomena based on their kinetics.

3.3.3.2.1 Cyclic Voltammetry (CV)

Cyclic Voltammetry (CV) is one of the most commonly used techniques to investigate electrochemical reactions. The basic principle involves sweeping the potential of a working electrode from an initial value (U) to a final value and then back again, at a constant scan rate (v, in mV/s), while measuring the resulting current (I). The applied potential varies linearly with time and can be described by the equation :

$$U(t) = U_0 \pm vt$$

The positive sign (+) indicates a scan toward more positive potentials, while the negative sign (–) corresponds to a scan toward more negative values. This technique is widely applied to study materials and interfaces in energy storage systems, especially solid-state batteries, as it provides key information on their electrochemical behavior.

CV allows the identification of :

- **Redox potentials (E and Ed) :** These are the voltages at which oxidation and reduction reactions occur in the electrode material.
- **Charge transfer :** By analyzing the current response, one can estimate the amount of charge involved in the redox processes, which relates to the battery's capacity.
- **Reaction kinetics :** The shape and symmetry of the CV curves reveal how fast the electrochemical reactions take place and whether they are reversible.
- **Material stability :** Irreversible peaks or changes over cycles can indicate degradation or instability of the electrode.

A typical CV experiment involves :

1. Sweeping the electrode potential from an initial to a final value and back at a fixed scan rate.
2. Recording the current response throughout the cycle.

The resulting CV curve plots current versus applied potential. Common features include :

1. **Current peaks :** Anodic peaks (positive current) are linked to oxidation, and cathodic peaks (negative current) to reduction. The position and size of these peaks provide insights into redox activity and reactivity.
2. **Curve shape :** The symmetry and shape of the loop can indicate the mechanism and reversibility of the reactions.
3. **The area under the peaks :** corresponds to the charge transferred, which can be used to evaluate the material's charge storage capacity.

3.3.3.2.2 Galvanostatic Cycling (charge–discharge)

This technique consists of applying a constant current to the electrochemical cell until the voltage reaches a predefined limit set by the user. Once this voltage is reached, the direction of the current is reversed. The process is repeated over multiple cycles, alternating between charging and discharging

the cell by switching the current direction. The data collected from these experiments are used to generate charge–discharge curves, which provide valuable information about the cell's specific capacity, cycling performance, and rate capability.

3.4 Conclusion

To thoroughly evaluate the properties and electrochemical performance of the synthesized electrolyte and electrode materials, a multidisciplinary approach combining several complementary characterization techniques was adopted. This integrated methodology enabled both a structural and functional understanding of the materials, which is essential for optimizing their application in lithium-based battery systems.

Structural characterization was primarily conducted using X-ray diffraction (XRD). This technique provided crucial insights into the crystallographic structure, enabling the identification of existing phases, assessment of phase purity, and detection of any phase transformations resulting from synthesis or electrochemical cycling. The diffraction patterns were analyzed to determine lattice parameters and to confirm the successful formation of targeted crystalline phases.

Morphological and microstructural analysis was performed using Scanning Electron Microscopy (SEM), which allowed the visualization of surface features at the micro- and nanoscale. SEM imaging was instrumental in revealing particle size distribution, surface roughness, porosity, and homogeneity of the electrode and electrolyte materials. To complement the morphological observations, Energy Dispersive X-ray Spectroscopy (EDS) was employed to map the elemental composition and spatial distribution of key elements within the samples. This ensured proper material synthesis and offered insights into the uniformity of composite materials.

To explore the electrochemical behavior, several key techniques were employed. Cyclic voltammetry (CV) was used to investigate the redox activity and electrochemical reversibility of the materials. CV profiles provided information about the potential windows of operation, reaction kinetics, and possible side reactions. Galvanostatic charge–discharge (GCD) tests were carried out to evaluate the specific capacity, coulombic efficiency, and cycling stability of the electrode materials under realistic working conditions. These tests directly reflect the charge storage performance and durability of the system.

Furthermore, Electrochemical Impedance Spectroscopy (EIS) was utilized to probe the ionic conductivity, interfacial resistance, and charge-transfer dynamics at various interfaces. By analyzing Nyquist plots and fitting them with appropriate equivalent circuits, it was possible to quantitatively assess the contributions from bulk material resistance, electrolyte/electrode interfacial impedance, and diffusion-related processes.

Taken together, the combined application of these structural, morphological, compositional, and electrochemical characterization techniques offers a comprehensive and multi-dimensional understanding of the synthesized materials. This integrative approach provides critical insights into the relationships between material properties and electrochemical performance, ultimately guiding the design and optimization of advanced materials for next-generation energy storage devices.

Chapter 4

Results and Discussion

4.1 Introduction

To evaluate the properties and performance of the synthesized NPO-Li electrolyte and its interaction with lithium, a series of structural, morphological, and electrochemical characterizations were performed. These analyses aimed to confirm the formation of the desired phases, assess the surface morphology and composition, and determine the electrochemical behavior of the material under cycling conditions.

X-ray diffraction (XRD) was used to identify the crystalline phases and assess structural integrity. Scanning Electron Microscopy (SEM), combined with Energy Dispersive X-ray Spectroscopy (EDS), provided insights into the surface structure and elemental distribution.

Electrochemical techniques such as cyclic voltammetry (CV), electrochemical impedance spectroscopy (EIS), and galvanostatic charge–discharge testing were employed to evaluate ionic conductivity, redox behavior, and cycling stability.

The results obtained from these techniques are presented and discussed in the following sections.

4.2 X-ray Diffraction (XRD) Results

X-ray diffraction (XRD) was performed to identify the crystalline phases present in the synthesized electrolyte and to verify the success of the synthesis process. A cobalt radiation source was used for excitation, providing suitable wavelength and resolution for phase identification in lithium-based compounds. The diffractogram was analyzed using *HighScore* software, which allows phase identification by comparing the experimental pattern with reference databases. This section presents and discusses the diffraction results obtained for the three samples.

4.2.1 First sample C1

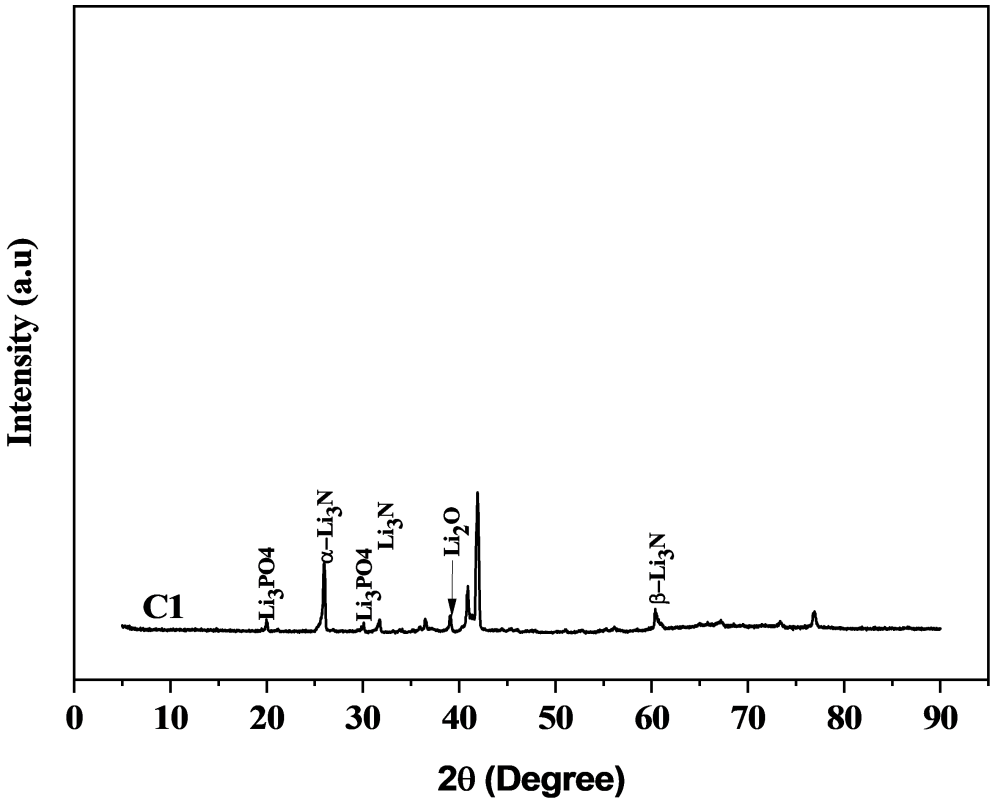

Figure 4.1 – XRD spectrum of C1 sample

The XRD pattern shows several well-defined peaks, confirming that the synthesized layer is crystalline. While the most intense peak appears around $2\theta \approx 39$–$41°$, indicating a dominant phase, smaller and less intense peaks were also observed. These minor peaks were matched to Li_3PO_4 and Li_3N, suggesting their presence in limited quantities. Li_3PO_4 is known for its chemical stability and helps improve interfacial compatibility, while Li_3N is a highly ionically conductive phase that supports lithium-ion transport. The relatively low intensity of their peaks indicates that these phases are not dominant in sample C1, which may limit ionic conductivity and overall performance. This result motivated us to increase the $LiNO_3$ concentration in subsequent samples to enhance the formation of these beneficial phases.

4.2.2 Second sample C2

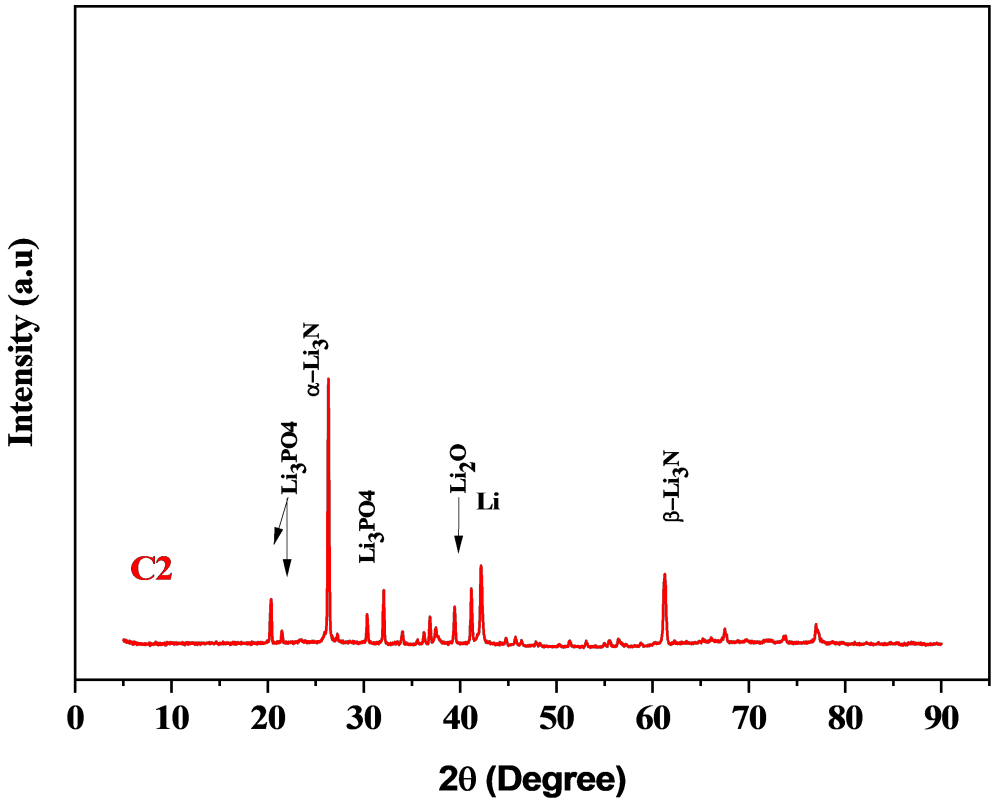

Figure 4.2 – XRD spectrum showing the desired phases C2

The XRD pattern of sample C2 shows a series of well-defined and intense peaks, confirming the crystalline nature of the synthesized layer. Unlike sample C1, the most intense peak observed in C2 corresponds to lithium nitride (Li_3N), indicating that it has become the dominant phase in this composition. Multiple peaks associated with Li_3N were detected, including both α-Li_3N and β-Li_3N, which suggests the formation of different polymorphic forms under the given synthesis conditions. In addition, peaks corresponding to Li_3PO_4 were also identified and were more intense than in C1, showing that this phase also increased with the modified composition. The enhancement in both Li_3N and Li_3PO_4 formation is directly linked to the increased concentration of $LiNO_3$ used in C2, which appears to promote the formation of these beneficial phases. Since Li_3N significantly contributes to lithium-ion conductivity and Li_3PO_4 enhances interfacial stability, their higher content in C2 indicates improved overall performance of the electrolyte layer. These findings confirm that adjusting the precursor concentration is an effective strategy for optimizing phase composition and boosting ionic transport.

4.2.3 Third sample C3

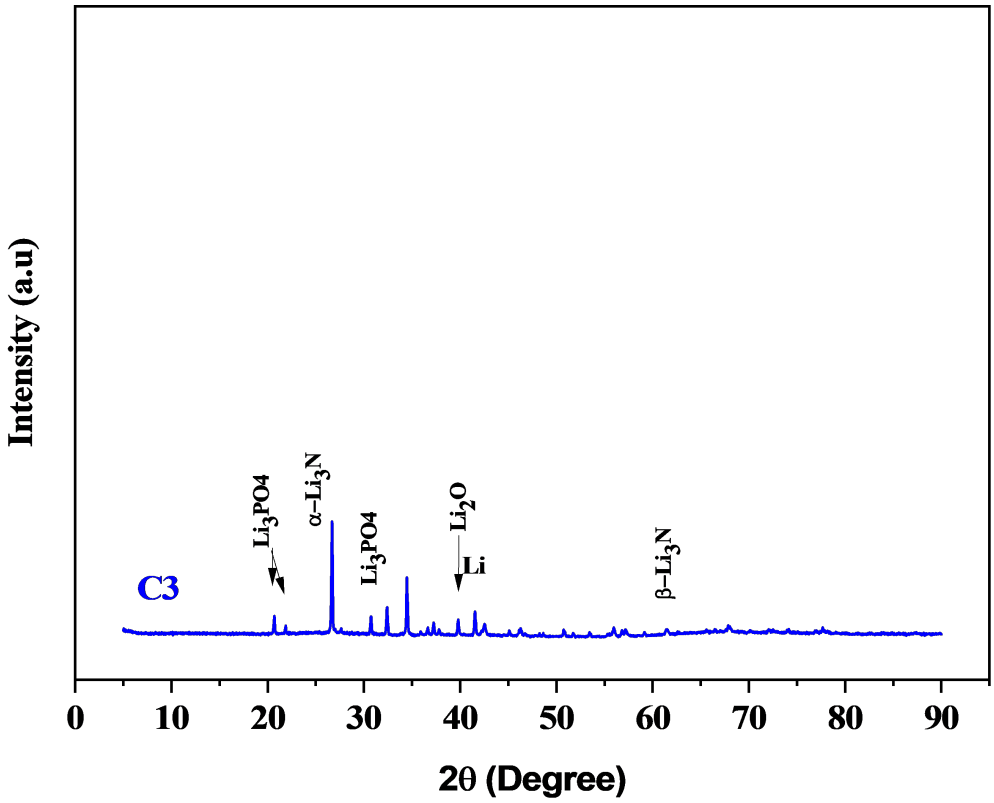

Figure 4.3 – XRD spectrum showing the desired phase C3

The XRD analysis of sample C3 revealed several intense and well-defined peaks corresponding to lithium nitride (Li_3N) and lithium phosphate (Li_3PO_4), confirming their successful formation as major phases. According to HighScore software, Li_3N was identified in multiple structural forms, including α-Li_3N and β-Li_3N, suggesting complex phase stabilization under the synthesis conditions used. Li_3N is widely recognized for its high lithium-ion conductivity and plays a critical role in enhancing ionic transport. Meanwhile, Li_3PO_4 was also matched with notable peaks, supporting its presence as a stable secondary phase that contributes to interfacial stability and chemical robustness. The combination of these conductive and stable phases indicates that the synthesized layer in sample C3 has a highly favorable structural profile for efficient lithium-ion movement and long-term electrochemical performance, making it a promising candidate for solid-state battery applications.

4.2.4 Concluding and Comparing the XRD Results of C1,C2 and C3

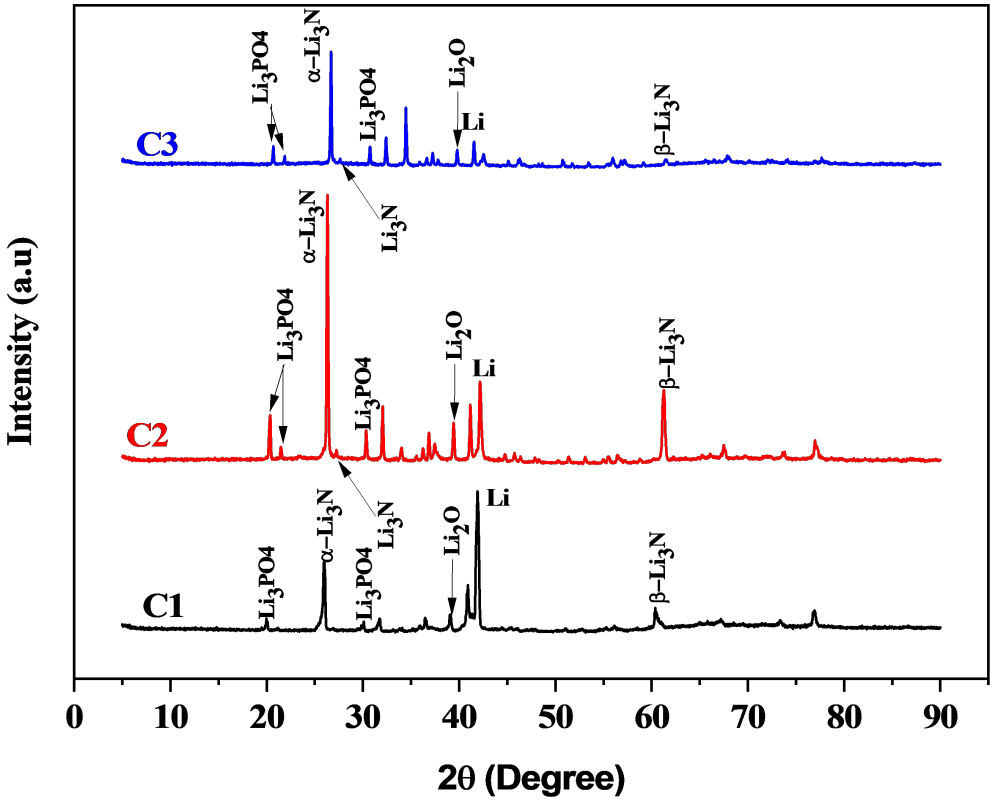

Figure 4.4 – Comparing XRD spectrums of C1,C2 and C3

To assess the properties and performance of the synthesized electrolyte and electrode materials, a combination of complementary characterization techniques was employed. Structural information was obtained through **X-ray diffraction (XRD)**, allowing phase identification and crystallographic analysis. **Scanning Electron Microscopy (SEM)**, supported by **Energy Dispersive X-ray Spectroscopy (EDS)**, was used to observe the surface morphology and elemental distribution of the materials.

In addition, electrochemical techniques such as **cyclic voltammetry (CV)**, **galvanostatic charge–discharge testing**, and **electrochemical impedance spectroscopy (EIS)** were implemented to evaluate ionic conductivity, electrochemical stability, and redox activity.

Together, these methods provide a comprehensive understanding of the physical and electrochemical characteristics of the materials. The following section presents and discusses the experimental results obtained from these techniques.

4.3 Scanning Electron Microscopy (SEM) Results

4.3.1 Fisrt sample C1

To provide additional insight into the surface morphology associated with this specific $LiNO_3$ concentration, SEM images from a previous PFE study *"Étude de Synthèse d'électrolyte solide inorganique NPO-Li pour la stabilité des batteries lithium tout solide"* by Mohamed Cherif Rayane IDDIR and Sondes MAHMAH are included. That work was conducted on a sample with the same composition, making the images relevant for illustrating the typical structural characteristics and surface features expected under similar synthesis conditions. These visual references help support the interpretation of the material's microstructural behavior.

4.3.1.1 Sample C1 After cycling

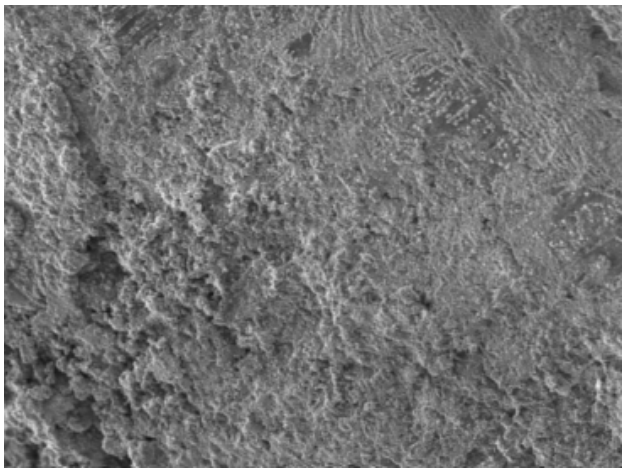

Figure 4.5 – Growth of a dendritic film (100 µm)

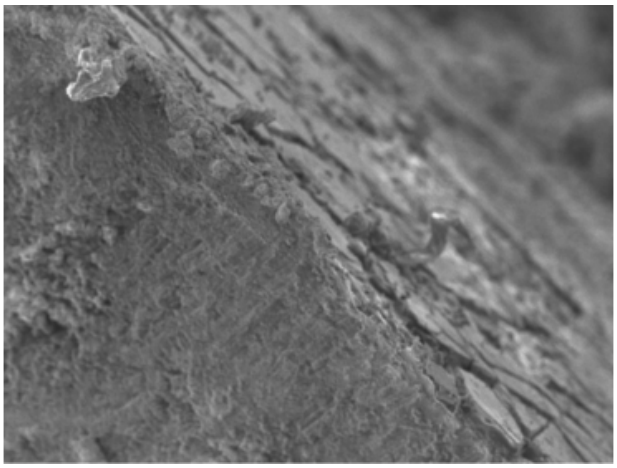

Figure 4.6 – Needle-like dendrite penetrating the surface (100 µm)

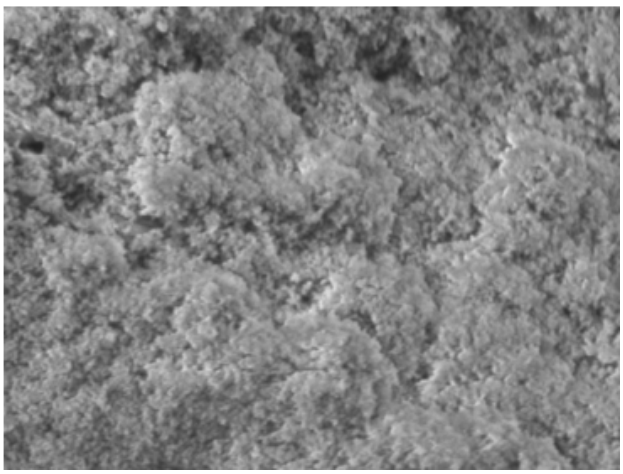

Figure 4.7 – Rough surface morphology (10 µm)

Figure 4.8 – Lithium metal–solid electrolyte interface (50 µm)

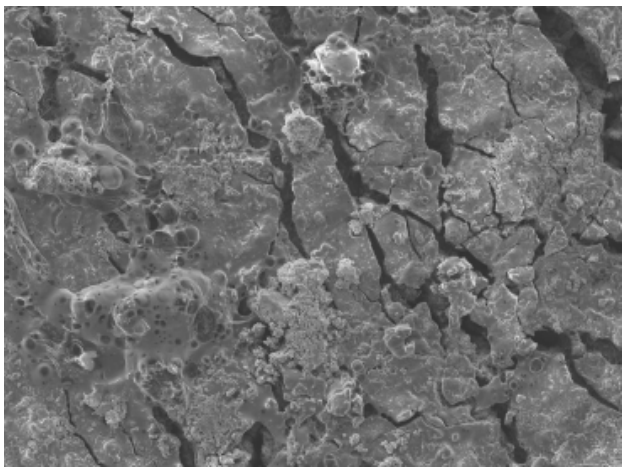

Figure 4.9 – Cracks and fractures observed on the surface of the sample (100 µm).

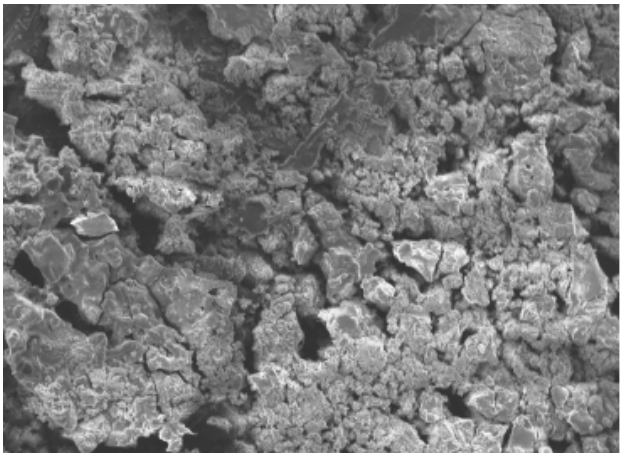

Figure 4.10 – Presence of dead lithium observed on the surface (10 µm).

In the figures, *needle-like lithium dendrites* are clearly visible, along with *nucleation sites* and *lithium propagation pathways*, which are characteristic of dendritic growth.

At the **interface between lithium metal and the solid electrolyte**, a distinct contrast in color and surface morphology is observed, suggesting the formation of a **solid electrolyte interphase (SEI)**.

The surface after cycling exhibits a noticeable *roughness*, likely resulting from the reaction between the solid electrolyte and the liquid electrolyte. Very deep and wide cracks are observed, extending across the entire surface and appearing to be fully developed. These fissures serve as preferential sites for *dendritic growth*.

Dendrites can be seen developing through these cracks and penetrating the surface, which may lead to **short circuits**.

The visible voids indicate *delamination* of the solid electrolyte and *poor interfacial contact* between the electrolyte and lithium metal.

Additionally, the presence of **dead lithium plates** is observed, indicating a separation of *inactive lithium* from the active lithium source. This results in a loss of active material and a significant reduction in the overall battery efficiency.

4.3.2 Second sample C2

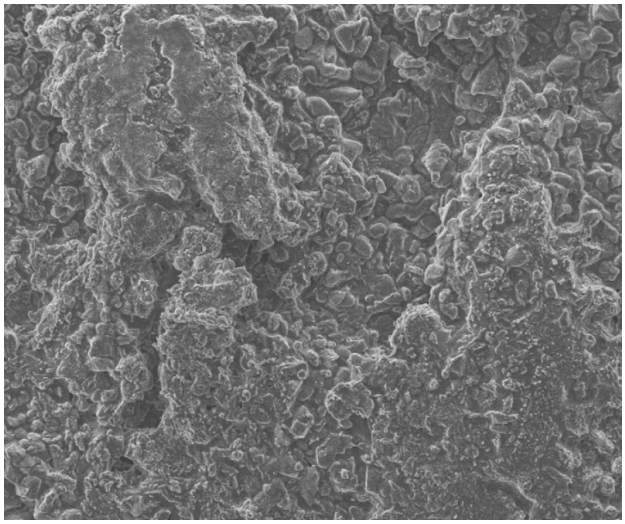

Figure 4.11 – The sample after cycling (100 µm) showing dead Lithium.

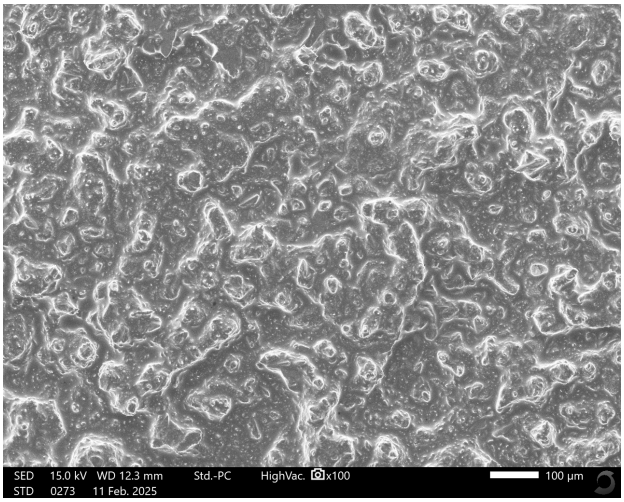

Figure 4.12 – The sample before cycling (100 µm).

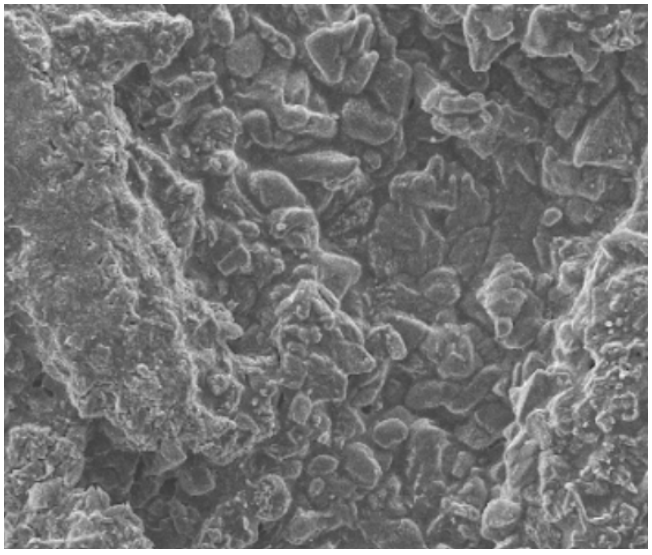

Figure 4.13 – Zoomed picture (100µm) of the sample C2 after cycling showing cracks

Before cycling, the surface appears intact and free of cracks, with a clearly visible layer uniformly deposited on the substrate, corresponding to the synthesized solid electrolyte.

After cycling, however, the surface morphology changes significantly. Cracks are observed across the structure, indicating mechanical degradation of the electrolyte. The image reveals the presence of two distinct surface morphologies ; the brighter zones correspond to areas where lithium has redeposited during cycling.

This redeposition appears in various forms, including lithium foam-like structures, dendrites, and possibly dead lithium, all of which suggest uneven lithium plating and stripping.

These observations point to instabilities at the lithium/electrolyte interface, which could affect battery performance and safety.

4.3.3 Third sample C3

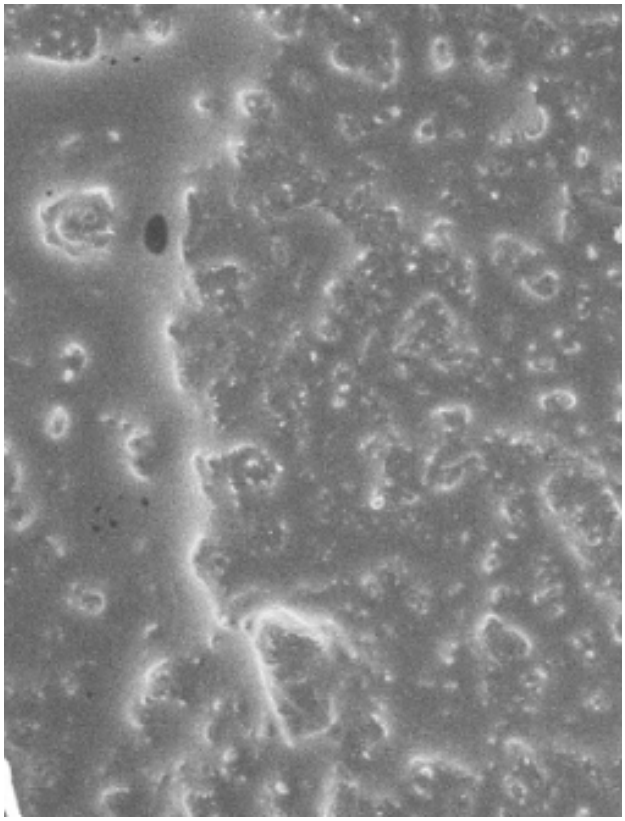

Figure 4.14 – Surface morphology of the sample before cycling (500 µm).

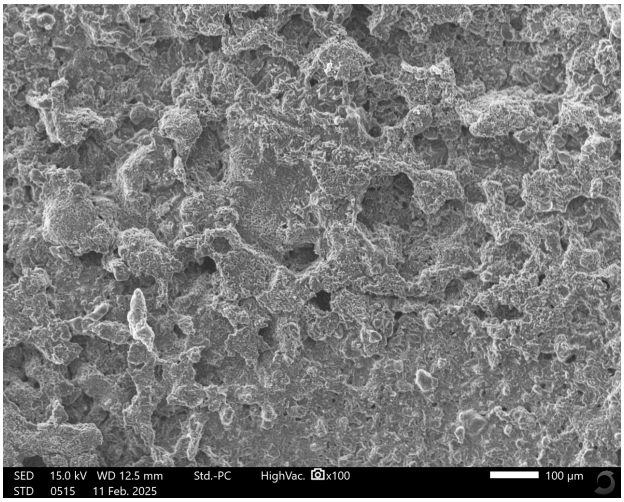

Figure 4.15 – Surface morphology of the sample after cycling (100 µm).

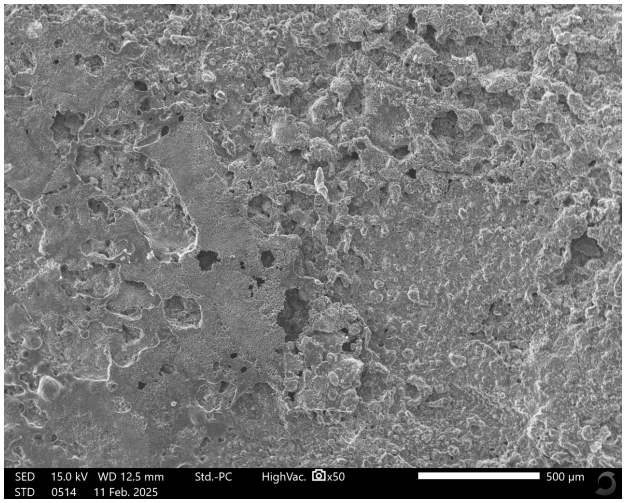

Figure 4.16 – Detailed view of the sample after cycling (500 µm) showing dead lithium.

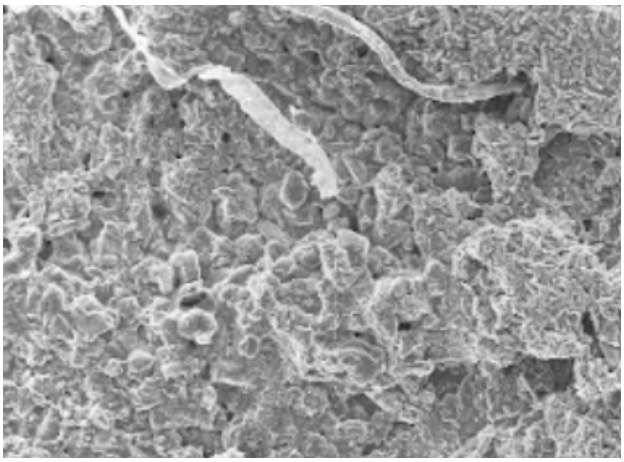

Figure 4.17 – Zoomed view of the electrode (500µm) showing dendritic lithium growth.

Before cycling, the surface shows no visible cracks, and the synthesized solid electrolyte layer is clearly deposited on the substrate with uniform coverage.

After cycling, only a few cracks are observed, and they appear less pronounced compared to other samples. This limited cracking indicates that the synthesized layer demonstrates improved mechanical resistance and better structural integrity under electrochemical cycling conditions.

The reduced formation of cracks suggests enhanced stability of the electrolyte, which may contribute to a more reliable lithium–electrolyte interface and improved long-term performance.

4.3.3.1 SEM imaging of the Silicon electrode interface after cycling in the sample C3

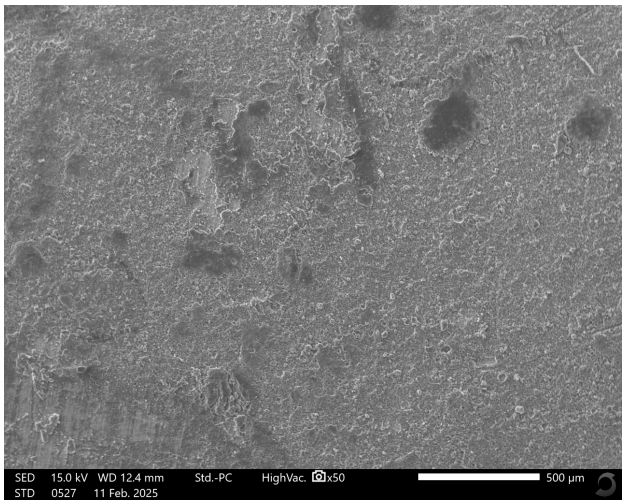

Figure 4.18 – Cracks and fractures observed (500 µm).

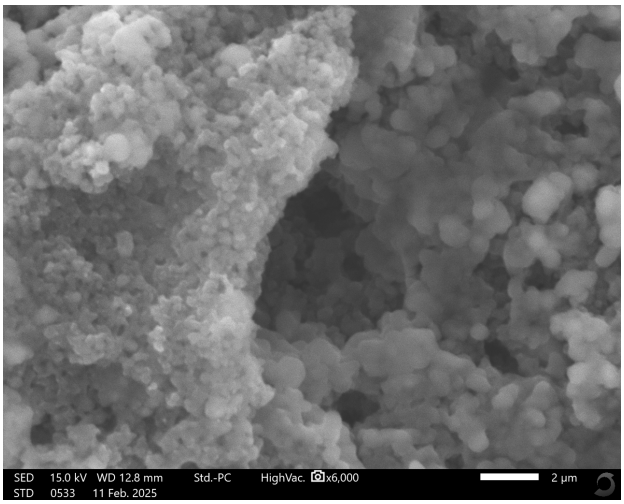

Figure 4.19 – Particle size and color variation between two regions (2 µm).

The image shows the surface of the silicon electrode after cycling in sample C3. Several cracks are visible across the surface, indicating mechanical stress induced by repeated charge–discharge processes. The brighter regions suggest the presence of a metallic structure, likely lithium, which migrated and redeposited during cycling. Interestingly, lithium appears to have deposited unevenly, accumulating in some zones while being absent in others. In addition, there is a noticeable variation in grain size between different areas of the surface. This heterogeneity is likely due to the volume expansion and contraction of silicon during lithiation and delithiation. Silicon undergoes significant structural changes as it reacts with lithium, which can lead to localized stress, grain deformation, and surface instability. These features reflect the complex and dynamic behavior of the silicon–electrolyte interface during battery operation.

4.3.4 Conclusion

The SEM observations provided valuable insights into the morphological changes occurring at the surface and interface of the electrode and electrolyte materials. Before cycling, the synthesized layers appeared uniform and free of cracks, confirming their good initial structural quality.

After cycling, notable variations were observed, including the formation of cracks, uneven lithium deposition, and changes in grain morphology. These changes reflect the effects of electrochemical stress and interfacial dynamics during repeated cycling.

Among the samples analyzed, sample C3 exhibited the most favorable structural behavior, showing fewer cracks and a more stable surface. This indicates enhanced mechanical resistance and improved interfacial compatibility between the electrode and the synthesized electrolyte.

These findings underscore the importance of compositional optimization to improve both the mechanical stability and the electrochemical performance of solid-state lithium batteries.

4.4 Energy Dispersive X-ray Spectroscopy (EDS)

Energy Dispersive X-ray Spectroscopy (EDS) was performed in conjunction with Scanning Electron Microscopy (SEM) to analyze the elemental composition of the synthesized materials. This technique allows for the detection and quantification of elements present on the sample surface by measuring the characteristic X-rays emitted in response to the electron beam.

The chemical reaction responsible for the formation of **phosphorus pentoxide ($\mathbf{P_2O_5}$)** from lithium phosphate (Li_3PO_4) is represented by the following equation :

$$3Li_3PO_4 \rightarrow 3Li_2O + P_2O_5 \tag{4.1}$$

This reaction illustrates the conversion of lithium phosphate into **lithium oxide ($\mathbf{Li_2O}$)** and phosphorus pentoxide (P_2O_5). Such a transformation typically occurs as a result of **decomposition** and chemical degradation of the solid electrolyte during cycling.

The detection of Li_2O and P_2O_5 on the material's surface is a strong indication of side reactions that can compromise the **chemical stability** of the electrolyte and negatively impact the overall performanceof the battery.

4.4.1 Lithium

Element	Line	Mass%	Atom%
O	K	70.69±0.43	75.58±0.46
F	K	23.64±0.56	21.29±0.50
Al	K	0.45±0.04	0.29±0.03
P	K	4.74±0.12	2.62±0.07
Cl	K	0.48±0.04	0.23±0.02
Total		100.00	100.00
Spc_001			Fitting ratio 0.0497

Figure 4.20 – Elemental Composition of the lithium metal

4.4.2 The First Sample C1

Element	Line	Mass%	Atom%
O	K	41.26±0.32	49.78±0.39
F	K	33.95±0.43	34.49±0.44
Al	K	3.31±0.08	2.37±0.06
Si	K	0.10±0.02	0.07±0.01
P	K	20.95±0.20	13.05±0.12
Cl	K	0.44±0.03	0.24±0.02
Total		100.00	100.00
Spc_003			Fitting ratio 0.0678

Figure 4.21 – Elemental Composition of Sample C1 (EDS)

The EDS results for sample C1 show a significant presence of **oxygen (O)** and **fluorine (F)**, with weight percentages of 41.26% and 33.95%, respectively. **Phosphorus (P)** is also present in notable quantity (20.95%), supporting the possible formation of **$\mathbf{Li_3PO_4}$**.

4.4.3 The Ssecond Sample C2

Element	Line	Mass%	Atom%
N	K	nd	nd
O	K	53.69±0.47	66.55±0.58
F	K	9.38±0.30	9.79±0.31
Si	K	0.21±0.03	0.15±0.02
P	K	36.72±0.29	23.51±0.19
Total		100.00	100.00
Spc_001			Fitting ratio 0.0346

Figure 4.22 – Elemental Composition of Sample C2 (EDS)

In sample C2, the EDS analysis reveals a much higher content of **oxygen** (53.69 wt%) and **phosphorus** (36.72 wt%), along with smaller amounts of **fluorine** (9.38 wt%) and **silicon** (0.21 wt%). The increase in P and O supports a more defined $\mathbf{Li_3PO_4}$-rich composition, which enhances interfacial stability. The overall elemental distribution in C2 aligns well with the improved phase formation observed in XRD results and reflects a better compromise between ionic conductivity and structural stability compared to C1.

4.4.4 The Third Sample C3

Element	Line	Mass%	Atom%
N	K	nd	nd
O	K	53.69±0.47	66.55±0.58
F	K	9.38±0.30	9.79±0.31
Si	K	0.21±0.03	0.15±0.02
P	K	36.72±0.29	23.51±0.19
Total		100.00	100.00
Spc_001			Fitting ratio 0.0346

Figure 4.23 – Elemental Composition of Sample C3 (EDS)

Sample C3 presents a similar elemental profile to C2, with high levels of **oxygen** (53.69 wt%), **phosphorus** (36.72 wt%), and **fluorine** (9.38 wt%). These results suggest a composition favorable to the formation of both **conductive** ($\mathbf{Li_3N}$) and **stable** ($\mathbf{Li_3PO_4}$) phases, particularly when considered alongside the structural findings from the diffraction analysis.

4.4.5 Conclusion

The EDS data from samples **C1**, **C2**, and **C3** show a clear evolution in elemental composition with increasing $\mathbf{LiNO_3}$ concentration. As the phosphorus and oxygen contents increase from C1 to C3, this trend supports the enhanced formation of $\mathbf{Li_3PO_4}$, known for its role in improving chemical stability and interfacial compatibility. Additionally, the compositional changes correlate with the increased formation of $\mathbf{Li_3N}$.

4.5 Electrochemical Characterization Results

4.5.1 Cyclic voltammetry (CV)

The CV measurements were performed with a potential scan from 0.005 V to 3 V for C1 and C2, and up to 3.3 V for C3, then reversed back, forming a triangular waveform.

The scan rate is 10 mV/s, meaning the voltage changes linearly with time according to the equation :

$$E(t) = E_0 \pm v \cdot t$$

In this equation : $E(t)$ is the instantaneous voltage (in volts) applied to the electrode at time t,
E_0 is the starting potential (in this case, 0.005 V),
v is the scan rate (10 mV/s = 0.01 V/s),
t is the time in seconds.

The sign $\pm$ indicates the direction of the scan :
+ during the forward sweep (increasing voltage),
during the reverse sweep (decreasing voltage).

The scan begins at the initial potential $E_0 = 0.005$ V, which is the point from which the voltage starts increasing.

The potential then rises linearly until it reaches the switching potential E_{max}, which represents the maximum voltage of the scan.

For samples C1 and C2, $E_{\text{max}} = 3.0$ V,
and for sample C3, $E_{\text{max}} = 3.3$ V.

Once the switching potential is reached, the scan is reversed and the potential decreases back to the initial value.

The final potential is equal to the initial potential, completing one full cycle of the triangular waveform used in the cyclic voltammetry process.

4.5.1.1 The First Sample C1

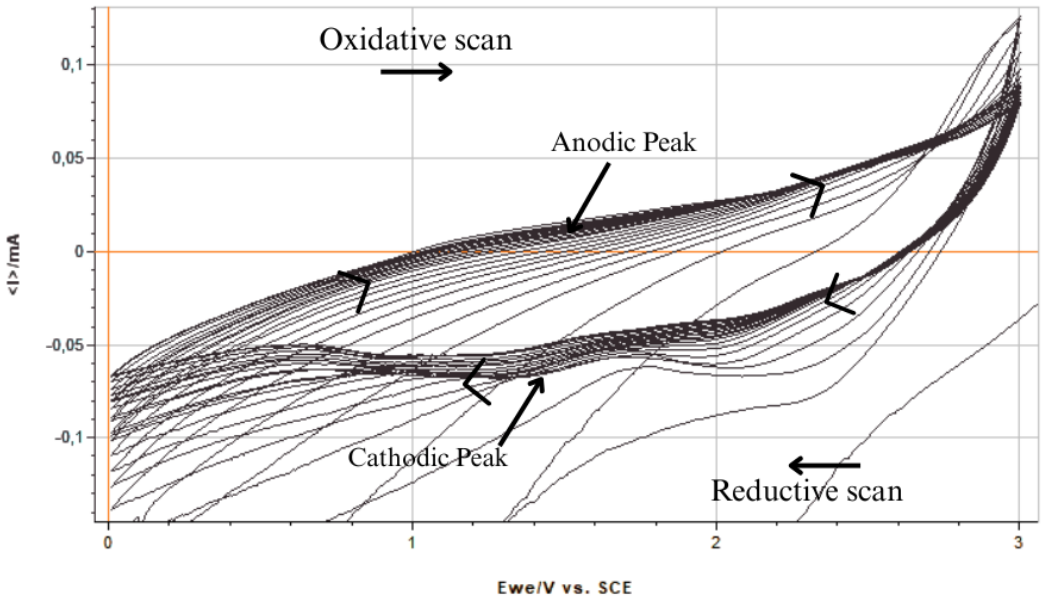

Figure 4.24 – Cyclic voltammetry graph of the cell with sample C1 after 21 cycles

Number of cycles : 21
Voltage range : 0.005 V to 3 V

-The voltammogram shows clear oxidation and reduction peaks, indicating reversible electrochemical behavior. The peaks suggest successful lithium plating and stripping, proving that electron and ion exchange occurs effectively.
The OX/RED Reactions
Reduction :

$$PO_4^{3-} + 4Li^+ + 4e^- \rightarrow P + 4Li_2O$$

Oxidation :

$$4Li \rightarrow 4Li^+ + 4e^-$$

Overall reaction :

$$PO_4^{3-} + 4Li \rightarrow P + 4Li_2O$$

Reduction :

$$Li_3N + 3Li^+ + 3e^- \rightarrow 3Li_2N$$

Oxidation :

$$3Li \rightarrow 3Li^+ + 3e^-$$

Overall reaction :

$$Li_3N + 3Li \rightarrow 3Li_2N$$

-After each cycle, there is a slight decay in peak current, likely due to diffusion limitations : ions take time to migrate across the electrolyte and reach the opposing electrode.

-The relatively wide potential window also allows for observation of side reactions or SEI layer evolution.

4.5.1.2 The Second Sample C2

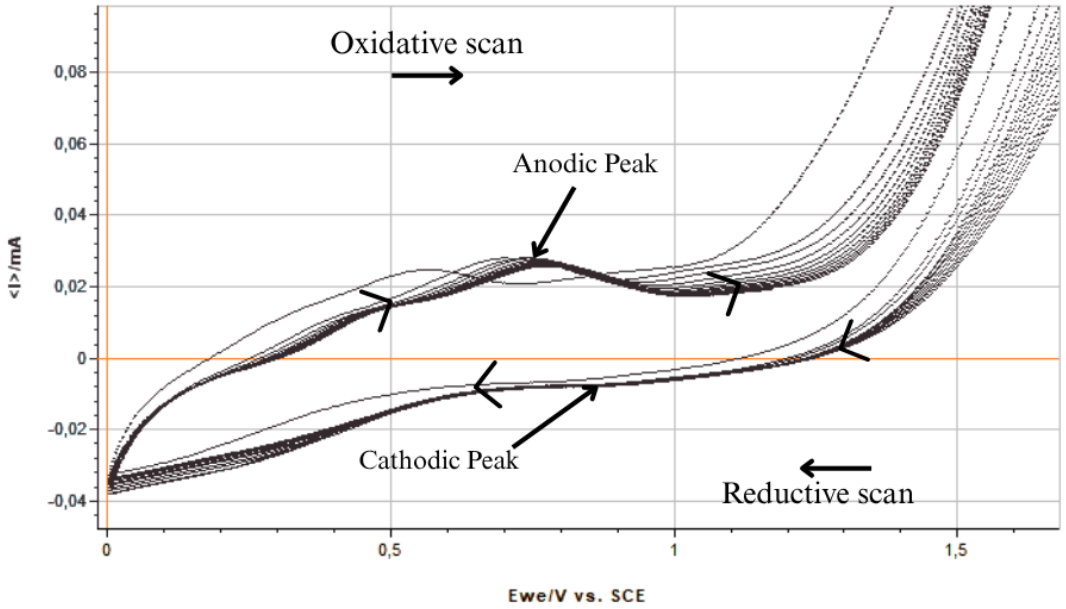

Figure 4.25 – Cyclic voltammetry graph of the cell with sample C2 after 23 cycles

Number of cycles : 23
Voltage range : 0.005 V to 3 V

-Similar to C1, oxidation and reduction peaks are present, confirming functional electrochemical activity. The peaks are less sharp and slightly lower in current, possibly due to a different concentration of NPO-Li that affects interfacial resistance.

The OX/RED Reactions
Reduction :

$$PO_4^{3-} + 4Li^+ + 4e^- \rightarrow P + 4Li_2O$$

Oxidation :

$$4Li \rightarrow 4Li^+ + 4e^-$$

Overall reaction :

$$PO_4^{3-} + 4Li \rightarrow P + 4Li_2O$$

Reduction :

$$Li_3N + 3Li^+ + 3e^- \rightarrow 3Li_2N$$

Oxidation :

$$3Li \rightarrow 3Li^+ + 3e^-$$

Overall reaction :

$$Li_3N + 3Li \rightarrow 3Li_2N$$

-As with C1, a decay is visible after the anodic peak, again due to diffusion-controlled processes.

4.5.1.3 The Third Sample C3

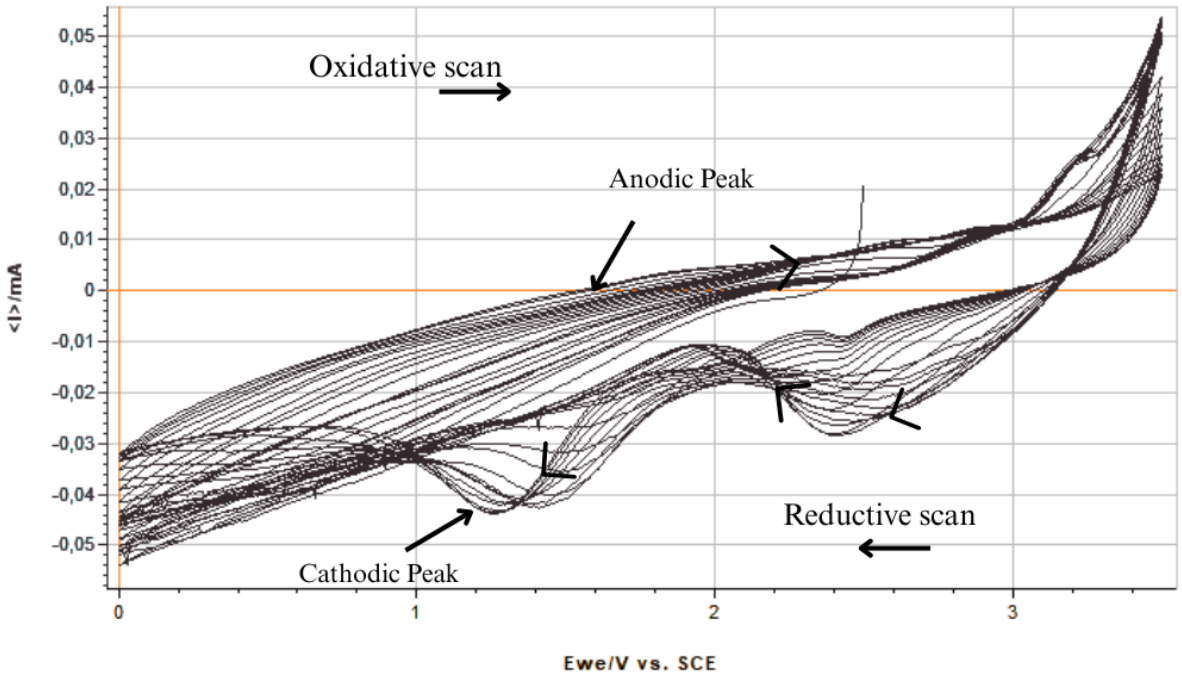

Figure 4.26 – Cyclic voltammetry graph of the cell with sample C3 after 21 cycles

Number of cycles : 21
Voltage range : 0.005 V to 3.3 V

-The extended potential range to 3.3 V allows better detection of oxidation processes. The CV shows pronounced redox peaks, even more structured than in C1 and C2, which might indicate a more defined electrochemical reaction due to the NPO-Li layer at this specific concentration.
The OX/RED Reactions
Reduction :

$$PO_4^{3-} + 4Li^+ + 4e^- \rightarrow P + 4Li_2O$$

Oxidation :

$$4Li \rightarrow 4Li^+ + 4e^-$$

Overall reaction :

$$PO_4^{3-} + 4Li \rightarrow P + 4Li_2O$$

Reduction :

$$Li_3N + 3Li^+ + 3e^- \rightarrow 3Li_2N$$

Oxidation :

$$3\text{Li} \rightarrow 3\text{Li}^{+} + 3e^{-}$$

Overall reaction :

$$\text{Li}_3\text{N} + 3\text{Li} \rightarrow 3\text{Li}_2\text{N}$$

-After the anodic peak, there is a clear decay or tailing in current, typical of ion diffusion limitations as lithium ions slowly migrate to the electrode surface.

-Some irregularities (small disturbances in the wave) could be due to interfacial resistance, bubble formation, or surface modifications during cycling.

4.5.1.4 Conclusion

All three CV graphs confirm the presence of redox activity (oxidation/reduction peaks), proving that the electrochemical system is functional and ion/electron exchange occurs at the electrode–electrolyte interface.

The decay in current after the anodic peak in each case is attributed to ion diffusion—as ions require time to move through the electrolyte, leading to slower current response.

Differences in curve shape and intensity reflect the influence of NPO-Li layer concentration, which affects reaction kinetics, resistance, and interface stability.

4.5.2 Electrochemical Impedance Spectroscopy (EIS)

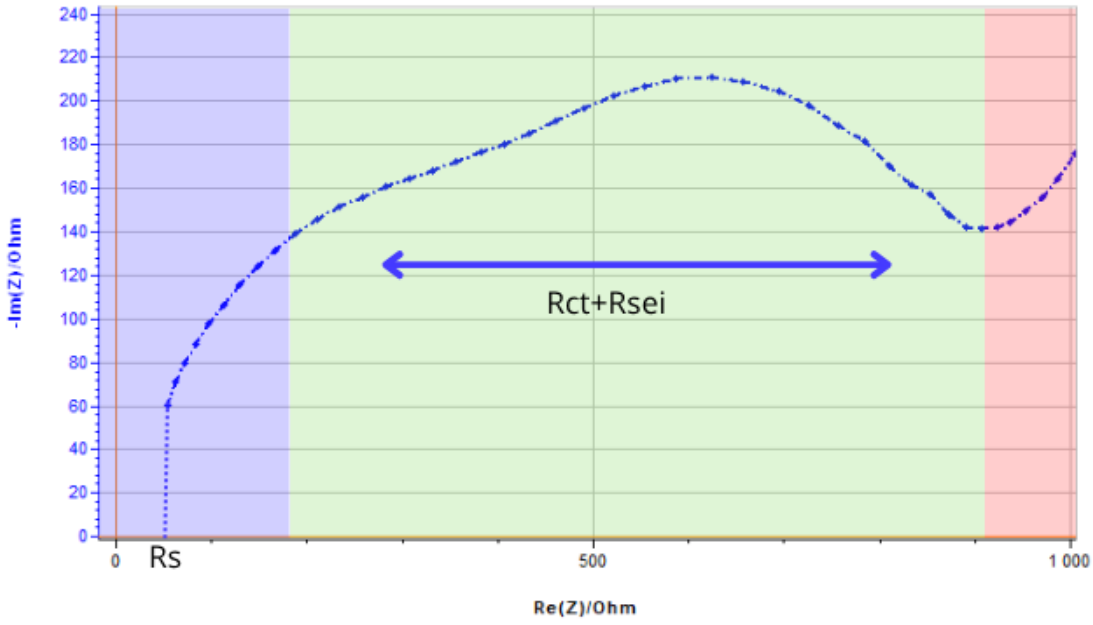

Figure 4.27 – Zoomed Nyquist Plot (High and Mid Frequencies)

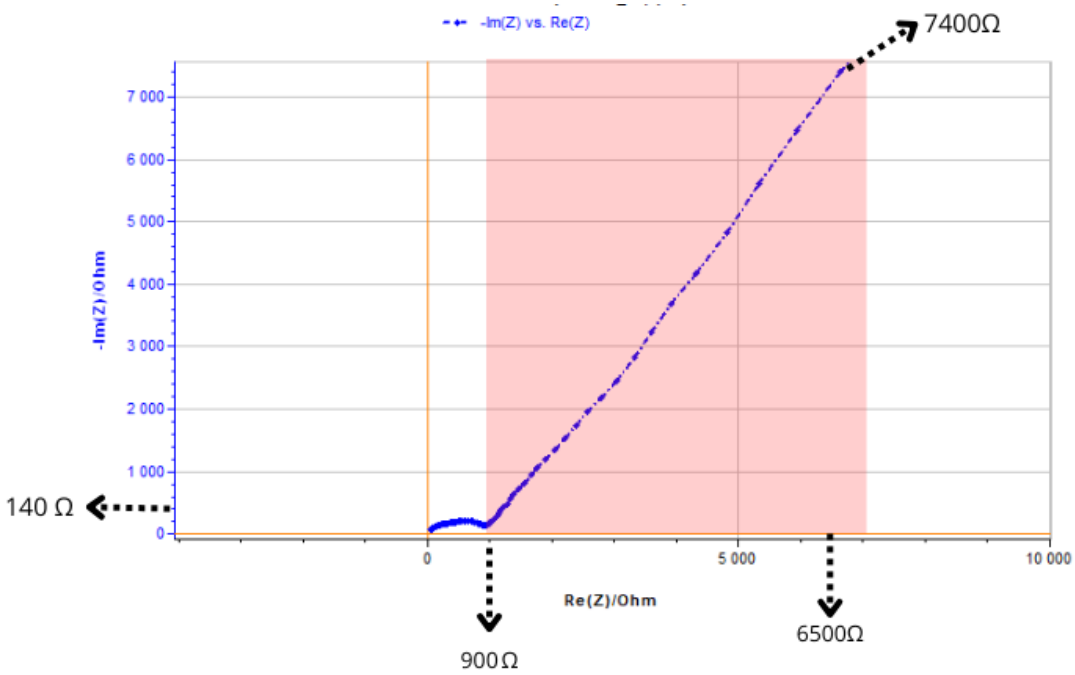

Figure 4.28 – Full Nyquist Plot (Full Frequency Range)

The Nyquist plot obtained from EIS characterization of Sample C1 reveals important information about the electrochemical behavior of the lithium metal cell. The graph displays the imaginary component of impedance ($-Z_{\text{im}}$) versus the real component (Z_{re}), and is interpreted based on the classical division of frequency domains into three regions : high, mid, and low frequency.

Frequency Range	Zone	Physical Meaning
High frequency (left, blue background)	Inductive effects	Artifacts from cell wiring, contact leads, and geometry
Mid frequency (center, green background)	Electrochemical processes	SEI resistance and charge transfer at both electrodes
Low frequency (right, red background)	Ion diffusion	Lithium ion transport through SEI or electrode porosity

Table 4.1 – Interpretation of Nyquist plot regions based on frequency domains

High Frequency Region (Blue Background)
At the left side of the plot (near the origin), the initial sharp rise in impedance may be attributed to parasitic inductive effects, often introduced by the measurement setup—such as cables, cell configuration, or connections. This region does not reflect the intrinsic behavior of the electrochemical cell, but rather setup-related impedance artifacts.

Mid Frequency Region (Green Background)
This region exhibits one or more semicircles, each associated with electrochemical processes at the electrode interfaces. These arcs can be decomposed into the following elements :

- SEI resistance (Solid Electrolyte Interphase) on the anode and cathode
- Charge transfer resistance at the electrode/electrolyte interfaces

From this region, the following parameters can be extracted :

- R_s : Solution resistance (intercept at low Z_{re})
- R_{ct} : Charge transfer resistance (width of the first arc)
- R_{SEI} : Resistance of the SEI (if a second arc is present)

Low-Frequency Region (Red Background)
In the rightmost region of the graph, a sloping line appears—this is the *Warburg tail*, which represents ion diffusion limitations within the cell.

It typically reflects lithium-ion diffusion through the SEI .

The more pronounced and extended the slope, the more dominant the diffusion impedance becomes. In this case, the long low-frequency tail suggests slow lithium-ion transport, likely through a relatively thick SEI or due to restricted diffusion pathways.

Parameter	**Symbol**	**Estimated Value**	**Notes**
Solution resistance	R_s	$\sim 60\,\Omega$	High-frequency intercept
SEI + charge transfer resistance	$R_{\text{SEI}} + R_{ct}$	$\sim 840\,\Omega$	Width of the semicircle
Warburg region start	—	$\sim 900\,\Omega$	Beginning of diffusion slope
Warburg region end	—	$\sim 6500\,\Omega$	End of diffusion tail
Imaginary impedance range	$-\text{Im}(Z)$	$140\,\Omega$ to $\sim 7500\,\Omega$	Indicates strong diffusional impact

Table 4.2 – Estimated EIS parameters from the Nyquist plot of Sample C1

4.5.2.1 Conlusion

The Nyquist plot of Sample C1 displays a well-defined sequence of impedance features :

- An initial intercept at $\sim 60\,\Omega$ corresponding to the solution resistance.
- A large semicircle ranging up to $\sim 900\,\Omega$, representing combined SEI and charge transfer resistance.
- A long, inclined tail beginning at $900\,\Omega$ and extending beyond $6000\,\Omega$ on the real axis and $8000\,\Omega$ on the imaginary axis. This is characteristic of Warburg impedance, confirming that the cell is limited by solid-state lithium-ion diffusion, most likely through the SEI or porous electrode structure.

The presence and clarity of these regions confirm a valid and interpretable EIS measurement, closely matching theoretical expectations. The data indicate a functional battery interface but with noticeable ion diffusion resistance, potentially linked to the SEI thickness or composition.

4.5.3 Galvanostatic charge and discharge

In a galvanostatic charge-discharge test, a constant current is applied to a battery cell, and the resulting voltage is recorded over time. During discharge, a constant negative current is applied, and the voltage decreases as lithium ions leave the anode. During charge, a constant positive current is applied, and the voltage increases as lithium ions are reinserted into the anode. The capacity of the cell is calculated as the product of current and time, expressed in milliampere-hours (mAh). Only the intervals during

which the current is constant and the voltage shows clear evolution (energy transfer is taking place) are used for capacity calculation.

Due to unsatisfactory cyclic voltammetry (CV) performance, Cell C2 was excluded from galvanostatic charge-discharge testing. Only Cells C1 and C3 underwent full galvanostatic cycling, and their capacity values were extracted from the corresponding current–time curves.

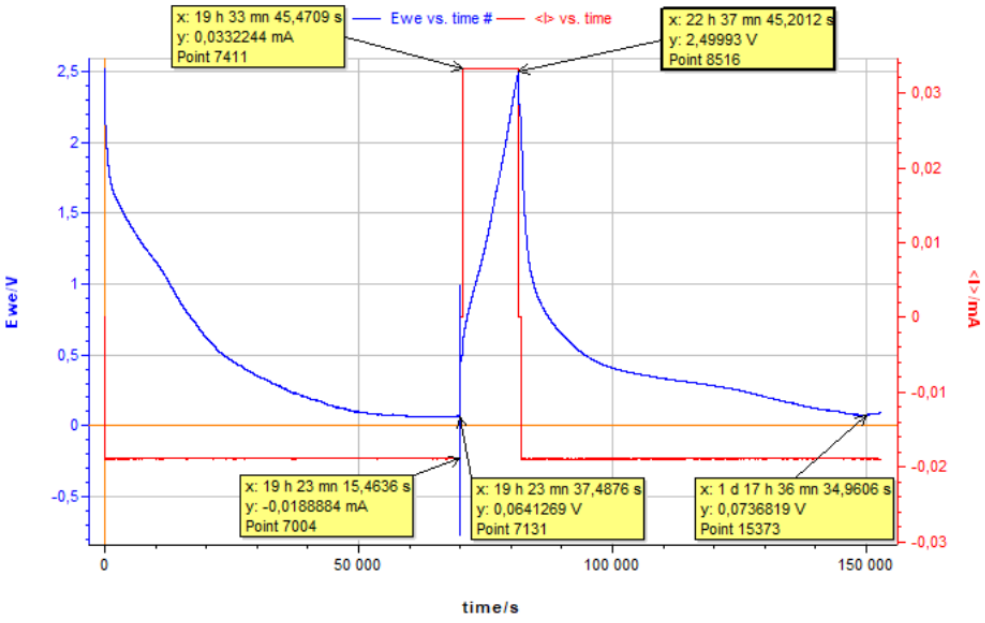

Figure 4.29 – Galvanostatic Charge–Discharge Profile of Cell C3

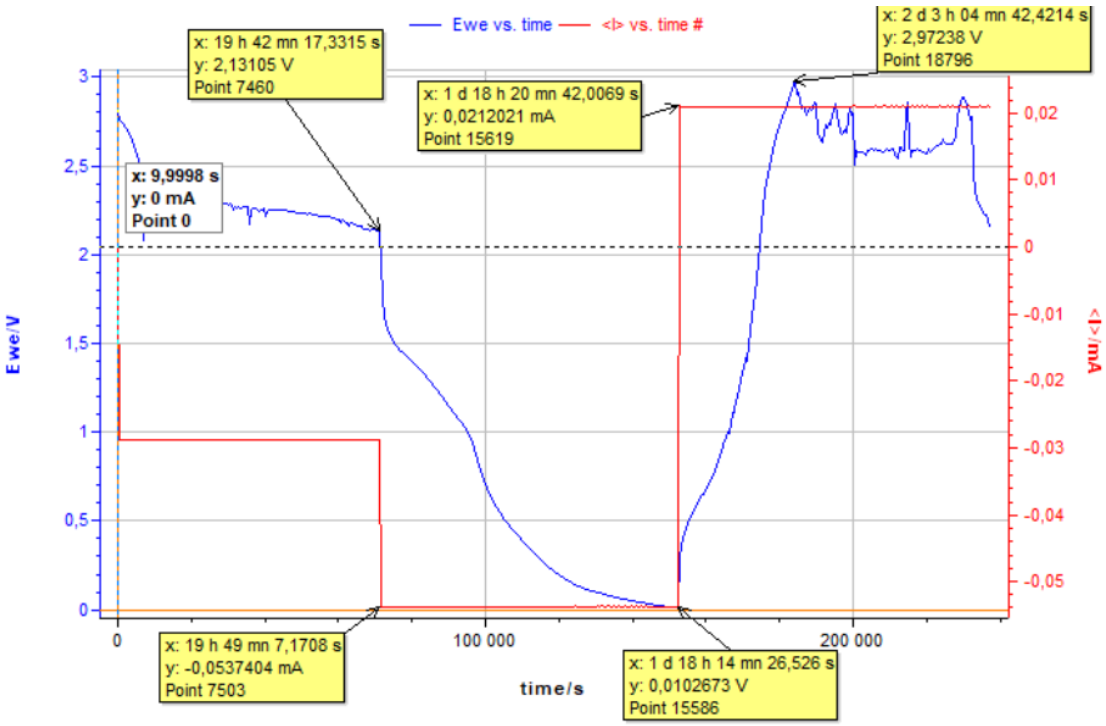

Figure 4.30 – Galvanostatic Charge–Discharge Profile of Cell C3

Cell	Phase	Current (mA)	Duration (h)	Capacity (mAh/cm²)
C1	Discharge	0.0188884	19.3936	0.3664
	Charge	0.0332244	3.2356	0.1075
C3	Discharge	0.0537044	22.1914	1.191
	Charge	0.0212021	22.9328	0.4864

Table 4.3 – Summary of galvanostatic charge–discharge parameters for Cells C1 and C3

4.5.3.1 Conclusion

A comparative analysis between Cells C1 and C3 reveals a significant improvement in the electrochemical performance of Cell C3. It delivered markedly higher discharge and charge capacities across the galvanostatic cycling process. Specifically, Cell C3 achieved a discharge capacity of 1.191 mAh, while Cell C1 reached only 0.3664 mAh. Similarly, the charge capacity of Cell C3 was 0.4864 mAh, in contrast to 0.1075 mAh for Cell C1. These results clearly demonstrate that Cell C3 can store and deliver more energy under identical conditions.

The performance enhancement is primarily attributed to the higher concentration of the NPO-Li protective layer applied to the lithium metal anode in Cell C3. In particular, the presence of Li_3N within this layer plays a crucial role. A greater amount of Li_3N leads to :

- Lower interfacial resistance,
- Improved ionic conductivity, and
- Faster electrochemical reaction kinetics.

These effects are reflected in the galvanostatic profiles by more stable voltage curves, longer discharge durations, and more efficient charge storage.

In Cell C3, the richer Li_3N content results in the formation of a more conductive and stable solid-electrolyte interphase (SEI). This facilitates uniform lithium-ion transport across the electrode–electrolyte interface and reduces polarization effects during cycling. Consequently, Cell C3 exhibits superior energy delivery and retention performance compared to Cell C1.

These findings support the conclusion that optimizing the NPO-Li layer composition—especially by increasing its Li_3N content—is an effective strategy for enhancing the efficiency, stability, and overall lifetime of lithium metal battery cells.

General Conclusion

The objective of this work was to improve the performance of a solid electrolyte material known as **NPO-Li**, which plays a dual role as both a **solid electrolyte** and a **protective SEI (solid electrolyte interphase)** layer.

By carefully controlling its composition and synthesis conditions, the aim was to enhance not only the **ionic conductivity** and **structural stability** of the electrolyte itself, but also the overall **electrochemical performance** of the electrode–electrolyte interface.

A comprehensive approach was adopted, combining :

- **Structural** characterization (XRD),
- **Morphological** analysis (SEM/EDS),
- **Electrochemical** testing (CV, EIS, galvanostatic cycling).

The results demonstrated that the formation of key phases such as $\mathbf{Li_3N}$ and $\mathbf{Li_3PO_4}$, under optimized conditions, contributed positively to the material's **conductivity and stability**.

Among the tested samples, some compositions showed significant improvements in **phase purity**, **porosity control**, and **interfacial behavior**.

This study confirms the potential of **compositionally engineered NPO-Li layers** to serve as efficient solid electrolytes and SEI-forming materials in advanced lithium battery systems.

These findings provide a **solid foundation** for future work aimed at designing **high-performance, all-solid-state batteries**.

Future Perspectives

- **Develop a more controlled deposition process** to ensure uniform layer thickness and minimize post-cycling porosity.
- **Explore the thermal stability** of the electrolytes.
- **Integrate the NPO-Li layer** into full solid-state battery configurations.
- **Evaluate long-term electrochemical stability** under extended cycling conditions.
- **Study the interfacial compatibility** between NPO-Li and various electrode materials.
- **Investigate the interfacial behavior** between the silicon electrode and the solid electrolyte.
- **Use grazing-incidence XRD** to detect surface phases more clearly.
- **Test the electrolyte** under different pressures and temperatures.

References

[1] Y. J. Chabal, K. Cho, and C. L. Hinkle. Safer high-performance electrodes, solid electrolytes, and interface reactions for lithium-ion batteries. https://qaci.sial.com/technical-documents/articles/materials-science/safer-highperformance-electrodes-solid-electrolytes.html, n.d. Also LIB Materials available from : https://www.aldrich.com/lib.

[2] Z. Khan, M. Vagin, and X. Crispin. Unknown title.

[3] Qaisar Abbas, Mojtaba Mirzaeian, Michael R. C. Hunt, Rizwan Raza, et al. Current state and future prospects for electrochemical energy storage and conversion systems. *Energies*, 13(21) : 5847, 2020. doi : 10.3390/en13215847. URL https://www.mdpi.com/1996-1073/13/21/5847.

[4] M. Mirzaeian, Q. Abbas, A. Ogwu, P. Hall, M. Goldin, M. Mirzaeian, and H.F. Jirandehi. Electrode and electrolyte materials for electrochemical capacitors. *International Journal of Hydrogen Energy*, 42 :25565–25587, 2017. doi : 10.1016/j.ijhydene.2017.08.093.

[5] Gary Clark. Essential guide to battery electrolyte, June 2025. URL https://holobattery.com/battery-electrolyte/. Accessed via Holobattery "Essential Guide to Battery Electrolyte".

[6] Naeblys. How a lithium ion battery works, 3d render, section. battery charging and discharging. ions flow from the anode to the cathode separated by a liquid electrolyte as the battery discharges energy, 2025. URL https://stock.adobe.com/images/how-a-lithium-ion-battery-works-3d-render-section-battery-charging-and-discharging-ions-flow-from-the-an 295099244. Illustration premium par Naeblys (licence standard/étendue).

[7] BYJU'S – The Learning App. Difference between primary cell and secondary cell, June 2025. URL https://byjus.com/chemistry/difference-between-primary-cell-and-secondary-cell/. Consulted via BYJU'S – The Learning App.

[8] Y. Yu, Y. Liu, and J. Xie. Title of the article. *ACS Applied Materials Interfaces*, 13(18), 2021. doi : DOIifavailable.

[9] X. Fan, X. Ji, L. Chen, J. Chen, T. Deng, F. Han, J. Yue, N. Piao, R. Wang, X. Zhou, X. Xiao, L. Chen, and C. Wang. N/a. *Nature Energy*, 4 :882, 2019.

[10] J. R. Nair, L. Imholt, G. Brunklaus, and M. Winter. N/a. *Electrochem. Soc. Interface*, 28 :55, 2019.

[11] H. Yang and N. Wu. N/a. *Energy Sci. Eng.*, 10 :1643, 2022.

[12] M. Weiss, F. J. Simon, M. R. Busche, T. Nakamura, D. Schröder, F. H. Richter, and J. Janek. N/a. *Electrochem. Energy Rev.*, 3 :221, 2020.

[13] X. Fan, X. Ji, L. Chen, J. Chen, T. Deng, F. Han, J. Yue, N. Piao, R. Wang, X. Zhou, X. Xiao, L. Chen, and C. Wang. Energy 2019. *Nat. Energy*, 4 :882, 2019.

[14] A. Hosseinioun and E. Paillard. Cross-linked polymer gel electrolytes. *J. Membr. Sci.*, 594 : 117456, 2020.

[15] J.-P. Hoffknecht, A. Wettstein, J. Atik, C. Krause, J. Thienenkamp, G. Brunklaus, M. Winter, D. Diddens, A. Heuer, and E. Paillard. Plasticized polymer electrolytes for advanced batteries. *Adv. Energy Mater.*, 13(2202789), 2023.

[16] N. Kamaya, K. Homma, Y. Yamakawa, M. Hirayama, R. Kanno, M. Yonemura, T. Kamiyama, Y. Kato, S. Hama, K. Kawamoto, and A. Mitsui. A lithium superionic conductor. *Nat. Mater.*, 10 :682, 2011.

[17] Y. Kato, S. Hori, T. Saito, K. Suzuki, M. Hirayama, A. Mitsui, M. Yonemura, H. Iba, and R. Kanno. High-power all-solid-state batteries using sulfide superionic conductors. *Nat. Energy*, 1 :16030, 2016.

[18] S. Yu, Q. Xu, X. Lu, Z. Liu, A. Windmüller, C.-L. Tsai, A. Buchheit, H. Tempel, H. Kungl, H.-D. Wiemhöfer, and R.-A. Eichel. Hybrid solid-state electrolytes for lithium batteries. *ACS Appl. Mater. Interfaces*, 13 :61067, 2021.

[19] M. Uitz et al. *J. Electrochem. Soc.*, 164 :A3503, 2017.

[20] F. Ma, Y. Zhang, Y. Zhao, H. Zhang, Y. Wang, and Y. Huang. Preparation and evaluation of high lithium ion conductivity $li_{1.3}al_{0.3}ti_{1.7}(po_4)_3$ solid electrolyte obtained using a new solution method. *Solid State Ionics*, 288 :235–239, 2016. doi : 10.1016/j.ssi.2016.02.007.

[21] Murata Manufacturing Co., Ltd. Basic lithium-ion battery (part 4) : What are solid-state batteries ?, March 2022. URL https://article.murata.com/en-global/article/basic-lithium-ion-battery-4. Série « The lithium-ion batteries changing our lives », supervisée par Ryoji Kanno.

[22] Isidor Buchmann. Battery packaging—a look at old and new systems. http://www.batteryuniversity.com/print-partone-9.htm, 2004. Accessed January 11, 2010.

[23] X. B. Cheng, R. Zhang, C. Z. Zhao, and Q. Zhang. Review—challenges for rechargeable li batteries. *Chemical Reviews*, 117 :10403, 2017.

[24] W. Li, H. Yao, K. Yan, G. Zheng, Z. Liang, Y.-M. Chiang, and Y. Cui. Improved lithium deposition via additive-modified electrolytes. *Nature Communications*, 6 :7436, 2015.

[25] C. P. Yang, Y. X. Yin, S. F. Zhang, N. W. Li, and Y. G. Guo. 3d current collector for dendrite-free lithium metal anodes. *Nature Communications*, 6 :8058, 2015.

[26] Z.-J. Zheng, Q. Su, Q. Zhang, X.-C. Hu, Y.-X. Yin, R. Wen, H. Ye, Z.-B. Wang, and Y.-G. Guo. Mof-coated 3d host for stable lithium metal anode. *Nano Energy*, 64 :103910, 2019.

[27] C. Yang, L. Zhang, B. Liu, S. Xu, T. Hamann, D. McOwen, J. Dai, W. Luo, Y. Gong, E. D. Wachsman, and L. Hu. 3d ion-conductive host for lithium metal anodes. *Proceedings of the National Academy of Sciences USA*, 115 :3770, 2018.

[28] Author(s) Unknown.

[29] S.C. Nagpure et al. Impacts of lean electrolyte on cycle life for rechargeable li metal batteries. *J. Power Sources*, 407 :53–62, 2018.

[30] Qingyu Wang, Bin Liu, Yuanhao Shen, Jingkun Wu, Zequan Zhao, Cheng Zhong, and Wenbin Hu. Confronting the challenges in lithium anodes for lithium metal batteries. *Advanced Science*, 8(17) :2101111, 2021. doi : 10.1002/advs.202101111.

[31] Joseph Nzabahimana, Zhifang Liu, Songtao Guo, Xianluo Hu, et al. Top-down synthesis of silicon/carbon composite anode materials for lithium-ion batteries : Mechanical milling and etching. *ChemSusChem*, 13(8) :2195–2210, March 2020. doi : 10.1002/cssc.201903155.

[32] Power Africa (USAID), CLDP, and ALSF. Understanding energy storage, June 2022. Page 7.

[33] P. Brault and A. Percheron-Guégan. Les supercondensateurs : une voie complémentaire aux batteries. In C. J. Allègre and D. Roux, editors, *L'énergie à découvert*, pages 131–133. CNRS Éditions, 2013. URL https://books.openedition.org/editionscnrs/10943?lang=en.

[34] S. Patoux. Stockage de l'énergie, aspects fondamentaux. In C. J. Allègre and D. Roux, editors, *L'énergie à découvert*, pages 123–130. CNRS Éditions, 2013.

[35] I. Shabbir and M. Mirzaeian. Feasibility analysis of different cogeneration systems for a paper mill to improve its energy efficiency. *Int. J. Hydrogen Energy*, 41 :16535–16548, 2016.

[36] C.F. Kutscher. *Principles of Sustainable Energy Systems.* Informa UK Limited, Colchester, UK, 3rd edition, 2018.

[37] A. Dehghani-Sanij, S. Dehghani, G. Naterer, and Y. Muzychka. Marine icing phenomena on vessels and offshore structures : Prediction and analysis. *Ocean Eng.*, 143 :1–23, 2017.

[38] A. Khajuria and N. Ravindranath. Climate change vulnerability assessment : Approaches dpsir framework and vulnerability index. *J. Earth Sci. Clim. Chang.*, 3, 2012.

[39] M.S. Guney and Y. Tepe. Classification and assessment of energy storage systems. *Renew. Sustain. Energy Rev.*, 75 :1187–1197, 2017.

[40] L. Bird, D. Lew, M. Milligan, E.M. Carlini, A. Estanqueiro, D. Flynn, E. Gomez-Lazaro, H. Holttinen, N. Menemenlis, A. Orths, et al. Wind and solar energy curtailment : A review of international experience. *Renew. Sustain. Energy Rev.*, 65 :577–586, 2016.

[41] L. Lu, X. Han, J. Li, J. Hua, and M. Ouyang. A review on the key issues for lithium-ion battery management in electric vehicles. *J. Power Sour.*, 226 :272–288, 2013.

[42] T.P. Mernagh. *A Review of Australian Salt Lakes and Assessment of Their Potential for Strategic Resources.* Geosci. Aust. Record 2013/39. Geoscience Australia, Canberra, Australia, 2013.

[43] T.C. Wanger. The lithium future-resources, recycling, and the environment. *Conserv. Lett.*, 4 : 202–206, 2011.

[44] H.D. Dawouda, T.M. Altahtamounia, M.M. Zaghoa, and N. Bensalahb. A brief overview of flexible cnt/pani super capacitors. *Mater. Sci. Nanotechnol.*, 1 :23–36, 2017.

[45] M. Watanabe and D.A. Tryk. Fuel cells : An overview with emphasis on polymer electrolyte fuel cells. In *Electrochemical Science for a Sustainable Society*, pages 51–94. Springer Science and Business Media LLC, Berlin/Heidelberg, Germany, 2017.

[46] H.L. Ferreira, R. Garde, G. Fulli, W. Kling, and J.P. Lopes. Characterisation of electrical energy storage technologies. *Energy*, 53 :288–298, 2013. doi : 10.1016/j.energy.2013.02.037.

[47] K. M. Abraham. Prospects and limits of energy storage in batteries. *The Journal of Physical Chemistry Letters*, 6 :830–844, 2015. Pages 1–6.

[48] Dae Kyeong Kim, Susumu Yoneoka, Ali Zain Banatwala, and Yu-Tack Kim. *Handbook on Battery Energy Storage System.* Asian Development Bank, December 2018. Pages 7–8.

[49] Junsheng Zheng. *Lithium-Ion Batteries and Li-Ion Capacitors : From Fundamentals to Practical Applications.* Elsevier, 2024.

[50] David Linden and Thomas B. Reddy. *Handbook of Batteries.* McGraw-Hill, 2002.

[51] A. J. Jacobson and L. F. Nazar. Intercalation chemistry. In *Encyclopedia of Inorganic and Bioinorganic Chemistry.* 2011.

[52] J. M. Tarascon and M. Armand. Issues and challenges facing rechargeable lithium batteries. *Nature*, 414(6861) :359–367, 2001.

[53] N. Meena, V. Baharwani, and D. Sharma. Charging and discharging characteristics of lead acid and li-ion batteries. In *Power and Energy Systems : Towards Sustainable Energy (PESTSE), 2014*. IEEE, 2014.

[54] Elton J. Cairns. Batteries – overview. In *Encyclopedia of Energy*, volume 1, pages 117–126. Elsevier, 2004. pages 117–118.

[55] Elton J. Cairns. Batteries – overview. In *Encyclopedia of Energy*, volume 1, pages 117–126. Elsevier, 2004. pages 119–121.

[56] Elton J. Cairns. Batteries – overview. In *Encyclopedia of Energy*, volume 1, pages 121–122. Elsevier, 2004. Page 121–122.

[57] Elton J. Cairns. Batteries – overview. In Cutler J. Cleveland, editor, *Encyclopedia of Energy*, volume 1, pages 123–127. Elsevier, 2004. Page 123–127.

[58] C. P. Grey and D. S. Hall. Title of the article. *Nature Communications*, 11 :6279, 2020. doi : DOIifavailable.

[59] J. R. Nair, L. Imholt, G. Brunklaus, and M. Winter. Electrochem. soc. interface. *Electrochem. Soc. Interface*, 28 :55, 2019.

[60] S. Sen, S. Malunavar, D. Radhakrishnan, C. Narayana, P. Soudant, R. Bouchet, and A. J. Bhattacharyya. Mol. syst. des. eng. *Mol. Syst. Des. Eng.*, 1 :391, 2016.

[61] J. Y. Song, Y. Y. Wang, and C. C. Wan. J. power sources. *J. Power Sources*, 77 :183, 1999.

[62] A. M. Stephan. Eur. polym. j. *Eur. Polym. J.*, 42 :21, 2006.

[63] K. Xu. Chem. rev. *Chem. Rev.*, 104 :4303, 2004.

[64] Z. Chang et al. Title... *Sci. Rep.*, 6 :28421, 2016.

[65] S. Sen et al. *J. Mater. Chem. A*, 9 :18701, 2021.

[66] P. G. Wolynes. *Ann. Rev. Phys. Chem.*, 31 :345, 1980.

[67] D. Hubble et al. *Energy Environ. Sci.*, 15 :550, 2022.

[68] J. B. Goodenough and K.-S. Park. *J. Am. Chem. Soc.*, 135 :1167, 2013.

[69] H. Pan et al. *Energy Fuels*, 34 :11942, 2020.

[70] S. Park et al. *Nat. Commun.*, 12 :838, 2021.

[71] Q. Wu et al. *ACS Appl. Energy Mater.*, 4 :10234, 2021.

[72] X. Ban et al. *J. Phys. Chem. C*, 122 :9852, 2018.

[73] F. Ahmed, I. Choi, M. d. M. Rahman, H. Jang, T. Ryu, S. Yoon, L. Jin, Y. Jin, and W. Kim. Title not provided. *ACS Appl. Mater. Interfaces*, 11 :34930, 2019.

[74] R. Bouchet, S. Maria, R. Meziane, A. Aboulaich, L. Lienafa, J.-P. Bonnet, T. N. T. Phan, D. Bertin, D. Gigmes, D. Devaux, R. Denoyel, and M. Armand. Title not provided. *Nat. Mater.*, 12 :452, 2013.

[75] F. Makhlooghiazad, L. A. O'Dell, L. Porcarelli, C. Forsyth, N. Quazi, M. Asadi, O. Hutt, D. Mecerreyes, M. Forsyth, and J. M. Pringle. Title not provided. *Nature Materials*, 21 :228, 2021.

[76] S. Parveen, P. Sehrawat, and S. A. Hashmi. Title not provided. *ACS Applied Energy Materials*, 5 :930, 2021.

[77] L. Bai, S. Ghiassinejad, J. Brassinne, Y. Fu, J. Wang, H. Yang, A. Vlad, A. Minoia, R. Lazzaroni, and J.-F. Gohy. Title not provided. *ACS Applied Materials & Interfaces*, 13 :44844, 2021.

[78] C. Cao, Z.-B. Li, X.-L. Wang, X.-B. Zhao, and W.-Q. Han. *Front. Energy Res.*, 2 :25, 2014.

[79] V. Thangadurai, S. Narayanan, and D. Pinzaru. *Chem. Soc. Rev.*, 43 :4714, 2014.

[80] A. Martínez-Juárez et al. *J. Phys. Chem. B*, 102 :372, 1998.

[81] H. Yamane et al. *Solid State Ion.*, 25 :183, 1987.

[82] H. Liu et al. *Chem. Mater.*, 32 :671, 2020.

[83] O. Bohnke et al. *Solid State Ion.*, 91 :21, 1996.

[84] Z. Liu et al. *ACS Energy Lett.*, 6 :298, 2021.

[85] M. Weiss, F. J. Simon, M. R. Busche, T. Nakamura, D. Schröder, F. H. Richter, and J. Janek. Title... *Electrochem. Energy Rev.*, 3 :221, 2020.

[86] L. Zhou et al. *Acc. Chem. Res.*, 54 :2717, 2021.

[87] H.-J. Deiseroth et al. *Angew. Chem., Int. Ed.*, 47 :755, 2008.

[88] A. Kuhn et al. *J. Mater. Chem. A*, 2 :6100, 2014.

[89] J. C. Bachman et al. *Chem. Rev.*, 116 :140, 2016.

[90] I. Hanghofer et al. *Chem. Mater.*, 31 :4591, 2019.

[91] D. H. S. Tan et al. *Science*, 373 :1494, 2021.

[92] S. Xu et al. *Adv. Funct. Mater.*, 31 :2004239, 2021.

[93] C.-L. Tsai et al. *Sustain. Energy Fuels*, 3 :280, 2019.

[94] Y.-G. Lee et al. *Nat. Energy*, 5 :299, 2020.

[95] S. Cangaz et al. *Adv. Energy Mater.*, 10 :2001320, 2020.

[96] F. Hippauf et al. *Energy Stor. Mater.*, 21 :390, 2019.

[97] P. Minnmann et al. *Adv. Energy Mater.*, 12 :2201425, 2022.

[98] T. Nagaura and K. Tozawa. Lithium ion rechargeable battery. *Prog. Batter. Sol. Cells*, 9 : 209–211, 1990.

[99] C. M. Julien, A. Mauger, A. Vijh, and K. Zaghib. *Lithium Batteries : Science and Technology*. Springer, 2015.

[100] Thomas G. Goonan. Lithium use in batteries. U.S. Geological Survey Circular 1371, 2011. URL https://pubs.usgs.gov/circ/1371/. Manuscript approved July 18, 2011. Edited by Anna N. Glover and Jane Eggleston.

[101] Green Batteries. Lithium-ion battery frequently asked questions. http://www.greenbatteries.com/libafa.html, 2009. Accessed January 11, 2010.

[102] Linda Gaines and Roy Cuenca. Costs of lithium-ion batteries for vehicles. Technical Report ANL/ESD-42, Argonne National Laboratory, 2000. URL http://www.transportation.anl.gov/pdfs/TA/149.pdf.

[103] Amy Hsiao and Brent Richter. Cost analysis of lithium-ion battery systems, 2008. Internal technical report.

[104] D.L. Anderson and Dalia Patiño-Echeverri. An evaluation of current and future costs for lithium-ion batteries for use in electrified vehicle powertrains, 2009. URL http://dukespace.lib.duke.edu/dspace/bitstream/10161/1007/1/Li-Ion_Battery_costs_-_MP_Final.pdf.

[105] Andrew Burke and Marshall Miller. Performance characteristics of lithium-ion batteries of various chemistries. In *EVS24 : International Battery, Hybrid and Fuel Cell Electric Vehicle Symposium*, Stavanger, Norway, 2009. May 13–16.

[106] P.A. Nelson, D.J. Santini, and James Barnes. Factors determining the manufacturing costs of lithium-ion batteries for phevs. In *EVS24 : International Battery, Hybrid, and Fuel Cell Electric Vehicle Symposium*, Stavanger, Norway, 2009.

[107] X. B. Cheng, R. Zhang, C. Z. Zhao, and Q. Zhang. Chem. rev. *Chemical Reviews*, 117 :10403, 2017.

[108] M. K. Aslam, Y. Niu, T. Hussain, H. Tabassum, W. Tang, M. Xu, and R. Ahuja. Nano energy. *Nano Energy*, 86 :106142, 2021.

[109] D. Lin, Y. Liu, and Y. Cui. Nat. nanotechnol. *Nature Nanotechnology*, 12 :194, 2017.

[110] K. Yan et al. Nat. energy. *Nature Energy*, 1 :16010, 2016.

[111] C. Jin et al. Nat. energy. *Nature Energy*, 6 :378, 2021.

[112] M. Wan et al. Nat. commun. *Nature Communications*, 11 :829, 2020.

[113] H. Ye et al. Acs cent. sci. *ACS Central Science*, 6 :661, 2020.

[114] W. Li et al. Nat. commun. *Nature Communications*, 6 :7436, 2015.

[115] H. Zhang et al. Angew. chem., int. ed. *Angewandte Chemie International Edition*, 57 :15002, 2018.

[116] H. Wang et al. Adv. sci. *Advanced Science*, 8 :2100684, 2021.

[117] Y. Cheng et al. Nano energy. *Nano Energy*, 63 :103854, 2019.

[118] H. Ye et al. Angew. chem., int. ed. engl. *Angewandte Chemie International Edition*, 58 :1094, 2019.

[119] X. Ke et al. Acs appl. mater. interfaces. *ACS Applied Materials Interfaces*, 10 :13552, 2018.

[120] C. P. Yang et al. Nat. commun. *Nature Communications*, 6 :8058, 2015.

[121] C.-Y. Wang et al. Nano energy. *Nano Energy*, 74 :104817, 2020.

[122] S. H. Wang et al. Nat. commun. *Nature Communications*, 10 :4930, 2019.

[123] Y.-Q. Feng et al. Nano energy. *Nano Energy*, 73 :104731, 2020.

[124] S. H. Wang, Y. X. Yin, T. T. Zuo, W. Dong, J. Y. Li, J. L. Shi, C. H. Zhang, N. W. Li, C. J. Li, and Y. G. Guo. Stable lithium metal anodes via regulating the concentration gradient of lithium ions at interface. *Advanced Materials*, 29 :1703729, 2017.

[125] Y.-Q. Feng, Z.-J. Zheng, C.-Y. Wang, Y.-X. Yin, H. Ye, F.-F. Cao, and Y.-G. Guo. Facile surface nanocrystallization enabling fast wettability of molten lithium. *Nano Energy*, 73 :104731, 2020.

[126] Z.-J. Zheng, Q. Su, Q. Zhang, X.-C. Hu, Y.-X. Yin, R. Wen, H. Ye, Z.-B. Wang, and Y.-G. Guo. Hybrid host design enabling uniform li deposition with low volume change. *Nano Energy*, 64 : 103910, 2019.

[127] J.B. Goodenough and Y. Kim. Challenges for rechargeable li batteries. *Chem. Mater.*, 22 : 587–603, 2010.

[128] M.S. Whittingham. Electrical energy storage and intercalation chemistry. *Science*, 192 :1126–1127, 1976.

[129] J.M. Tarascon and M. Armand. Issues and challenges facing rechargeable lithium batteries. *Nature*, 414 :359–367, 2001.

[130] S. Megahed and B. Scrosati. Lithium-ion rechargeable batteries. *J. Power Sources*, 51, 1994.

[131] M. et al. Winter. Before li ion batteries. *Chem. Rev.* doi : 10.1021/acs.chemrev.8b00422.

[132] J. et al. Lu. State-of-the-art characterization techniques for advanced lithium-ion batteries. *Nat. Energy*, 2 :17011, 2017.

[133] J. et al. Zheng. Understanding the unique interfaces between concentrated electrolytes and electrodes. *Adv. Sci.*, 2017.

[134] J. et al. Qian. High rate and stable cycling of lithium metal anode. *Nat. Commun.*, 6 :6362, 2015.

[135] Z. et al. Zeng. Non-flammable electrolytes with high salt-to-solvent ratios for li-ion and li-metal batteries. *Nat. Energy*, 3 :674–681, 2018.

[136] S. et al. Chen. High-voltage lithium-metal batteries enabled by localized high-concentration electrolytes. *Adv. Mater.*, 1706102 :1–7, 2018.

[137] X. et al. Ren. Localized high-concentration sulfone electrolytes for high-efficiency lithium-metal batteries. *Chem*, 4 :1877–1892, 2018.

[138] Y. et al. Li. Atomic structure of sensitive battery materials and interfaces revealed by cryo-electron microscopy. *Science*, 358, 2017.

[139] M.J. et al. Zachman. Cryo-stem mapping of solid–liquid interfaces and dendrites in lithium-metal batteries. *Nature*, 560 :345–349, 2018.

[140] W. Xu et al. Lithium metal anodes for rechargeable batteries. *Energy Environ. Sci.*, 7 :513–537, 2014.

[141] K. Nishikawa et al. In situ observation of dendrite growth of electrodeposited li metal. *J. Electrochem. Soc.*, 157 :A1212, 2010.

[142] X.-B. Cheng et al. Recent advances in energy chemistry between solid-state electrolyte and safe lithium-metal anodes. *Chem*, 5 :74–96, 2019.

[143] D. Lu et al. Failure mechanism for fast-charged lithium metal batteries with liquid electrolytes. *Adv. Energy Mater.*, 5 :1400993, 2015.

[144] Yuanhao Shen, Jingkun Wu, Zequan Zhao, Cheng Zhong, Wenbin Hu, Qingyu Wang, and Bin Liu. Confronting the challenges in lithium anodes for lithium metal batteries. *Advanced Science*, 8(17) :2101111, 2021. doi : 10.1002/advs.202101111.

[145] M. Arakawa and J. Yamaki. Lithium electrode cycleability and morphology dependence on current density. *Journal of Power Sources*, 43 :27–35, 1993.

[146] K.-H. Chen et al. Dead lithium : mass transport effects on voltage, capacity, and failure of lithium metal anodes. *Journal of Materials Chemistry A*, 2017. doi : 10.1039/c7ta00371d.

[147] J. Zheng et al. Research progress towards understanding the unique interfaces between concentrated electrolytes and electrodes for energy storage applications. *Advanced Science*, 4 :1–19, 2017.

[148] E. Peled and S. Menkin. Review—sei : Past, present and future. *Journal of The Electrochemical Society*, 164 :A1703–A1719, 2017.

[149] X.B. Cheng, R. Zhang, C.Z. Zhao, and Q. Zhang. A review of solid electrolyte interphases on lithium metal anode. *Advanced Science*, 3 :1–20, 2015.

[150] J. M. Tarascon and M. Armand. Issues and challenges facing rechargeable lithium batteries. *Nature*, 414 :359–367, 2001.

[151] D. Larcher, S. Beattie, M. Morcrette, K. Edstrom, J.-C. Jumas, and J.-M. Tarascon. Recent findings and prospects in the field of pure metals as negative electrodes for li-ion batteries. *Journal of Materials Chemistry*, 17 :3759–3772, 2007.

[152] M. Obrovac and L. Krause. Reversible cycling of crystalline silicon powder. *Journal of The Electrochemical Society*, 154 :A103–A108, 2007.

[153] C. K. Chan, H. Peng, G. Liu, K. McIlwrath, X. F. Zhang, R. A. Huggins, and Y. Cui. High-performance lithium battery anodes using silicon nanowires. *Nature Nanotechnology*, 3 :31–35, 2008.

[154] L. Pan, H. Wang, D. Gao, S. Chen, L. Tan, and L. Li. Silicon/carbon composites for high-performance lithium-ion batteries. *Chemical Communications*, 50 :5878–5880, 2014.

[155] R. Yi, F. Dai, M. L. Gordin, S. Chen, and D. Wang. Micro-sized si-c composite with interconnected nanoscale building blocks as high-performance anodes for lithium-ion batteries. *Advanced Energy Materials*, 3 :295–300, 2013.

[156] N. Liu, K. Huo, M. T. McDowell, J. Zhao, and Y. Cui. Rice husk-derived silicon nanomaterials for high-performance lithium battery anodes. *Scientific Reports*, 3, 2013.

[157] J. Song, S. Chen, M. Zhou, T. Xu, D. Lv, M. L. Gordin, T. Long, M. Melnyk, and D. Wang. Microscale silicon/carbon composites as high-performance anodes for practical application in lithium-ion batteries. *Journal of Materials Chemistry A*, 2 :1257–1262, 2014.

[158] G. Hwang, H. Park, T. Bok, S. Choi, S. Lee, I. Hwang, N.-S. Choi, K. Seo, and S. Park. Porous si anodes for lithium-ion batteries using a scalable nacl-templating method. *Chemical Communications*, 51 :4429–4432, 2015.

[159] J. Graetz, C. Ahn, R. Yazami, and B. Fultz. Nanocrystalline and thin film germanium electrodes with high lithium capacity and high rate capabilities. *Electrochemical and Solid-State Letters*, 6 :A194–A197, 2003.

[160] N. Liu, Z. Lu, J. Zhao, M. T. McDowell, H.-W. Lee, W. Zhao, and Y. Cui. A pomegranate-inspired nanoscale design for large-volume-change lithium battery anodes. *Nature Nanotechnology*, 9 :187–192, 2014.

[161] L. Y. Yang, H. Z. Li, J. Liu, Z. Q. Sun, S. S. Tang, and M. Lei. Facile synthesis of porous si/c composites with superior lithium storage performance. *Scientific Reports*, 5, 2015.

[162] M. Li, J. Gu, X. Feng, H. He, and C. Zeng. Micro/nano hierarchical porous silicon particles as high-performance anode materials for lithium-ion batteries. *Electrochimica Acta*, 164 :163–170, 2015.

[163] J. Wen, Y. Yu, and C. Chen. Challenges and opportunities for rechargeable lithium batteries. *Materials Express*, 2 :197–212, 2012.

[164] M. Ge, X. Fang, J. Rong, and C. Zhou. Review of porous silicon nanomaterials for lithium-ion battery anode applications. *Nanotechnology*, 24 :422001, 2013.

[165] D. Ma, Z. Cao, and A. Hu. Si-based anode materials for li-ion batteries : a mini review. *Nano-Micro Letters*, 6 :347–358, 2014.

[166] N. Nitta and G. Yushin. High-capacity anode materials for lithium-ion batteries : current status and future perspectives. *Particle & Particle Systems Characterization*, 31 :317–336, 2014.

[167] M. L. Terranova, S. Orlanducci, E. Tamburri, V. Guglielmotti, and M. Rossi. Nanostructured silicon-based anodes for lithium-ion batteries : a review. *Journal of Power Sources*, 246 :167–177, 2014.

[168] X. Su, Q. Wu, J. Li, X. Xiao, A. Lott, W. Lu, B. W. Sheldon, and J. Wu. Silicon-based nanomaterials for lithium-ion batteries : a review. *Advanced Energy Materials*, 4 :1300882, 2014.

[169] X. H. Liu, H. Zheng, L. Zhong, S. Huang, K. Karki, L. Q. Zhang, Y. Liu, A. Kushima, W. T. Liang, and J. W. Wang. Anisotropic swelling and fracture of silicon nanoparticles during lithiation. *Nano Letters*, 11 :3312–3318, 2011.

[170] M. K. Y. Chan, C. Wolverton, and J. P. Greeley. First principles simulations of the electrochemical lithiation and delithiation of faceted crystalline silicon. *Journal of the American Chemical Society*, 134 :14362–14374, 2012.

[171] X. H. Liu, L. Zhong, S. Huang, S. X. Mao, T. Zhu, and J. Y. Huang. Size-dependent fracture of silicon nanoparticles during lithiation. *ACS Nano*, 6 :1522–1531, 2012.

[172] M. T. McDowell, I. Ryu, S. W. Lee, C. Wang, W. D. Nix, and Y. Cui. Studying the kinetics of crystalline silicon nanoparticle lithiation with in situ transmission electron microscopy. *Advanced Materials*, 24 :6034–6041, 2012.

[173] Z. Sun, X. Song, P. Zhang, and L. Gao. Facile synthesis of carbon–silicon hybrid hollow spheres for high performance lithium-ion battery anodes. *RSC Advances*, 4 :20814–20820, 2014.

[174] Z. Sun, S. Tao, X. Song, P. Zhang, and L. Gao. Carbon-coated silicon hollow spheres as high-performance anode materials for lithium-ion batteries. *Journal of The Electrochemical Society*, 162 :A1530–A1536, 2015.